Forms and fluxes of carbon: Surface to deep

Alberto Vitale Brovarone, Kevin Wong, Donato Giovannelli, Benoit de Pins, Fabrice Gaillard, Malcolm Massuyeau, Fabrizio Nestola, Martha Giovanna Pamato, Isabelle Daniel

Forms and fluxes of carbon: Surface to deep

Alberto Vitale Brovarone[a,b,c], Kevin Wong[a], Donato Giovannelli[d,e,f,g,h], Benoit de Pins[d], Fabrice Gaillard[i], Malcolm Massuyeau[j], Fabrizio Nestola[k], Martha Giovanna Pamato[k], and Isabelle Daniel[l], [a]Dipartimento di Scienze Biologiche, Geologiche e Ambientali (BiGeA), Alma Mater Studiorum Università di Bologna, Bologna, Italy; [b]Institut de Minéralogie, de Physique des Matériaux et de Cosmochimie (IMPMC), Sorbonne Université, Muséum National d'Histoire Naturelle, UMR CNRS 7590, IRD UR206, Paris, France; [c]Institute of Geosciences and Earth Resources, National Research Council of Italy, Pisa, Italy; [d]Department of Biology, University of Naples Federico II, Naples, Italy; [e]National Research Council—Institute of Marine Biological Resources and Biotechnologies (CNR-IRBIM), Ancona, Italy; [f]Department of Marine and Coastal Science, Rutgers University, New Brunswick, NJ, United States; [g]Marine Chemistry, Geochemistry Department—Woods Hole Oceanographic Institution, Falmouth, MA, United States; [h]Earth-Life Science Institute, Tokyo Institute of Technology, Tokyo, Japan; [i]CNRS, BRGM, ISTO, UMR 7327, Université d'Orléans, Institut des Sciences de la Terre (ISTO), Orléans, France; [j]Institut für Mineralogie, Westfälische Wilhelms-Universität Münster, Münster, Germany; [k]Department of Geosciences, University of Padova, Padova, Italy; [l]Universite Claude Bernard Lyon1, LGL-TPE, UMR 5276, CNRS, Ens de Lyon, Universite Jean Monnet Saint-Etienne, Villeurbanne, France

Abstract

Carbon is an essential element for the coevolution of Earth and life, and its largest fraction is stored in the deep Earth. The availability of carbon at the Earth's surface or shallow subsurface over the past 3.8 billion years has been modulated by this reservoir of deep carbon, which has played a fundamental role in the emergence and diversification of life. In turn, major geobiological changes at the Earth's surface have profoundly affected the chemical fingerprints and morphological forms of carbon entering the deep Earth through subduction. This chapter presents an overview of the geology of deep carbon, from its origins and forms throughout the Earth's history, to its movements and fluxes between shallow and deep reservoirs.

Keywords

Abiotic organics; Biotic and abiotic carbon; Carbon budgets; Carbon cycle; Carbon fluxes; Carbon in melts; Deep carbon; Coevolution of Earth and life; Origin of carbon; Metamorphic carbon degassing

Key points

- We present the origins and forms of deep carbon throughout the Earth's history
- We summarize the reservoirs of deep carbon from the core to the crust
- We review the available estimates of carbon fluxes from the surface to the deep Earth and vice-versa

Introduction

Carbon (C) is an essential element for life and the functioning of our planet. Its presence and quantity in the biosphere and atmosphere has largely been controlled by exchange with the large carbon reservoir in the deep Earth throughout the Earth's history (Berner, 1994; Hazen and Schiffries, 2013). Deep carbon is recycled through tectonic (or mechanical), metamorphic, magmatic, and fluid-rock interaction processes, and — within the parameter space for life — through biologically-mediated processes. However, the largest fraction of Earth's carbon is stored in deep Earth reservoirs such as the mantle and the core (Dasgupta and Hirschmann, 2010). Because of that, the distribution, movements, and fluxes of deep carbon within and between geological reservoirs are still largely unconstrained and model-dependent (Dasgupta, 2013; Wood et al., 2013). The long-term carbon cycle on our planet is primarily controlled by plate tectonics, with convergent plate margins and subduction driving the input of surface carbon into the deep Earth and volcanism and diffuse degassing acting as the main pathway for the return of carbon to the Earth's surface (Halama and Bebout, 2021; Jarrard, 2003; Kelemen and Manning, 2015; Lee et al., 2019; Plank and Manning, 2019; Werner et al., 2019).

Defining the boundary between surface and deep carbon is not straightforward, as the two reservoirs are intimately connected. Deep carbon represents the largest fraction of carbon on Earth and controls its long-term, or geological, cycle ($\sim 10^{23}$ mol; Lee et al., 2019). On the other hand, surface carbon represents a much smaller reservoir (10^{21}–10^{22} mol; Hayes and Waldbauer, 2006; Javoy et al., 1982), but is central for - and profoundly affected by - biological activity with important implications on the types, sizes and chemical fingerprints of both solid carbon being transferred from the surface to the deep Earth at subduction zones, and deep carbon degassing into the atmosphere. The emergence and diversification of life over the Earth's history has substantially affected the diversity, distribution, and signatures of carbon-bearing geological materials (Hazen et al., 2019), thereby affecting deep carbon processes and chemical fingerprints. This includes subsurface life that acts on deep carbon to alter its composition.

Given the diverse interconnections among processes acting at various depths within the crust and mantle, and the complex interplay between geological and biological processes, the potential solution to identify a boundary between surface and deep carbon can be found in the respective sizes and response times of carbon in the various reservoirs. Lee et al. (2019) defined the limit between endogenic (deep; Earth's lithosphere and mantle) and exogenic (surface; oceans, atmosphere, biosphere, reactive marine sediments) carbon at 10^7 Gt mass of carbon (where 1 Gt = 10^{15} g) and 10,000–100,000 years of residence time, with endogenic carbon being richer in carbon and slower in response time relative to exogenic carbon. In the lithosphere and mantle reservoir, the residence time of carbon is estimated to be in the range of 1 million to 1 billion years, in comparison to the <100,000 year timescales typical of the exogenic carbon cycles (Lee et al., 2019).

Starting from the origin of deep carbon on Earth, this chapter presents a summary of the most common forms of deep carbon, their movements — from solids to fluid phases — and fluxes. Although carbon in the biosphere is considered exogenic (response time <10,000 years; Lee et al., 2019), this chapter also presents some key aspects of carbon in the biosphere. This is because of the central role of life in controlling the amounts, forms, and chemical signature of carbon not only at the Earth's surface, but also in the subsurface where endogenic and exogenic processes together act to modulate the fluxes of carbon between the surface and the deep Earth.

Origins of deep carbon

Isotopic constraints on Earth's bulk carbon are consistent with a chondritic origin (Broadley et al., 2022). The carbon content of non-carbonaceous enstatite chondrites and carbonaceous chondrites could explain the concentration of carbon and the $^{13}C/^{12}C$ ratio of the bulk silicate Earth (BSE; Hirschmann, 2018; Marty et al., 2016). A similar chondritic provenance of most life-forming elements, i.e., hydrogen and nitrogen, is also consistent with the elemental and isotopic abundances for these elements (Broadley et al., 2022). It therefore seems likely that carbon and other life-forming elements were delivered to Earth during planetary accretion. The geological history of carbon thus started with the earliest planetary events that have shaped planet Earth (Fig. 1).

Carbon was first delivered by chondrite-like materials on small planetary bodies that formed within the first 1–3 millions of years of the solar system, via a mechanism termed 'pebble accretion' (Johansen and Lambrechts, 2017; Li et al., 2016). During this early stage, radioactive heating was intense enough to induce melting of these bodies, enabling magma ocean and core differentiation. Upon this early differentiation, carbon was greatly partitioned into the core (Li et al., 2016), but due to the combination of low gravity and high temperature, outgassing and loss of gaseous carbon was certainly prevailing. This implies that the carbon content of these small planetary bodies was low. It was only when the size of these planet-forming bodies reached diameters of ~1000 km that gravity was strong enough to limit gas escape. Carbon incorporation in the planet interior then became considerable, with the particularity that under the prevailing reducing conditions, a significant, amount of carbon must have been dissolved in the forming core (Li et al., 2016; see Section "Carbon in the Earth's core") and outgassed into the atmosphere (Gaillard et al., 2022a). The proportion of carbon being dissolved in the magma ocean (the Hadean BSE) was in comparison small (Gaillard et al., 2022a,b).

Once pebble accretion ended, planetary growth occurred via collisions, a highly energetic process capable of partly or totally ejecting the atmosphere into space (Chen and Jacobson, 2022). Since the magma ocean atmosphere was primarily composed of carbon species, collisions mostly caused carbon loss. Secondary atmospheres were subsequently formed by the degassing of the planetary interior after these impacts. The primordial carbon delivered by chondrites has therefore been mostly lost to space or partitioned into the core, which, in both cases, constitutes an irreversible mechanism, subtracting some carbon from the BSE (Gaillard et al., 2021). Accordingly, non-carbonaceous (>3000 ppm C) and carbonaceous (several wt% C) chondrites actually contain more carbon than BSE (Gaillard et al., 2021), which has a carbon concentration ranging from 140 ppm (Hirschmann, 2018) to >500 ppm (Marty et al., 2013, 2016; see also Section "Carbon throughout the Earth's mantle"). It has also been hypothesized that large impacts, such as that forming the Moon, could have contributed a substantial amount of carbon and other volatiles to the BSE, as opposed to facilitating overall carbon loss (Grewal et al., 2019).

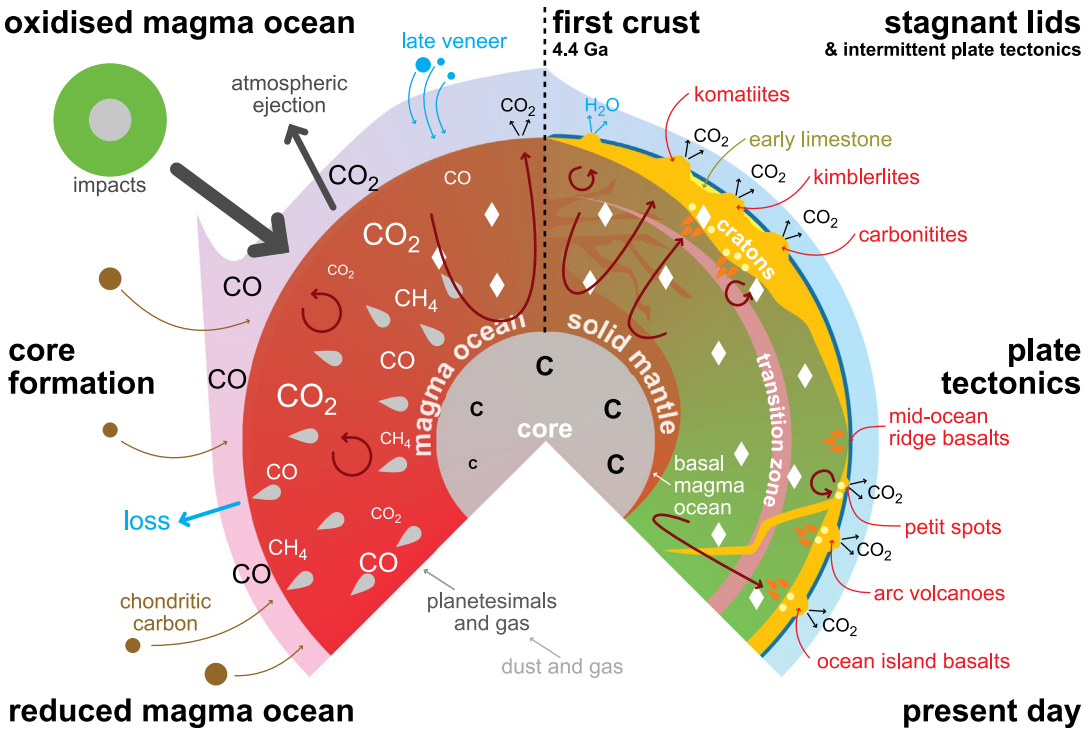

Fig. 1 The geological history of deep carbon summarized in a clockwise time line sketch – starting bottom left – (see Section "Origins of deep carbon" for details). It shows the evolution of deep carbon from the early accretion of planet Earth, where magma ocean processes prevailed and drove core-mantle-atmosphere exchanges, to the present-day solid-state convection regime wherein mantle-crust-atmosphere exchanges are dominated by plate tectonics.

On large bodies such as the Earth, a thick magma ocean could develop with high pressures prevailing at its base. When pressure exceeds 15–20 GPa, ferric-iron-rich silicate melts (with $Fe^{3+}/Fe_{tot} \sim 0.1–0.2$) are stable in equilibrium with molten Fe-rich alloys (Armstrong et al., 2019). At lower pressure, under otherwise similar conditions, such melts would contain only ~5% ferric iron. Vigorous convection from the base to the top of the magma ocean implies that such ferric-iron-rich silicate melts would buffer a high oxygen fugacity when exposed to surficial conditions. This implicitly assumes that the Fe-rich molten alloys remain at the base of the magma ocean due to negative buoyancy forces. Consequently, while early and thin magma oceans outgassed mostly CO, late and deep magma oceans outgassed mostly CO_2. The early redistribution of oxygen from CO_2 at shallow conditions to Fe_2O_3 (i.e., Fe^{3+}) in the deep magma ocean may have caused the first diamond precipitation in the interior of Earth as illustrated in Fig. 1 (Armstrong et al., 2019).

The solidification of the magma ocean is a complicated stage, blending thermomechanical and thermochemical processes (Ballmer et al., 2017; Hier-Majumder and Hirschmann, 2017; Korenaga, 2021). It is yet unclear how magma ocean carbon could behave during this solidification. If a deep basal magma ocean survived this process (Labrosse et al., 2007), we could expect substantial quantities of dissolved carbon species to be sequestered therein.

Most models suggest that the atmosphere forming at the end of the magma ocean was CO_2-dominated, with pressures ranging from 90 to 200 bar depending on the size of the degassing magma ocean (Gaillard et al., 2022a; Sossi et al., 2020). Assuming water was efficiently degassed from the solidifying mantle during the early Hadean, it has been proposed that its condensation in the form of early oceans could have efficiently pumped in atmospheric carbon into the deep Earth via carbonate mineral precipitation in a context of early plate tectonics and vigorous rock alteration (Sleep et al., 2011; Korenaga, 2021). This implies an early sequestration of deep carbon in the mantle via subduction of surface carbon.

A comparison between the mass of carbon outgassed by the magma ocean in the early Hadean and the present-day mass of surface carbon (atmosphere + oceans + crust) indicates surprisingly similar numbers of $110 \pm 50 \times 10^{21}$ g C (Gaillard et al., 2022a). This mass of surficial carbon is also indistinguishable from the mass of carbon constituting the dense Venusian atmosphere. A similar conclusion has been reached for nitrogen (Gaillard et al., 2022a), which can be explained by the very low fluxes of nitrogen involved in both present-day planetary outgassing and burying via subduction with respect to the size of the atmospheric reservoir (Gaillard et al., 2022a; Hirschmann, 2018). This may indicate that a surficial reservoir of carbon formed early in the history of planet Earth and has been only moderately affected by the subsequent 4.5 billion years of geological history. The balance of subduction versus outgassing might have maintained a steady state regime, although there are still many uncertainties in the actual fluxes of carbon involved in such geodynamic cycles (see Section "Carbon movement within and between deep reservoirs"; Dasgupta and Hirschmann, 2010; Iacono-Marziano et al., 2009; Kelemen and Manning, 2015) and it is difficult to discuss such processes further.

Toward the end of Earth's formation, a meteoritic bombardment — the so-called 'late veneer' — delivered significant portions of highly siderophile elements to the Earth in chondritic proportions, thereby elevating their BSE concentrations despite core differentiation (e.g., Walker, 2009; Wang and Becker, 2013). A volatile-rich late veneer, as suggested by Wang and Becker (2013), could have supplied a substantial proportion (20%–100%) of the carbon now comprising BSE. However, subsequent studies have cast doubt on the possibility of a solely late veneer contribution to BSE volatiles, including carbon. A simple mass balance calculation has shown that the mass of material required to account for the BSE carbon inventory ($\sim 2 \pm 1$ wt%) is equal to, or greater than, the mass delivered by the late veneer (0.1–2.0 wt%; Mikhail and Füri, 2019). Ruthenium, a highly siderophile element replenished in BSE by the late veneer, has an isotopic composition in Earth's mantle distinct from carbonaceous chondrite-derived material; this suggests that the late veneer was unlikely to be composed of the volatile-rich carbonaceous chondrites from which Earth's carbon is derived (Fischer-Gödde and Kleine, 2017). Instead, it is reasonable to suggest that the bulk of Earth's carbon was obtained during the principal stages of planetary accretion, as discussed above, with a minor fraction of carbon subsequently added by a late veneer (e.g., Hirschmann, 2016). This is supported by isotope fractionation modeling of sulfur and chalcophile elements, which suggests that planetary differentiation is sufficient to account for volatile element concentrations in the BSE with less than 40% delivered by the late veneer (Wang et al., 2023).

Once the magma ocean was solidified, volcanism on Earth was mostly mafic (i.e., forming basaltic lavas), accompanied by superhot lavas such as Mg-rich komatiites (Fig. 1, top). No constraint allows us to understand the carbon outgassed by these magmas. The oldest available constraints are probably encapsulated within diamonds; diamonds older than 3.0 Ga host peridotitic inclusions, whereas younger diamonds prevalently host eclogitic inclusions (Shirey and Richardson, 2011; see Section "Diamonds as clues on deep and super-deep carbon movements" for a full discussion on inclusions in diamond). This is possibly a signature of the initiation of plate tectonics at the end of the Archean eon.

Cratons are thick (>200 km) and cold lithospheric blocks which have experienced little, if any, geological activity since the Archean. They host kimberlites, which constitute the dominant form of extrusive rocks containing diamonds (see Section "Diamonds over (geological) time"). Mantle xenoliths found in kimberlites and in many other intraplate lavas have revealed that mantle metasomatism, i.e., melt-fluid-rock interactions taking place at the base of lithosphere (O'Reilly and Griffin, 2013), is an important process, modifying the physical and compositional properties of cratonic mantle lithosphere and possibly storing an important amount of carbon (see Section "Sub-continental lithospheric mantle"; Aulbach et al., 2017; Hirschmann, 2018). To some extent, lithospheric diamonds can be seen as resulting from such metasomatism, and Ca-Mg carbonate minerals have also been widely observed. A hidden carbon reservoir might thus have continuously formed over time (Hammouda et al., 2021) by melt-fluid-rock interactions taking place in cratonic, non-cratonic, and even oceanic lithosphere (Aulbach et al., 2017; Delpech et al., 2023; Foley and Fischer, 2017; Hammouda et al., 2021; Hirano and Machida, 2022; Hirschmann, 2018; O'Reilly and Griffin, 2013).

The final picture of the geological history of carbon corresponds to the present-day outgassing of volcanoes — mid-ocean ridges, petit spots, hot spots, volcanic arcs, etc. (Fig. 1) — which are sourced by various reservoirs built by 4.5 billion years of geodynamic processes with a key role played by subduction processes (Aiuppa et al., 2017; Dasgupta and Hirschmann, 2010; Hammouda et al., 2021; Hirano and Machida, 2022; Plank and Langmuir, 1998). Carbon isotopic measurements of volcanic gasses in arc settings suggest the major involvement of sedimentary carbonates in degassing, with the possibility of crustal assimilation processes short-circuiting the deep carbon cycle (Section "Movements of deep carbon in melts"; Iacono-Marziano et al., 2009; Mason et al., 2017).

Carbon at the interface between the geosphere and biosphere

Deep carbon movements and transformations on Earth result from complicated and interconnected geological and biological processes. A large fraction of solid carbon in the crust is formed through biological processes and their successive solid-state transformations. For example, carbonate minerals can be synthesized by various organisms that grow a carbonate shell such as coccolithophores and other phytoplankton, be precipitated as a result of microbial metabolism such as in chemosynthetic ecosystems on the seafloor, or can also be dissolved by endoliths and other microorganisms during their metabolic reactions. The organic component of biological matter, or its transformation, represents the largest fraction of organic carbon on the surface of our planet. The main biological processes interacting with carbon and their related fluxes are presented in Fig. 2.

While biology might appear as a thin veneer on the surface of our planet, its interactions with the solid Earth are far reaching (Vernadsky, 1926). Life originated on this planet between 3.8 and 4.0 Ga, and soon after its appearance it has taken control over several surface and near-surface chemical cycles, deeply impacting the movement, speciation, and quantity of elements on Earth (Falkowski et al., 2008). Subducted organic carbon material as old as 3.0 Ga, as reflected from the carbon isotopic signature of diamonds (Howell et al., 2020), reveals that the biosphere has extended its reach far beyond the habitable area of the near planetary surface, and it is possible that today no Earth carbon reservoir, with the exception perhaps of the core, is devoid of the fingerprints of life.

This section introduces the contribution of biology to deep carbon processes and fluxes, reflecting on the complex geo-biological interactions that underpin the interplay between the fast and slow carbon cycle.

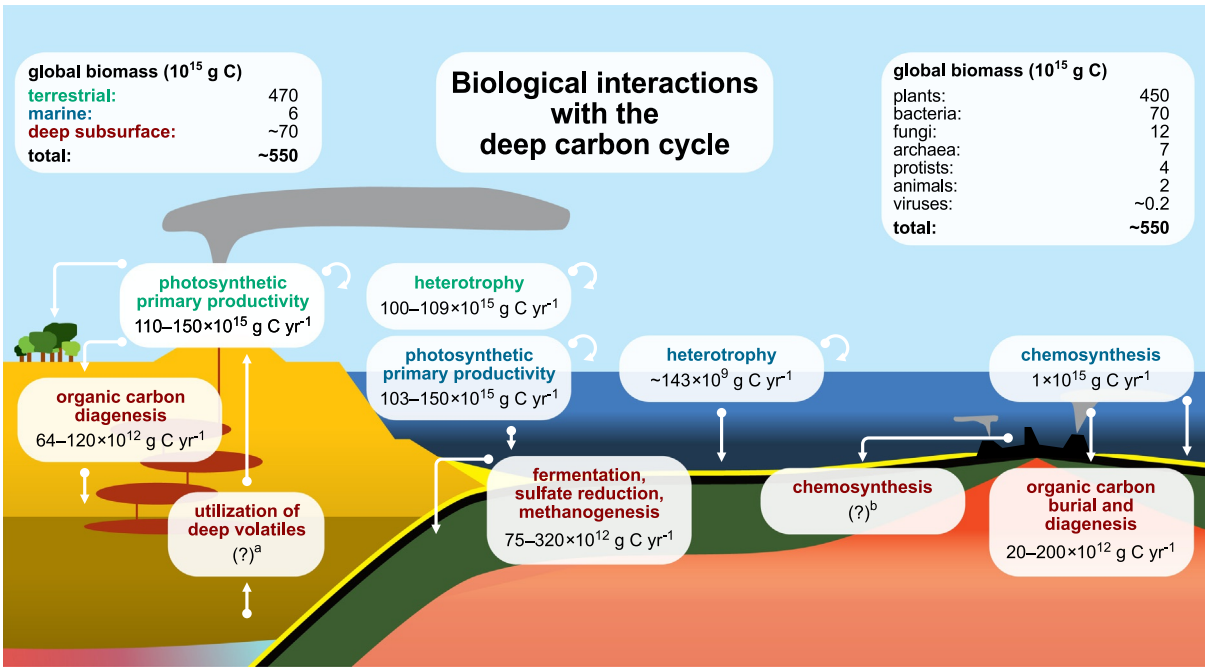

Fig. 2 Summary of the major biological processes interacting with carbon that have direct effects and interactions with the deep carbon cycle. Major processes are colored according to the division between terrestrial (green), marine (blue) and deep subsurface (red) processes. Global estimates of biomass are reported (Bar-On et al., 2018). Gross (photosynthetic) primary productivity on land: 110–150 $\times$ 10^{15} g C yr^{-1} (Jian et al., 2022; Lu et al., 2024). Organic carbon diagenesis: 64–120 $\times$ 10^{12} g C yr^{-1} (Kump and Arthur, 1999). Heterotrophy at the ocean surface: 143 $\times$ 10^{9} g C yr^{-1} (del Giorgio and Duarte, 2002). Gross (photosynthetic) primary productivity in the ocean: 103–150 $\times$ 10^{15} g C yr^{-1} (Huang et al., 2021a,b). Water column chemosynthesis (in the photic zone, dark ocean and surface marine sediments): ~1 $\times$ 10^{15} g C yr^{-1} (Middelburg, 2011). Marine organic carbon burial and diagenesis: 20–200 $\times$ 10^{12} g C yr^{-1} (Cartapanis et al., 2018; Dunne et al., 2007; Hayes et al., 2021; Jahnke, 1996). Oceanic sediment methane production is 75–320 $\times$ 10^{12} g C yr^{-1} (Valentine, 2002). Utilization of deep volatiles in the continental crust (and oceanic crust) is still unconstrained (subscript a), but likely to be significant; see Barry et al. (2019) and Fullerton et al. (2021) for estimates at the Costa Rican convergent margin (~10^{8}–10^{10} mol C yr^{-1}). Both continental and oceanic subsurface chemosynthesis is currently unconstrained (subscript b).

Carbon's central role in life

Carbon is not merely a ubiquitous element; it is the cornerstone of biochemistry on Earth. Its ability to form stable, complex molecules with a variety of elements, especially hydrogen, oxygen, nitrogen, phosphorus, sulfur and minute amounts of metals underpins the chemistry of life. From the complex carbohydrates that fuel cellular processes to the intricate information storage systems of nucleic acids, carbon forms the scaffolding upon which life is built. Additionally, different carbon species play crucial roles in energy generation and electron transfer reactions that sustain life. Reduced carbon compounds like methane (CH_4) and carbon monoxide (CO) serve as energy sources for chemolithotrophic microorganisms, while oxidized forms like carbon dioxide (CO_2) and bicarbonate (HCO_3^-) act as electron acceptors in various metabolic pathways.

Carbon is incorporated into building blocks through the process of carbon fixation, either starting from CO_2, HCO_3^-, CO, CH_3-group and CH_4 as carbon sources. These carbon species are taken up by cells and incorporated into organic molecules following diverse carbon fixation pathways. To date, six carbon fixation pathways are known, namely the Calvin-Benson Cycle, the Arnon-Buchanan cycle, the Wood-Ljungdahl pathway, the hydroxypropionate bicycle, the 4-hydroxybutyrate pathway, the hydroxypropionate/hydroxybutyrate cycle and the dicarboxylate/hydroxybutyrate cycle (Fuchs, 2011). Of the six pathways, the Calvin-Benson cycle (most frequently called the Calvin cycle) was the first one to be elucidated and it is the pathway that currently dominates carbon fixation on the surface of planet Earth, probably due to the robustness of its enzymes to atmospheric molecular oxygen. Used by phototrophs, including plants, algae and cyanobacteria, and a number of chemolithotrophic (that is non-photosynthetic autotrophs) bacteria, the Calvin cycle accounts for the large majority of the organic carbon produced under the influence of the sun on the surface of the planet. Organic carbon produced using this pathway fractionates relative to the source carbon ($\Delta^{13}C$) between −20‰ and −30‰, generally producing organic carbon with a distinctive $\delta^{13}C$ (VPDB) isotopic signature between −25‰ and −28‰, providing a unique marker for tracking carbon fixed using oxygenic photosynthetic processes (Fuchs, 2011).

The other five carbon fixation pathways play a key role in anaerobic microorganisms inhabiting marine sediments today, a variety of extreme environments, and the continental and oceanic subsurface. The Arnon-Buchanan cycle, also known as the reverse tricarboxylic acid (TCA) cycle or reverse Krebs cycle, is abundant in anoxygenic phototrophs, and a large number of anaerobic and microaerophilic chemolithotrophic microorganisms. Its $\delta^{13}C$ carbon isotopic fractionation ($\Delta^{13}C$) is much smaller than the Calvin cycle, and generally between −2‰ and −12‰. Recently, it has been shown to be dominant in subsurface ecosystems at convergent margins (Fullerton et al., 2021; Rogers et al., 2023), and it has been previously identified as a key carbon fixation pathway in deep-sea hydrothermal vents (Hügler and Sievert, 2011; Sievert and Vetriani, 2012). The Wood-Ljungdahl pathway, also known as the reductive acetyl-CoA pathway, has been originally described in acetogenic bacteria and it is active in a number of strictly anaerobic bacteria and archaea, including methanogens and sulfate reducing bacteria, both of which play a key role in linking the fast and slow carbon cycle. The Wood-Ljungdahl pathway is capable of producing some of the most ^{13}C-depleted organic carbon on this planet, with carbon isotopic fractionation $\Delta^{13}C < -30$‰ and reported values as low as −65‰ Freude and Blaser, 2016. The methane produced using this pathway by methanogens is also distinctively depleted in ^{13}C ($\delta^{13}C < -45$‰) compared to abiotic and thermogenic methane sources (Whiticar, 1999). This "light" carbon isotopic signature can be retained in authigenic carbonate minerals (that is carbonate minerals directly precipitated within the sedimentary sequences rather than exported from the surface) created in chemosynthetic environments by the oxidation of methane, and can reach extreme $\delta^{13}C$ values below −70‰. This is a value markedly different from the carbonate minerals created by photosynthetic organisms with a $\delta^{13}C \sim 0$‰. The remaining carbon fixation pathways play a minor quantitative role in ecosystems, with the exception of the hydroxypropionate/hydroxybutyrate cycle that is used by the ammonia-oxidizing archaea that dominate carbon fixation in the dark oceanic water column (Könneke et al., 2014). These examples highlight the diversity of interactions that life has with carbon as a building block, and they suggest that the isotopic signature of organic carbon and carbonates subducted and recycled in the deep Earth might have important local variations depending on the microbial processes involved.

Beyond its structural role, carbon compounds play critical energetic roles in ecosystems, especially in environments where light and oxygen are scarce. Reduced carbon forms such as CO and CH_4 can serve as electron donors (i.e., energy sources) in microbial redox energy reactions and are important energy sources especially in subsurface environments. Oxidized carbon forms, such as CO_2 and HCO_3^- can instead be used as terminal electron acceptors (i.e., oxidants) in microbial redox metabolic reactions, and are quantitatively important in several ecosystems despite the low Gibbs free energy released. Diverse organisms, both aerobic and anaerobic, can utilize these carbon compounds as substrates in their redox metabolism, altering the quality and quantity of the carbon cycling through diverse geological reservoirs. While oxidized carbon molecules (i.e., CO_2 and HCO_3^-) can only be used in conjunction with hydrogen (H_2) as electron donor to generate compounds such as CH_4 and acetate, the reduced carbon forms, and in particular methane can be coupled to a diverse array of electron acceptors by taxonomically and metabolically diverse microorganisms (Hay Mele et al., 2023). Methane can be oxidized aerobically at the expense of oxygen (O_2) by aerobic methanotrophs, as well as anaerobically coupled to diverse electron acceptors such as sulfate (SO_4^{2-}), iron (Fe^{3+}), manganese (Mn^{4+}) and nitrite (NO_2^-) (Guerrero-Cruz et al., 2021).

The deep subsurface biosphere

While the interaction of life with carbon is at the basis of the fast — and near-surface — carbon cycle (Lee et al., 2019), the discovery of the deep subsurface biosphere has revolutionized our understanding of the interaction of life with the deep carbon cycle. Since

first proposed in the early 1990s (Gold, 1992), the deep biosphere has constantly challenged our understanding of the limit and adaptation of life and its interaction with the solid Earth (Colman et al., 2017). After 30 years of research we know that up to 14% of Earth's biomass is stored in the subsurface (Bar-On et al., 2018), and microbial communities thrive kilometers below the surface, inhabiting diverse environments within the Earth's crust, oceanic sediments, and subseafloor (Kallmeyer et al., 2012; Magnabosco et al., 2018). This hidden biosphere exhibits remarkable metabolic diversity, with organisms adapted to extreme conditions of temperature, pressure, and nutrient availability, and it is capable of interacting with geological processes at extremely diverse spatial and temporal scales, matching scale processes such subduction, organic matter diagenesis and geological volatile cycling (Giovannelli et al., 2022).

Communities in the deep subsurface are largely composed of bacteria and archaea, along with a very small number of eukaryotic microbes (Bar-On et al., 2018). These microorganisms exhibit remarkable adaptations that allow them to exploit redox energy couples provided by the geosphere — such as hydrogen or methane — together with organic carbon produced in situ biotically, and potentially abiotically, or derived from the surface. Their distribution is controlled by diverse factors such as energy availability, geochemistry, temperature, pressure and available liquid water and pore space (Heuer et al., 2020). A key factor controlling their distribution appears to be temperature, with the current upper limit for life set at 122 °C in the laboratory (Takai et al., 2008) and believed to be around 135 °C in natural ecosystems (Heuer et al., 2020; Merino et al., 2019). Current data suggests that the deep subsurface biosphere extends from a few meters below the surface to 3–5 km in marine and continental settings respectively (Magnabosco et al., 2018), with theoretical studies suggesting that under favorable conditions, such as those found in cold subduction zones, the habitable zone could extend up to 15–20 km depth (Plümper et al., 2017). These depths, together with the diversity of metabolic processes and the ability to interact with geological processes over long timescales (Lloyd, 2020), allow subsurface microbial communities to impact carbon and other volatiles cycling at planetary scales (Barry et al., 2022; Giovannelli et al., 2021, 2022). The upper lithosphere can thus be seen as a giant biofilter (Giovannelli et al., 2021), harboring microbial communities capable of altering the influx (mainly in marine sediments) and the outflux (in the oceanic and continental crust) of carbon materials, affecting the quantities of carbon recycled, its redox state and its isotopic signature.

Impact of life and organic carbon on the deep carbon cycle

The biological production of organic matter and its subsequent deposition and burial lead to significant transformations in carbon reservoirs, which can ultimately be subducted and recycled within the Earth's interior (Fig. 2). This process introduces vast quantities of carbon into Earth's lithosphere and beneath, contributing to the formation of fossil fuel deposits and shaping the composition of deep carbon reservoirs. The evolution of oxygenic photosynthesis and the subsequent rise of oxygen in the atmosphere led to a shift from carbonate-based to organic-carbon-based burial of carbon at the beginning of the Proterozoic eon (Galvez et al., 2020), highlighting the profound influence of biological evolution on deep carbon cycling.

The metabolic activities of deep life significantly impact deep carbon cycling. Microorganisms facilitate the transformation of various carbon species, contributing to processes such as methanogenesis, hydrocarbon oxidation, and carbonate mineral precipitation. These activities alter the composition and mobility of carbon in deep reservoirs, influencing long-term carbon storage and release. For instance, methanogenesis in deep subsurface environments contributes to the global methane budget, while microbial oxidation of hydrocarbons can impact the quality and recovery rates of oil and gas reservoirs. Additionally, microbial processes contribute to the precipitation and dissolution of carbonate minerals, playing a role in the long-term carbon cycle.

Despite significant advancements in our understanding of the deep biosphere and its interactions with deep carbon, many questions remain unanswered. Quantifying the total biomass and metabolic activity of deep life remains a challenge due to limitations in sampling and detection methods. Additionally, most deep subsurface organisms remain uncultured, hindering our understanding of their metabolic capabilities and their role in biogeochemical cycles. Furthermore, the impact of anthropogenic activities and natural environmental changes on deep life and deep carbon cycling requires further investigation. Addressing these open questions is crucial for developing a comprehensive understanding of the Earth system and its response to environmental change. Further research at the interface of geochemistry and microbiology promises to illuminate the intricate interplay between deep carbon and the biosphere, revealing the hidden secrets of Earth's deepest realms.

Biogenic carbon: From the surface to the subsurface of the planet

The vast majority of inorganic carbon enters the biosphere through the Calvin cycle enzyme rubisco (Raven, 2009). Rubisco is an ancient enzyme that appeared in archaea from ~4.0 Ga. Over time, it evolved into the primary carbon-fixing enzyme, notably in phototrophs like cyanobacteria and terrestrial plants, facilitating the historical accumulation of biogenic carbon on Earth (i.e., carbon that is either part of, or derived from, living organisms).

At the Earth's surface — on the land and the marine photic zone — biogenic carbon fixation is mostly ensured by plants and microalgae respectively through photosynthesis (Bar-On et al., 2018). It is estimated that gross primary productivity, a metric quantifying the amount of CO_2 removed from the atmosphere every year to fuel photosynthesis, is evenly distributed between land and ocean, each contributing ≈100–150 Gt C yr^{-1} (Fig. 2; Huang et al., 2021a, Huang et al., 2021b; Jian et al., 2022; Lu et al., 2024). These primary producers form the basis of terrestrial and marine food webs, as they are consumed by heterotrophs, which build their biomass out of this fixed biogenic carbon. When these organisms die, their organic matter — when not decomposed — can accumulate and become buried under layers of sediment. On land, biogenic carbon-rich organic matter can for instance be

preserved from decomposition by mud or acidic water, eventually forming peat deposits that, over millions of years, transform into coal. Overall, ≈0.2 Gt C are buried in the ground each year (Kandasamy and Nagender Nath, 2016). Alternatively, this terrestrial biogenic carbon can be transported to the oceans by water motion and wind (with an estimated terrestrial carbon input to the ocean of 1.4 ± 0.5 Gt C yr^{-1}; Kwon et al., 2021). There, it joins a pool of biogenic carbon that is fixed in situ by photosynthetic phytoplankton. While most biogenic carbon at the ocean surface is recycled by local consumption (respiration by heterotrophic organisms), a small fraction of it (≈10 Gt C yr^{-1}) sinks or is transported down (by migrating animals or ocean circulation), and eventually joins the deep sea organic carbon stock (Siegel et al., 2023).

Variations in global and regional climate, tectonic activity, and the development of large depositional basins have played critical roles in determining the rates of carbon accumulation and the formation of these different deposits. These carbon reservoirs are therefore not uniformly distributed across the planet. Large coal deposits, for instance, are often found in regions that were historically forested and subject to specific geological conditions favoring the preservation of organic material. Oil and natural gas fields are frequently associated with marine sedimentary basins that accumulated vast amounts of organic matter. In the deep sea, most biogenic carbon comes from the surface. However, primary productivity performed by chemolithotrophs, which obtain energy by the oxidation of environmental electron donors (e.g., ammonium, nitrite, ferrous iron, sulfide), can significantly contribute to the organic carbon pool (≈0.1 Gt C yr^{-1} in the deep ocean; Middelburg, 2011). Nitrification, the oxidation of ammonia to nitrite and nitrate, is understood to be the dominant chemolithotrophic metabolism in the deep ocean, while diverse ecosystems (e.g., hydrothermal vent, cold seeps, mud volcanoes, whale falls, oxygen minimum zones) host diverse communities of chemolithotrophs, further contributing to the total rate of non-phototrophic biogenic carbon fixation in the ocean (0.77 Gt C yr^{-1}; Middelburg, 2011).

All the biogenic carbon that is not recycled back into inorganic carbon (by respiration or fermentation) can eventually be buried under layers of sediment. There, the fate of biogenic carbon is an important component of the process of diagenesis, the process by which sedimentary deposits are transformed into a sedimentary rock over the years (Fig. 2). This is largely influenced by local biotic processes (LaRowe et al., 2020). While, in the upper layers of shallow sediments, aerobic respiration remineralizes biogenic carbon, in the deeper layers, and, by extension in all deep-ocean sediments, anaerobic respiration and fermentation processes dominate. The most prevalent one is sulfate reduction (Canfield and Des Marais, 1991). Sulfate-reducing microorganisms use the abundant oceanic sulfate as an electron acceptor to oxidize biogenic carbon (Jørgensen et al., 2019). Interestingly, sulfate is not the most favorable oxidizer thermodynamically (as compared to nitrate or ferric oxide), however its greater abundance in seawater makes it the dominant electron acceptor in the anaerobic oxidation of biogenic carbon in marine sediments. Deeper below, where sulfate is scarce, another metabolism, methanogenesis, is prevalent (e.g., Bojanova et al., 2023). Methanogens reduce organic matter or CO_2 into methane, releasing biogenic carbon that can seep up. Between the sulfate and methane zones lies the sulfate-methane transition zone (SMTZ), where both species cohabit. Within the SMTZ, a third metabolism, the anaerobic oxidation of methane, is dominant. Anaerobic oxidation of methane uses the sulfate to oxidize methane produced below by methanogens, thereby releasing CO_2 and hydrogen sulfide. Stable isotope analysis can track these stratified metabolisms, as each reaction leaves a characteristic isotopic signature, yielding a range of signatures in diagenetic samples (Meister et al., 2019).

A part of biogenic carbon in sediment remains unalterable. Chemically, intermolecular cross-links (Kunhi Mouvenchery et al., 2012) or abiotic modifications, such as sulfurization or peptide deamination (Abdulla et al., 2018; Burdige, 2005), decrease the bioavailability of the organic matter in the sediments. Physically, the phenomenon of sorption of organic matter to mineral surfaces also protects biogenic carbon remineralization by encapsulating it, denaturing extracellular enzymes, and limiting molecular diffusion. In the long run, the quantity of biogenic carbon buried therefore depends on the balance between a continuous input from sedimenting biological matter and its oxidation by local microbial life, in parallel with the ongoing process of sorption and the abiotic alteration of the matter, protecting this carbon from further oxidation.

Finally, another component of the deep carbon cycle is the 'carbonate pump' which contributes to carbon sequestration in the subsurface. Calcifying organisms use dissolved inorganic carbon in seawater to build calcite platelets called coccoliths. Upon their death, these organisms contribute to the accumulation of biogenic carbonate sediments on the ocean floor. Over geological timescales, these sediments can undergo lithification, forming carbonate rocks such as limestone (Folk, 1980).

Of the 10 Gt of biogenic organic carbon transported from the surface to the deep ocean annually, only 0.02–0.2 Gt C yr^{-1} is eventually incorporated in ocean sediments (Cartapanis et al., 2018; Dunne et al., 2007; Hayes et al., 2021; Jahnke, 1996). Most of this biogenic carbon is therefore accumulating at various depths until it is eventually reoxidized, effectively sequestering it away from surface ocean and atmospheric exchange over timescales ranging from months to millennia, depending on the depth.

Effect of life on carbon fluxes to and from the deep Earth

Over geological timescales, organic-matter-rich sediments can be subducted into the Earth's mantle along convergent plate boundaries (Fig. 2; Section "Subduction of crustal carbon"). Microbial communities can survive in sediments that are subducted to depths of several kilometers, where they continue to influence the transformation of carbon (Barry et al., 2019; Debret et al., 2022; Fryer et al., 2020; Plümper et al., 2017). In particular, these communities can rely on the interaction with fluids associated with serpentinizing forearc mantle: reduced volatile species from these fluids (e.g., H_2, CH_4) encounter more oxidized redox couples from the subducted crust, thereby supporting deep chemolithotrophic life (Mottl et al., 2003; Ohara et al., 2012; Vitale Brovarone et al., 2020a). Chemolithotrophy leads to the formation of partially reduced organic carbon compounds (e.g., lipids, carbohydrates,

proteins, hydrocarbons), which may either be subducted further into the deep mantle or, heated under high-pressure conditions, can decompose and release remineralized carbon (CO_2, CH_4).

The subduction of biogenic carbon has significant implications for volcanic activity and the global carbon cycle. Organic carbon and carbonates carried into subduction zones can decrease the melting point of the mantle, leading to enhanced magma generation (Plank and Manning, 2019; see Section "Movements of deep carbon in melts"). This magma, when it reaches the Earth's surface through volcanic eruptions, releases substantial amounts of CO_2 back into the atmosphere together with variable amounts of reduced carbon compounds (e.g., Giggenbach, 1996; Symonds et al., 1994). The amount and speciation of carbonic fluids released at volcanic arcs may be directly influenced by surface biology. For example, recent examination of melt inclusions from a global collection of Cenozoic arc magmas has shown that latitudinal variations in phytoplankton production may directly influence the redox state of the resulting arc magmas (Hu et al., 2024).

Degassing and rising fluids containing reduced carbon species (and other reduced compounds, e.g., H_2, NH_3, H_2S) have the potential to fuel subsurface life on their way to the surface, as evidenced by the abundance of chemolithotrophic microbial communities thriving in various volcanic and gas-seeping ecosystems. Information regarding the quantitative impact of subsurface life on the carbon recycled to the surface are limited, but suggests that potentially large amounts of the carbon compounds (and other volatiles) recycled to the surface might be altered and sequestered by the subsurface biosphere in the overriding crust. For example, recent work suggests that subsurface microbial communities present in the forearc region of convergent margins can sequester into biomass up to 90% of the carbon recycled to the surface, reducing the carbon going to the mantle by up to 40% (Barry et al., 2019; Fullerton et al., 2021). Dissolved organic carbon in the sampled forearc springs has $\delta^{13}C$ signatures indicative of chemolithotrophic activity utilizing CO_2 originating from the subducting plate (Fullerton et al., 2021). Additionally, near-surface microbial communities associated with areas where reduced fluids and gas are recycled to the surface utilize these compounds for their metabolism, further influencing the diversity and fate of carbon molecules and impacting the carbon cycle. In this context, the interactions between subsurface life and the solid Earth play a significant role in the deep carbon cycle, impacting and altering the flux between the Earth's interior and surface. Constraining the contribution of life in altering the quality and quantity of carbon recycled to the surface will be of key importance to understand the interactions and feedbacks between biology and the solid Earth.

Deep carbon forms

The deep forms of carbon are diverse and include multiple redox states and coordination numbers depending on their origin and location within the deep Earth (Fig. 3). The most common solid carbon forms are carbonate minerals, organic matter, graphite, diamond, and carbides. Their movement is largely controlled by redox changes and solubility. This section covers the deep reservoirs of the Earth from the core to the crust, passing through the mantle.

Carbon in the Earth's core

Earth's core is located 2890 km below the surface and is primarily made of iron (85%) and nickel (5%). Small amounts of lighter siderophile elements, including hydrogen, oxygen, sulfur, silicon, and carbon are mandatory to match the density deficit and velocity excess of the Preliminary Reference Earth Model (PREM; Dziewonski and Anderson, 1981). As the Earth's core constitutes 32% of the mass of our planet, even minute amounts of carbon in the core (between 0.1 and 0.5 wt% C depending on estimates) make it the largest planetary carbon reservoir, containing approximately 90% of the bulk Earth carbon budget (see Fischer et al., 2020, and references therein).

As the Earth's core is not directly accessible, estimates of its carbon content rely on our interpretation of various observations. The seismic velocity and elastic parameters of the Earth's core indicate that it is ~10% less dense than iron-nickel alloy under the core pressure-temperature range (136–364 GPa and 4000 K at the core-mantle boundary, CMB) primarily due to the presence of light elements. Comparison of elemental concentrations in BSE relative to primitive meteorites and the volatility trend of elements indicates that the core is enriched in sulfur, hydrogen, and carbon as far as light volatile elements are concerned. Isotopic fractionation during core formation leads to one of the highest estimates of core carbon concentrations (0.5–2.0 wt%; Wood et al., 2013).

The relative enrichment of the core in carbon relative to the BSE was acquired when the core segregated from the mantle silicate reservoir during the collisional accretion stage of the Earth, which extended 10–100 million years after the initial solar nebula processes (see Section "Origins of deep carbon"; Barboni et al., 2017; Jacobson et al., 2014). The metal delivered to the growing Earth that ultimately formed the core existed as droplets that equilibrated at least partially with the magma ocean, while themselves sinking due to the higher density of the metal phase relative to silicate melt. The environment, depth, and redox conditions under which carbon partitioned between silicate and metal phases largely dictated the carbon content of the Earth's core. At low to moderate pressure and high temperature, carbon is siderophile. Our modern societies have largely taken advantage of this behavior, expanding our understanding of carbon partitioning behavior in metals through the production and intensive use of steel (i.e., iron carbide), and developing adjustable properties depending on the addition of other siderophile elements (e.g., chromium and often nickel to obtain stainless steel). The high cosmochemical abundance of carbon, coupled with its low BSE abundance (0.01%), has led to the suggestion that carbon dissolved extensively into the core, and that its concentration in the core is on the order of 2–4 wt% C. This opens the idea that carbon could be a major element in the inner core, which may contain high-pressure carbides such as

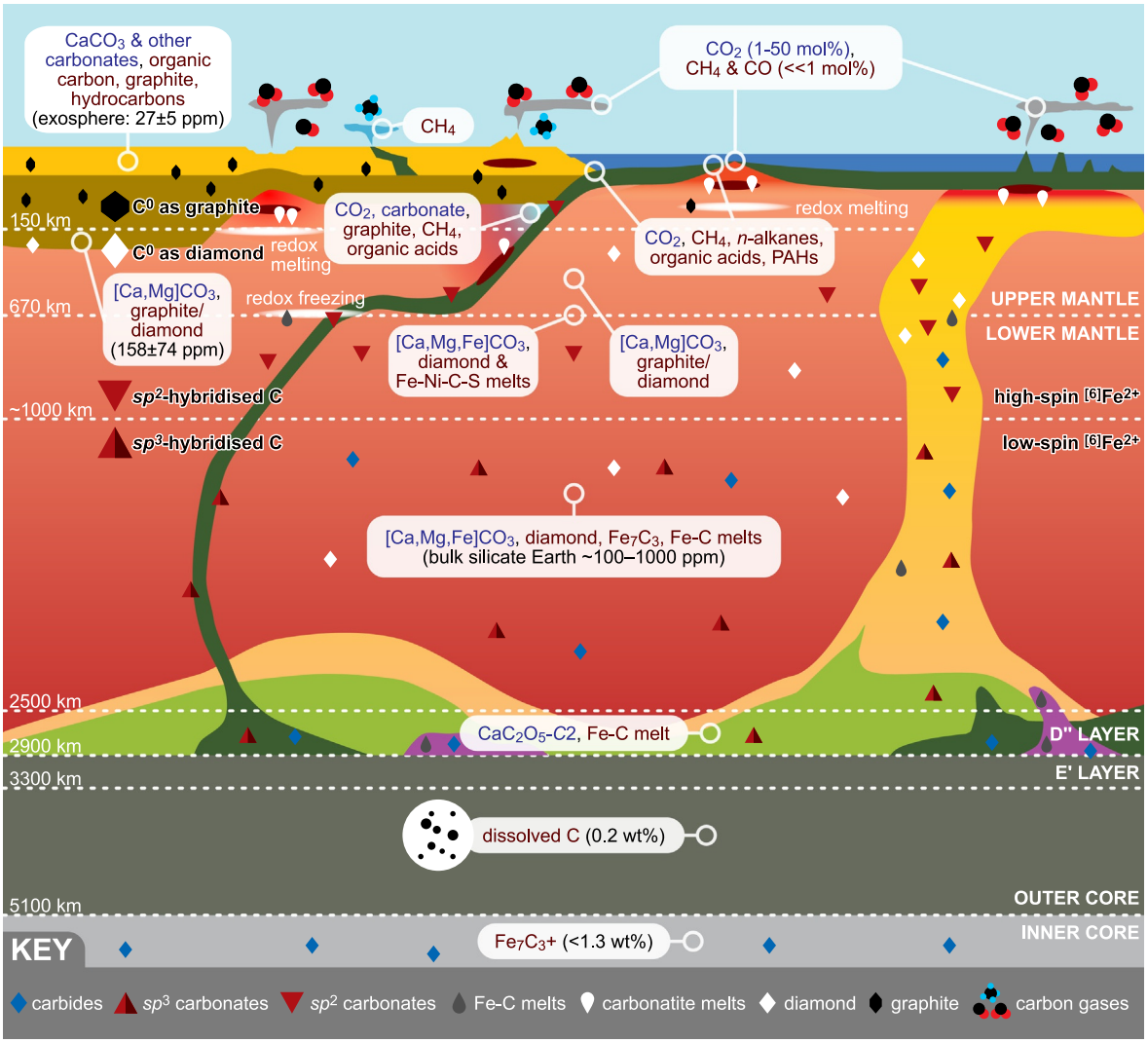

Fig. 3 Schematic diagram illustrating the distribution, forms, and budgets of deep carbon in the Earth. Carbon in the core is distributed between solid iron carbides in the inner core and dissolved phase in the liquid outer core (Fischer et al., 2020). In the lowermost mantle, carbon is present as sp^3-hybridized carbonate, diamond, iron carbides, and fluids and melts; carbonate is sp^2-hybridized at the mantle transition zone and in the upper mantle (Stagno et al., 2019). Redox freezing at these pressures will convert carbonate into diamond as it descends into the lower mantle; likewise, redox melting will convert diamond into carbonate during decompression (e.g., Foley, 2021; Rohrbach and Schmidt, 2011). In the lithosphere, carbon takes multiple forms, including graphite (or diamond in thick sub-continental lithospheric mantle), carbonate minerals, and organic carbon (e.g., Hazen et al., 2013a). During mantle melting, carbon is incompatible in mantle minerals and will join the melt phase as carbonatite melts (e.g., Jones et al., 2013) or dissolved CO_2 in silicate melts, which exsolves into a vapor at low pressures (e.g., Dixon et al., 1995). Volcanic gas speciation is controlled by the redox conditions of the magma and exsolving gas (e.g., Giggenbach, 1996). Fluid-rock reactions, such as those at sub-seafloor conditions or during subduction, and metamorphism can generate other carbon forms, including methane (CH_4) (e.g., Connolly and Cesare, 1993; Holloway, 1984; Kelley et al., 2005; Vitale Brovarone et al., 2020a), organic acids and polycyclic aromatic hydrocarbons (PAHs; Andreani and Ménez, 2019, Debret et al., 2022).

Fe_3C or Fe_7C_3 (Wood, 1993; Dasgupta et al., 2013a). Therefore, Fe-C alloy binaries have been extensively investigated under extreme pressure-temperature conditions. Their density and elastic properties were measured, as a viable composition model of the core must account for the density deficit and seismic characteristics of the core. For the inner core, both experiments and theory suggest that carbon and hydrogen are key impurity elements to explain the Poisson ratio (V_p/V_s) observed in the inner core as compared to pure iron. Among candidate Fe-C alloys and carbides, Fe_7C_3 is a good candidate from its ability to match the anomalously low V_s and high Poisson ratio of the inner core, in addition to reproducing the density deficit and having the highest electrical resistivity among all Fe-C alloys (Zhang et al., 2018a). A caveat is its density, which may be too low to match the inner core density, and would more generally imply a high carbon concentration in the core. This contradicts experiments performed at the pressures and temperatures expected in a deep magma ocean during formation of Earth's core which demonstrate that carbon becomes much less siderophile at depth (Fischer et al., 2020). Fischer et al. estimated that the core likely contains a maximum of

0.09 ± 0.04 to 0.20 ± 0.10 wt% C, which is in agreement with most of the theoretical atomistic and experimental mineral physics studies that were performed at or close to core pressures.

As the composition of the core is central to our understanding of the Earth's accretion and the terrestrial magnetic field, hundreds of studies focusing on mineral physics, cosmochemical constraints, or geochemical experiments have attempted to decipher the composition of the Earth's inner or outer core and provide a match with the seismic properties of the core. Depending on the chosen theoretical or experimental parameters and strategies, the pressure-temperature range covered by these studies, and the cocktail of light elements considered, results vary. Recent results still propose that the carbon concentration in the outer core spans one order of magnitude between 0.1 and 2.0 wt% (Bajgain et al., 2021). Existing data are yet insufficient to resolve the competing models of core composition because of limited data coverage in the relevant challenging pressure-temperature-composition space and uncertainties in experimental measurements and theoretical simulations. In their recent review, Hirose et al. (2021) propose a likely range of composition for the outer and inner core, with approximately 0.2 wt% and 0–1.3 wt% C respectively, depending on the concentration of other light elements.

Future progress and better constraints on the core composition and carbon budget could arise from the investigation of the interactions between melt and solid at the inner core boundary, as techniques and methods progressively allow us to reach inner core boundary pressure (330 GPa); inner core boundary temperatures, which may be as high as 7000 K, have not yet been attained. This would inform us on the evolution of Earth's magnetic field through time. The thermal and compositional evolution of Earth's core is related to the growth of the inner core. Since light elements control the liquidus temperature of Fe alloy and therefore the crystallization of the core during secular cooling, they could substantially increase the thermal conductivity of the outer core with profound implications for core thermal evolution and geodynamics. Inner core viscosity and dynamics are also certainly dependent on the light element composition through diffusion rate, grain growth rate and shear modulus, with virtually nothing known at this stage.

Moving upwards through the Earth to the outermost part of the core, seismology has revealed a ∼400 km thick low-velocity and low-density layer named the E′ layer (Fig. 3), which is characterized by a steep V_p gradient (Brodholt and Badro, 2017; Helffrich and Kaneshima, 2010; Kaneshima, 2018; Kaneshima and Helffrich, 2013; Kaneshima and Matsuzawa, 2015). The E′ layer is interpreted as a remnant of the chemical exchange between the early formed core and the whole-Earth magma ocean. The stagnation of such a layer over time necessitates buoyancy relative to the underlying convecting outer core, which could be explained by an enrichment in oxygen and depletion in silicon, but probably not at the 100-km scale. Presence of a significant amount of carbon in the E′ layer is unlikely, as adding carbon slightly decreases the density of liquid iron and increases its V_p (Morard et al., 2017; Nakajima et al., 2015).

Despite the challenges to reach the pressure and temperature conditions characteristic of the core-mantle boundary and deeper, the knowledge of the physical properties of Fe alloys and melts including carbon and other light elements has incredibly improved over the last decades. Even for the lowest estimated carbon contents (∼0.2 wt%), the largest carbon reservoir of planet Earth is its core, which hosts at least 90% of the whole Earth carbon budget and is where carbon has been sequestered since the final stages of core formation.

Carbon at the interface between the core and the lowermost mantle

The lowermost mantle above the core-mantle boundary, referred to as the D″ layer, displays multiple seismic features (Fig. 3). It is also a strong thermal boundary layer, with temperatures increasing from an average mantle adiabat of about 2500 K at 2600 km depth (e.g., Stixrude et al., 2009) to a core-mantle boundary temperature of about 4000 K. The D″ layer is both vertically and laterally highly heterogeneous, and it is layered on a kilometer scale in the lower 50 km (Sidorin et al., 1999; Thybo et al., 2003). Because of diffraction of seismic waves by the core, the resolution in this layer is lower than in the overlying mantle and hinders access to fine details. Velocity profiles show large lateral heterogeneities in this region. Estimates of the thickness of the D″ layer suggest that it ranges from 100 km to about 400 km. Within this layer, unusually low wavespeeds have been measured beneath the African continent and the Pacific Ocean, and these regions are known as large low-shear-velocity provinces (LLSVPs) and exhibit a density excess of about 1.25% compared to the surrounding mantle. Most active volcanic hotspots on Earth's surface are located above and at the boundaries of LLSVPs.

Adjacent to the LLSVPs, seismic observations show ultra-low velocity zones (ULVZs), often in contact with the core-mantle boundary. ULVZs are not ubiquitous. They also have a density excess and a low seismic velocity feature as indicated by their name. Their V_p and V_s reduction is about 10% and 30%, respectively (e.g., Lay, 2005). Although the presence of ULVZs and LLSVPs is not questioned, their origin and composition remain uncertain and there are multiple conceptual models that are consistent with seismic tomography results and the geochemistry of the hotspot lavas of oceanic islands, which are commonly assumed to result from the partial melting of large rising mantle plumes deeply rooted in the LLSVPs and ULVZs (see reviews by Garnero et al., 2016; Weis et al., 2023).

The ULVZs may represent partially leaky 'windows' between the D″ layer and the outer core. Such localized core-mantle exchanges are supported by geochemical investigations of plume-related volcanic rocks. Recent isotopic measurements have revealed a negative correlation between the $^{182}W/^{184}W$ and $^{3}He/^{4}He$ ratios in major plume-related suites of oceanic island basalts (see review by Weis et al., 2023). Plumes giving rise to ocean island basalts with low $^{182}W/^{184}W$ ratios might have sampled core metal, most likely via some ULVZs located in the root zones of plumes (Rizo et al., 2019).

The location of LLSVPs and ULVZs between regions of sinking tectonic plates is intimately associated with the long-term dynamics of the convecting mantle, although it is unclear whether they are inherited from the early evolution of the mantle and related with remnants of the deep magma ocean, or they developed over time (e.g., McNamara, 2019; Flament et al., 2022). As long-lived structures, stable or slowly mobile at the core-mantle boundary over hundreds of millions of years, they will be negatively buoyant relative to the convecting mantle, and their composition is likely correlated to the observations of their increased intrinsic density and seismic velocity reduction.

Among the multiple models of LLSVPs and ULVZs, we focus here on the potential role of carbon-bearing phases that may explain the density excess and low shear wave pattern of LLSVPs. Enhanced iron content in deep mantle mineral assemblages is the easiest way to account for the density excess and low velocity of LLSVPs and ULVZs, and low partial melting could also explain the low-velocity features. Liu et al. (2016) proposed that metallic Fe-C produced in subducted slabs beyond a depth of 250 km may partially melt at core-mantle boundary conditions, since the eutectic melting curve of the Fe-C system crosses the geotherm near Earth's core-mantle boundary. At the eutectic, the Fe-C melt could contain 2 wt% C at the pressure and temperature conditions of the core-mantle boundary (Fei and Brosh, 2014; Lord et al., 2009). If concentrated into isolated patches, such a metallic melt could induce the seismically observed density and velocity features of ULVZs as it is twice as dense as the surrounding mantle. These hypotheses connect peculiar features near Earth's core-mantle boundary to subduction of the oceanic lithosphere through the deep carbon cycle. Depending on the melt fraction and wetting angle, Liu et al. (2016) distinguished three types of dynamics of the Fe-C melt in ULVZs that could have different seismic signatures, and may explain the laterally varying electrical conductivity in the D″ layer: (a) ULVZs containing solid phases that have become iron-rich through reaction with Fe-C melt; (b) ULVZs containing 9–16 vol% non-wetting Fe-C melt coexisting with a small degree of silicate melt in a solid silicate matrix; (c) ULVZs containing 5–11 vol% Fe-C melt that wets the solid silicate matrix and will ultimately merge with the core, explaining some of the W isotopic signature sampled by ocean island basalts (Rizo et al., 2019).

The seismic features of the hot and dense LLSVPs, including seismic anisotropy, are generally consistent with the presence of bridgmanite, $CaSiO_3$-perovskite (or Davemaoite; Thomson et al., 2019). They have recently appeared to be also consistent with the high-pressure polymorphs of CaC_2O_5 (Wang et al., 2024), with a structure that is based on CO_4 groups (tetracarbonates) with sp^3-hybridized carbon. In particular the symmetry change from orthorhombic *Fdd2* to monoclinic *C2* leads to a density increase of 5.8% and a V_s decrease of 7.4%, and to elastic parameters of CaC_2O_5-*C2* consistent with seismic observations within LLSVPs. The orthorhombic to monoclinic transition in CaC_2O_5 occurs at 80 GPa, broadly consistent with the top of LLSVP piles. More generally, the elastic properties of the polymorphs of CaC_2O_5 that may form by the reaction between $CaCO_3$ and CO_2 in deep subducting slabs from transition zone conditions and deeper are in good agreement with the Primary Reference Earth Model. This would connect the deep carbon cycle from the oceanic crust to the lowermost mantle and back to ocean island basalts. Given similarities in elastic properties between $CaSiO_3$-perovskite and CaC_2O_5-*C2*, it may be challenging to evaluate the actual amount of oxidized carbon present in LLSVPs. Their fate may be better estimated through their isotopic signature in suites of ocean island basalts.

Should there be remnants of the basal magma ocean, sp^3 hybridized tetracarbonates are less siderophile, and thus large amounts of it may be stranded instead in the deep mantle. These tetracarbonates may therefore provide a possible source for carbon-rich emissions registered at the surface in suites of ocean island basalts (Cerantola et al., 2023).

Carbon throughout the Earth's mantle

Carbon is a trace element in the Earth's convecting mantle. Estimates of the carbon content in the bulk silicate Earth generally reconstructed from noble gas content are estimated to vary between 500 and 1000 ppm (Marty et al., 2013, 2016). Ratios of C to elements that partition in a similar manner in the mantle, such as Ba or Nb, yield a BSE estimate of 110 ± 40 ppm for the mantle, and 140 ± 40 ppm for the BSE (Hirschmann, 2018). When estimated from elements that behave geochemically like carbon but are refractory in a cosmochemical sense, concentrations of ∼192 ppm and ∼350 ppm C are derived from U and Ba respectively (Lee et al., 2019).

The concentration of carbon in the lower and upper mantle is substantially different. Measured carbon fluxes near hot spots are much higher than those for the depleted mid-ocean ridge basalt (MORB)-source mantle indicative of a higher concentration of carbon in the lower mantle. The most comprehensive and detailed analysis of the carbon content in MORBs showed very-fine-scale variations in their mantle source, with carbon fluxes from the mantle to the surface varying by over three orders of magnitude at the segment scale along mid-ocean ridges (Hauri et al., 2019). Integration over the entire length of ridges yields a global carbon flux in the form of CO_2 of 1.3–1.5 × 10^{12} mol yr^{-1} (16–18 Mt. C yr^{-1}) and a mean content of 100 ppm C in the depleted mantle source of MORB (Cottrell et al., 2019, Hauri et al., 2019; Le Voyer et al., 2019).

Measurement of carbon solubility in the major minerals of the upper mantle, transition zone and lower mantle shows that carbon is virtually insoluble in the silicate minerals, at the level of a ppm or less (Keppler et al., 2003; Shcheka et al., 2006). This implicitly requires that carbon is stored in accessory, nominally carbon-rich phases such as elemental carbon in the form of graphite or diamond, carbides, hydrocarbons in regions rich in hydrogen or carbonates, with oxidation numbers ranging between −4 and +4 depending on pressure, temperature and oxygen fugacity (fO_2). As such, the diversity of carbon-rich phases is diagnostic of the vertical and lateral heterogeneities in the convecting mantle. Over geological time, the forms of carbon-rich phases are controlled by the degree of oxygenation of the mantle and are diagnostic of its evolution through time.

Reduced lower mantle and transition zone

Rock samples from depths of 300 km and below are scarce; the deeper, the scarcer. Observations rely almost exclusively on inclusions within the few super-deep diamonds that have been collected through time in cratons (see Section "Carbon movement within and between deep reservoirs"). Observations of natural samples are complemented by experimental and theoretical studies to assess the redox state and carbon-hosting phases in the deep mantle.

The deepest natural messengers from the mantle are the 'CLIPPIR' diamonds (Cullinan-like, Large, Inclusion Poor, Pure, Irregular, and Resorbed) that formed at lower mantle conditions and were brought back to the surface (see Shirey et al., 2013, 2019, and references therein). Their most common inclusion is a composite metallic Fe-Ni-C-S mixture. The metallic inclusions are comprised of cohenite $(Fe,Ni)_3C$, interstitial Fe-Ni alloy, segregations of Fe-sulfide, and minor occasional Fe-Cr-oxide, Fe-oxide, and Fe-phosphate. A thin fluid layer of CH_4 and lesser H_2 is trapped at the interface between the inclusion and surrounding host diamond. The mixture is commonly interpreted to have been trapped as a molten metallic liquid. Their depth is bracketed to depth between 360 and 750 km by inclusions containing high-pressure silicate minerals such as retrogressed $CaSiO_3$-perovskite (Davemaoïte) or majoritic garnet.

The Fe-Ni-C-S inclusions in CLIPPIR diamonds are unique physical samples of an Fe-rich metallic liquid from the deep mantle, which confirm the fundamental process of Fe^{2+} disproportionation at depth, also called 'redox freezing'. Indeed, the Earth's mantle oxygen fugacity is buffered by ferric-ferrous (Fe^{3+}-Fe^{2+}) equilibria and decreases with increasing depth. This has been measured in natural garnet peridotites (Woodland and Koch, 2003), and confirmed by experiments that tested garnet oxythermobarometry equilibria under relevant high-pressure conditions (Stagno et al., 2013, and references therein). Theoretical analysis of the mantle fO_2 evolution with increasing depth (Ballhaus, 1995; Ballhaus and Ronald Frost, 1994) predicts that an isochemical mantle composition becomes reduced by ~0.6 log units in fO_2 per GPa as a result of molar volume changes of redox equilibria and changing mantle mineralogy. At lower mantle conditions, experimental studies have shown that aluminous bridgmanite and majoritic garnets are sinks for ferric iron, which in turns forces ferrous iron disproportionation into ferric silicates and Fe-metal (e.g., McCammon, 1997; Frost and McCammon, 2008). This is thought to generate up to about 1 wt% metal in the lower mantle and establishes a carbon-reducing environment in much of the deep mantle, where the forms of carbon would be diamond, metal and carbides (Fig. 3).

Experimental work has also assessed the relevant carbon phases in the lower mantle. At the base of the upper mantle, the Fe-Ni-C solidus at 10 GPa is low (1150–1250 °C) compared to mantle geotherms, which may indicate that Fe-Ni-C alloys are stable as molten phases, potentially limited in size to the grain scale. Cohenite $[Fe,Ni]_3C$ observed in the CLIPPIR diamonds likely forms together with metal and diamond at ~10 GPa or 350 km depth at intermediate Ni# between 0.11 and 0.24 (Rohrbach et al., 2014). In the deeper mantle, where carbon is at least locally more abundant, carbides in the form of molten Fe_7C_3 along with diamond are expected to be the phases hosting carbon (Dasgupta and Hirschmann, 2010). The presence of 100–200 ppm of sulfur prevents the formation of carbides and favors the precipitation of diamonds, thus explaining the Fe-Ni-S inclusions in the CLIPPIR diamonds. Whether such small fractions of melt and/or carbides affect seismic attenuation and V_p and V_s remains an open question.

Some super-deep diamonds show a wide range of carbon isotope compositions extending to very low values (e.g., $\delta^{13}C$ ~0‰ to −25‰), which are interpreted as the result of the contribution of crustal material (see Section "Carbon movement within and between deep reservoirs"; Howell et al., 2020). Others, like the super-deep diamonds from Kankan (Guinea) and their inclusions, have very narrow multi-isotope signatures that are typical of a mantle that has experienced little or no crustal interaction. The latter isotopic signature could be explained by a slight hydration of the uppermost lower mantle by a hydrated subducted oceanic lithosphere that destabilizes carbides to form diamond and would be consistent with a lower-mantle barrier for carbon subduction (Regier et al., 2020). Upon infiltration into the deep mantle, oxidized carbonate minerals are submitted to 'redox freezing' and reduced to diamond ± carbides as described above; whether carbonate rocks are preserved and enter the deep mantle through subduction therefore remains controversial and might actually display some significant lateral variability within the mantle.

A few inclusions hosted in super-deep diamonds have also shown the presence of solid carbonate minerals, including calcite, magnesite and ferromagnesite (Brenker et al., 2007; Kaminsky et al., 2016; see Section "Diamonds and their solid carbon inclusions" for additional details), suggesting that oxidized carbon in the form of carbonate minerals could be stable, at least locally. A recent estimate of redox state at the conditions of the transition zone was proposed based on the ferric iron content of majorite inclusions in diamonds (Kiseeva et al., 2018), which increased linearly as a function of pressure and is likely due to the oxidizing effect of CO_2-rich fluids rather than Fe^{2+} disproportionation. This would correspond to an fO_2 value about 2 log units above the iron-wüstite buffer.

Observations of carbonate inclusions and their potential local stability in the deep mantle have been complemented by a wealth of experimental and theoretical studies investigating the stability of mineral endmembers (i.e., $CaCO_3$, $MgCO_3$, $FeCO_3$) and their solid solutions at high pressures and temperatures, with the aim of assessing the fate of subducted oxidized carbon that may be potentially transferred deep in the mantle (see reviews by Boulard et al., 2020; Merlini et al., 2020). At Earth's surface, carbonate minerals mainly occur as calcite ($CaCO_3$) and dolomite ($CaMg(CO_3)_2$). In the lower mantle, they react with silicate minerals such as pyroxenes and bridgmanite to form ferromagnesite ($[Mg,Fe]CO_3$), which is considered the dominant carbonate phase in the deep mantle. Independent of their reactivity toward silicate minerals, oxides, or reduced carbon, all carbonate minerals are stabilized at the conditions of Earth's lower mantle through a series of high-pressure phase transitions; no fewer than 20 new carbonate structures have been discovered so far (Merlini et al., 2020). The main feature occurs at mid-lower mantle conditions, where new crystal structures including tetrahedrally coordinated sp^3-hybridized carbon form a systematic class of carbonates, nesocarbonates, cyclocarbonates, and inocarbonates, with complex crystal chemistries analogous to silicate structures.

In the mid-lower mantle, the spin crossover of Fe^{2+} from high spin to low spin changes the physical and chemical properties of iron in minerals (Badro, 2014, and references therein), including Fe-bearing carbonates (e.g., Fu et al., 2017; Liu et al., 2014; Mattila et al., 2007). As the expected changes in the elastic parameters across the transition are large, there has been hope that this would help to detect seismically ferromagnesite in the deep lower mantle. Unfortunately, both the iron content and the fraction of magnesioferrite that would produce a detectable 1% shear velocity decrease compared to non-carbonated lithologies is exceedingly high (Chariton et al., 2020).

The carbonate phase that is most likely to survive in the mid-lower mantle and deeper (>1800 km, 80–90 GPa) is $CaCO_3$. Carbonate minerals entrained in cold slabs in the form of magnesite or dolomite react with silicate $CaSiO_3$ to form $CaCO_3$ with sp^3-hybridized carbon ($CaCO_3$-*P*21/*c*-*h*; Lv et al., 2021). The presence of such carbonates is unlikely to be directly detected, as the change in cation within a carbonate mineral would not be observable seismically. However, $CaCO_3$ produced in the deep mantle would carry a higher calcium isotopic composition ($\delta^{44/40}Ca$), distinct from the much lower Ca isotope signature of surface-derived $CaCO_3$. If preserved in diamond inclusions and returned to the surface, ^{44}Ca-enriched $CaCO_3$ could be used to trace the presence of oxidized carbon in the lowermost mantle.

The carbon-depleted oxidized upper mantle

The upper mantle gradually became more oxidized by 1.5 log units between ~3.0 Ga and 1.9 Ga when fO_2 values reached levels near the FMQ buffer, as recorded by mid-ocean ridge basalts and metabasalts over geological time (Aulbach and Stagno, 2016). Their redox is largely controlled by the initial ferric iron content of the mantle and the geotherm, as elemental carbon turns into carbonates while ferric iron is reduced to ferrous iron during redox melting (see Stagno and Fei, 2020).

Therefore, below approximately 90 km in the asthenosphere, the oxidized form of carbon is carbonate, either as dolomite or melt depending on the thermal regime. Evidence of the carbonate forms present in the mantle is provided by solid carbonate inclusions within diamond (see Section 5.5.3) with Mg-rich and Ca-rich dolomite stable in peridotitic and eclogitic assemblages, respectively (Falloon and Green, 1989; Hammouda, 2003). As silicate minerals react with this carbonate, the latter tend to be mostly in the melt phase. At depths greater than approximately 150–180 km, the asthenospheric mantle is too reducing for carbon to stay in its oxidized form and only graphite or diamond is present, as discussed above. Hence, the region located in the depth range of 90 km to 150–180 km is where carbonatitic melts are most likely to be produced and subsequently impregnate the surrounding mantle through metasomatism, fostering movement of carbon in the upper mantle (see Section "Movements of deep carbon in melts", and review by Hammouda and Keshav, 2015). The presence and composition of dolomite in the upper mantle are critical for the composition of carbonatitic melts.

When in its elemental zero oxidation state, the upper stability limit of diamond is at 150–170 km depth for the present-day mantle geotherm, and diamond is replaced by graphite upon ascent and vice-versa upon descent, though with a slow kinetics. If sufficient hydrogen is present, C-O-H fluids containing CO_2, CH_4, and more complex ionic species in variable proportions (Sverjensky and Huang, 2015; Sverjensky et al., 2020) may also be present and facilitate graphite or diamond crystallization (e.g., Holloway, 1984; Luque del Villar et al., 1998; Stachel et al., 2017).

Sub-continental lithospheric mantle

The sub-continental lithospheric mantle (SCLM) acts as a sluice gate between the Earth's interior and exosphere. Substantial volumes of carbon and other volatile elements have accumulated in the SCLM over long periods of geological time before they are liberated during continental rifting and magmatism (Gibson et al., 2020; Gibson and McKenzie, 2023). Direct evidence for carbon accumulation in the SCLM exists in the form of carbon-rich mantle xenoliths, which are observed at numerous sites around the globe representative of thick continental crust and lithosphere (Chen et al., 2018; Ducea et al., 2005), and at continental rifts where thick continental lithosphere is tectonically ruptured (Casagli et al., 2017; Rooney et al., 2017; Trestrail et al., 2017). Such xenoliths appear to be neither compromised in their carbon concentrations during their ascent, nor reflective of preservation bias (e.g., Hirschmann, 2018). Additionally, alkaline low-SiO_2 silicate melts encountered in juvenile continental rift settings require low degrees of melting in environments with abundant CO_2 concentrations, further betraying the nature of their sub-lithospheric source region (Foley et al., 2009).

Foley and Fischer (2017) outline three principal means of sequestering carbon in the SCLM. Firstly, some carbon is emplaced during the initial formation of the SCLM. In this case, it may be assumed that the cratonic lithospheric mantle formed through the accretion of island arcs (e.g., Lee, 2006); the initial cratonic lithosphere is therefore reflective of sub-arc mantle wedge lithosphere and will therefore host a similar concentration of carbon.

Secondly, gradual addition of small fraction carbon-rich asthenospheric melts that ascend into the lithosphere from the underlying asthenosphere will passively contribute toward the SCLM carbon budget. At the base of the lithosphere, the temperature is generally lower than in the convective asthenosphere. Small-fraction low-SiO_2, high-CO_2 mantle melts are therefore stable at these conditions, and can rise and freeze, causing so-called mantle metasomatism (Aulbach et al., 2017, 2020; Grégoire et al., 2000; Hirschmann, 2010; Massuyeau et al., 2021; McKenzie, 1989; Yaxley et al., 1998; O'Reilly and Griffin, 2010). Small fractions of carbonate melt derived from the convecting mantle may end up frozen within layers near the bottom of the lithosphere as a result of their low volumes and the reduced conditions in the SCLM (McKenzie, 1989; Sleep, 2009), or metasomatize the SCLM itself. Metasomatism therefore re-enriches depleted lithosphere by reintroducing volatiles and incompatible elements. This process is broad enough that it is documented in both cratonic and oceanic lithosphere, and it has been shown to produce H_2O- and CO_2-bearing phases such as carbonates. Mantle xenoliths from Ethiopia and Tanzania appear to have been altered by carbonate

fluids in this manner (Rudnick et al., 1993; Trestrail et al., 2017). Sometimes, lithospheric metasomatism results in mantle rejuvenation; in other words, the base of the lithospheric lid is transformed into asthenospheric convective domains (Aulbach et al., 2017; Foley, 2008, 2011; Liu et al., 2019; Tappe et al., 2007).

A third, more active means of sequestering mantle carbon is through the episodic passage of mantle plumes in the underlying asthenosphere. In contrast to gradual accumulation of carbon in the SCLM, plume-related enrichment would deliver carbon derived from enriched mantle sources during lithospheric metasomatism (Foley et al., 2009). However, the high temperatures of convective plumes may partially destabilize fusible metasomes in the lithosphere, thereby remobilizing volatiles within the SCLM (Rooney et al., 2014) as opposed to emplacing them. Further carbon may be deposited in the SCLM from the diapirism of carbonates delivered into the mantle through subduction (Ducea et al., 2022). Xenoliths from the West Antarctic Rift demonstrate that multiple discrete periods of metasomatism may be recorded and correlated with different SCLM refertilization events, including subduction (Broadley et al., 2016). Similarly, the metasomatism of xenoliths from the Kaapvaal craton has been attributed to subduction-derived fluids (e.g., Jackson and Gibson, 2023).

Because of these multiple contributing factors that may sequester carbon in the SCLM, literature estimates of SCLM carbon content are both broad and uncertain. Further uncertainty is introduced through the necessity to estimate the mass of the SCLM, which is combined with SCLM carbon concentrations to assess total SCLM carbon budgets. The widest range in the literature is provided by assuming fixed bulk mantle volumes and carbon concentrations representative of mantle lithosphere ($3.5–350 \times 10^{21}$ g C, corresponding to 100–1000 ppm C; Kelemen and Manning, 2015). Following the three principal carbon addition methods listed in the previous paragraphs (initial sequestering at formation; gradual addition; plume addition), Foley and Fischer (2017) suggest an initial SCLM carbon budget of 3.2×10^{21} g C, which has increased by an order of magnitude to 37.5×10^{21} g C over geological time through the gradual addition of carbon from small-fraction melts and plumes, corresponding to an SCLM mantle carbon concentration of 860 ppm. However, Hirschmann (2018) argues that this value is unrealistic owing to the high carbon concentrations required by the infiltrating plume magmas of Foley and Fischer (>10 wt% C in silicate melts, necessitating a convecting mantle of ~2 wt% CO_2; c.f. 100–1000 ppm, Section "Carbon throughout the Earth's mantle").

The largest single estimate of 60×10^{21} g C is derived from assumptions made about the frequency of kimberlite emplacement at depth within the SCLM (Sleep, 2009). In contrast, bulk rock analyses of SCLM xenoliths suggest a value closer to $10 \pm 5 \times 10^{21}$ g C (100 ± 20 ppm; Hirschmann, 2018), which is similar to a recent combined volumetric-geochemical estimate of $7 \pm 3 \times 10^{21}$ g C at a concentration of 140 ± 56 ppm (Gibson and McKenzie, 2023). From further subdivision of the carbon within lithospheric mantle, Gibson and McKenzie estimate that cratonic mantle contains ≥45% of the total lithospheric carbon budget under continents and oceans; off-craton mantle, which is more prone to rifting, will therefore have substantially lower carbon concentrations (93 ± 61 ppm versus 158 ± 74 ppm) and lower carbon residence time than cratonic mantle. This vast amount of sub-lithospheric carbon would be sequestered in the lower cratonic lithosphere as diamonds in sub-continental peridotites and eclogites owing to their highly depleted and refractory compositions (Foley, 2011; Section "Diamonds as clues on deep and super-deep carbon movements"), and/or in hydrous dike assemblages comprising carbonate, phlogopite, and clinopyroxene (Foley and Fischer, 2017). Amphibole-bearing lithospheric metasomes may also host substantial carbon, as evidenced by xenoliths (e.g., Rooney et al., 2017). Such carbonated lithologies may contribute toward seismic discontinuities observed within cratonic lithosphere (Saha et al., 2021).

As carbon is an incompatible element in the mantle, the SCLM will be devolatilized during continental rifting (Gonzalez and Gorczyk, 2017; Gorczyk and Gonzalez, 2019). Changes in temperature and oxidation state, and reactions with infiltrating fluids and melts will result in the destabilization of carbon-bearing phases in the SCLM and the mobilization of carbon, which will migrate upwards toward the rift surface (Foley and Fischer, 2017). Redox melting is likely to dominate in the earliest stages of continental rifting. Significant oxidation of the SCLM, possible through the infiltration of small-fraction asthenospheric melts, will result in the oxidation of diamond into carbonate, thereby mobilizing carbon into low-SiO_2 carbonate-rich melts such as carbonatites or nephelinites (Foley, 2011). At later stages of rifting, carbon will depress the peridotite solidus and facilitate mantle melting (Section "Movements of deep carbon in melts"; e.g., Dasgupta and Hirschmann, 2006). Decompression of the upwelling asthenosphere under thinning rifting lithosphere, especially in the presence of a mantle plume, will result in the formation of silicate melts which will overshadow the low-volume, low-fraction, volatile-rich melts generated in the earlier stages of rifting. The heat supplied from lithospheric thinning and asthenospheric melts will destabilize carbon-bearing phases present in the SCLM (Gorczyk and Gonzalez, 2019), forcing an upwards-migration of carbon into the continental crust. The gradual focusing of melts under rift zones over time into a narrow volcano-tectonic locus (Brune et al., 2023) will concentrate carbon derived from a broad area into a narrow region under the rift.

During the mechanical process of rifting, advection of unstable cratonic keel material may concentrate the carbon mobilized toward continental rifts, further increasing fluxes of CO_2 seen at rift zones (Muirhead et al., 2020). Cratonic cores themselves do not degas CO_2 significantly, in contrast to the rift zones that border them (Muirhead et al., 2020). As cratonic mantle can contain ≥45% of the overall lithospheric carbon budget (Gibson and McKenzie, 2023), mobilization of cratonic carbon in this manner may substantially enhance the quantity of carbon feeding into rift zones. Through this mechanism, carbon-rich magmas such as carbonatites may be generated without necessitating a carbon-enriched mantle source (Fischer et al., 2009).

Silicate melts generated during decompression melting at continental rifts will ascend through the SCLM and pond at or within the crust (Section "Movements of deep carbon in melts"). At this stage, melts may interact with crustal carbonate minerals and sources of biogenic carbon, resulting in further CO_2 release through thermal decarbonation (e.g., Mason et al., 2017). The solubility of CO_2 in magmas will decrease with decreasing pressure (Dixon et al., 1995), thereby resulting in extensive degassing of magmatic

bodies within the continental crust. At active continental rift zones and rift volcanoes, vast degrees of diffuse and active carbon degassing are characterized worldwide (Brune et al., 2017; Cappelli et al., 2023; Foley and Fischer, 2017; Hunt et al., 2017; Lee et al., 2016; Tamburello et al., 2018; Wong et al., 2019), with carbon isotope ratios marking a strong affinity with a mantle-derived magmatic source (e.g., Blomgren et al., 2019; Bräuer et al., 2018; Correale et al., 2019; Frondini et al., 2008; Muirhead et al., 2020). The difference in CO_2 concentrations between undegassed crustal melt inclusions and parental mantle-derived magmas (determined through CO_2-incompatible trace element ratios) is sufficient to account for the considerable fluxes of diffuse CO_2 degassing at continental rifts (Iddon and Edmonds, 2020; Wong et al., 2023).

Sub-oceanic lithospheric mantle

Carbon may also be sequestered within sub-oceanic lithospheric mantle. At mid-ocean ridges, asthenospheric carbon mobilized by mantle melting is focused toward the ridge axis, where a significant quantity degasses into the water column. In addition, a portion of the mobilized carbon is directed toward the flanks of the spreading ridge, where it is sequestered through the metasomatism of the juvenile sub-oceanic lithospheric mantle (Keller et al., 2017). As oceanic plates age, their underlying mantle lithosphere will thicken, and by doing so it will accumulate additional small-fraction carbon-rich asthenospheric melts in the developing lithosphere. Furthermore, xenoliths collected from the base of the Pacific plate suggest that later extensional stresses in the lifetime of the oceanic plate such as plate flexure may induce further metasomatism (Pilet et al., 2016). Carbon present in the oceanic lithosphere in this manner is believed to contribute to observed seismic low-velocity zones and velocity contrasts (Keller et al., 2017). The controls on CO_2 sequestration within oceanic lithosphere include mantle temperature, mantle CO_2 content, and melt productivity/fertility (Keller et al., 2017), which are known to vary substantially across the present-day ridge system (e.g., Le Voyer et al., 2019). In combination with the difficulty in accessing the lower oceanic lithosphere, there is likely to be substantial uncertainty in quantifying the carbon budget of the lithosphere underlying oceanic plates. Following geodynamic models and tomographic estimates of lithospheric mass, recent first order estimates suggest that $0.5–2.2 \times 10^{21}$ g C may be stored within present-day unaltered sub-oceanic lithospheric mantle (Gibson and McKenzie, 2023; Müller et al., 2022).

Deep carbon in the crust

In the continental crust, solid carbon will take multiple different forms depending on the pressure, geothermal gradient, and oxidation state of the local environment (e.g., Hazen et al., 2013a; Oganov et al., 2013). Voluminous solid continental carbon phases can be broadly subdivided into two principal forms. The largest fraction of crustal carbon is represented by inorganic carbon in carbonate minerals, in which oxidized carbon is present within the bicarbonate anion (CO_3^{2-}) bonded in mineral structures to a wide selection of cations, which account for about 80% of total crustal carbon (Berner, 2004; Hayes and Waldbauer, 2006). The second largest form of solid crustal carbon, accounting for about 20% of total carbon, is organic matter, in which carbon is present in its reduced form (Hazen et al., 2013a; see chapter in this book by Derry, 2024). It includes biogenic organic matter, petrogenic or detrital graphitic carbon in sedimentary rocks, and abiotic forms of condensed reduced carbon (Beyssac and Rumble, 2014; Galy et al., 2008; Luque del Villar et al., 1998).

A large fraction of crustal solid carbon, both organic and inorganic, in the crust formed through biological processes and their successive solid-state transformations. Carbonate minerals can be synthesized by various organisms that grow a carbonate shell, or result from biology-mediated chemical reactions, as discussed in Section "Origins of deep carbon" above. Over the past 150 million years, deposition of calcareous plankton in deep-sea sediments, mainly coccoliths and foraminifera, has increased and currently accounts alone for more than half of global carbonate sedimentation (Berner, 2004; Milliman, 1974). Organic carbon accumulates in rocks during sedimentary processes and is progressively transformed to carbonaceous materials and graphitic carbon by diagenesis and metamorphic processes (see discussion above). Carbonate minerals and organic matter can also form abiotically in the crust, through multiple processes ranging from silicate weathering at the Earth's surface, to deep crustal fluid-rock interactions. The following sections describe the forms and distribution of carbon in the main crustal reservoirs.

Continental crust

The continental crust is an important reservoir of carbon. Recent estimates derived from statistical analysis of lithological distributions suggest that ~20% of present-day continental crust is composed of carbonate rocks (Walton and Shorttle, 2024), which operate as the largest store of crustal carbon at the present-day (Hirschmann, 2018). However, the distributions and forms of carbon on and within present-day and geologically historic continental crust is highly heterogeneous, complicating our capacity to estimate the carbon budget of the crust. Here, we summarize the current understanding of carbon reservoirs in the continental crust.

Crustal carbonate and organic matter are distributed within both the sedimentary and crystalline materials that comprise the bulk continental crust (Hirschmann, 2018). Of these two carbon forms, carbonate is perhaps more commonly analyzed, while data on reduced carbon is sparse in comparison (Derry, 2014; Hartmann et al., 2012; see chapter in the current Treatise, Derry (2024)). Carbon in the continental crust dates back to 4.0 Ga, coinciding with some of the earliest records of life on the planet (Schidlowski, 1988). Primordial Earth had a primarily silicate crust, which has been gradually carbonated over time as a consequence of continuous deep-Earth degassing (Alcott et al., 2024). From present-day records of lithological preservation, it is estimated that ~5% of total preserved Precambrian crustal volume comprises carbonate rocks, which are principally biogenic stromatolitic and abiotic precipitated carbonate rocks deposited in oceanic environments and preserved on continental crust (Walton and Shorttle, 2024). After the Cambrian and Ordovician radiations of biomineralizing marine life (Gilbert et al., 2022), there is a substantial

increase in the proportion of carbonate preserved in continental crust (~20–25%); similarly, a decrease in the fraction of accumulated carbonate minerals is recorded within crustal sections in the aftermath of the Permian-Triassic extinction (Walton and Shorttle, 2024). This ongoing carbonate accumulation within Earth's continental crust has had substantial consequences for the co-evolution of life and the geosphere and atmosphere (e.g., Alcott et al., 2024; Duncan and Dasgupta, 2017, Isson et al., 2020). The abundance of carbonate minerals present with the bulk Earth crust is therefore both affected by and in turn affects surface biogeochemical cycles (see Section "Carbon at the interface between the geosphere and biosphere").

In the continental lithosphere (crust and uppermost non-convecting mantle), the principal form is also carbonate minerals (Hazen et al., 2013a; Oganov et al., 2013). Of these minerals, the most abundant carbonate minerals in the Earth's crust are calcite (β-$CaCO_3$) and dolomite ($CaMg(CO_3)_2$), which are present within massive sedimentary and metamorphic carbonate formations that account for 90% of crustal carbonate minerals (Reeder, 1983). Calcite is additionally one of the most common cement minerals found within siliciclastic sedimentary rocks (Manning et al., 2013). Aragonite (λ-$CaCO_3$), the orthorhombic polymorph of the trigonal calcite, is a metastable form of carbonate which principally originates from biomineralization, and is therefore found in substantial proportions on continental shelves where it is sourced from the dissolved bicarbonate anion in seawater by marine biomineralizers (e.g., Gilbert et al., 2022). Other key but minor carbonate minerals include magnesite ($MgCO_3$), which forms through the carbonation of Mg-rich igneous and metamorphic rocks or through authigenic precipitation (e.g., Scheller et al., 2021), and siderite ($FeCO_3$), a principal component of Precambrian banded iron formations (e.g., Klein, 2005). At the time of writing, 614 carbonate minerals are registered by the online mineral database mindat.org, n.d. (i.e., filtering by 'CO_3^{2-}'; retrieved June 2024), illustrating the broad and diverse nature of carbonate minerals on Earth at the present day (Hazen et al., 2013b). Carbonate minerals are also generated through chemical weathering of silicate rocks, which consumes atmospheric CO_2 (Gaillardet et al., 1999; Hartmann et al., 2012; Stewart et al., 2019; Urey, 1952) and has hence been correlated to long-term climate modulation (e.g., Gernon et al., 2021; Johansson et al., 2018).

Oxidized carbon in crystalline continental basement is present in igneous and metamorphic rocks as carbonate minerals or as fluid inclusions (e.g., Lowenstern, 2001; Skelton, 2011). In magmatic systems, mobile carbon, present as a vapor phase or dissolved within silicate magmas, typically takes the form of CO_2 (typically 1–50 mol%), with its more reduced gaseous forms CO and CH_4 much lower in concentration (typically $\ll$1 mol%; Giggenbach, 1996; Symonds et al., 1994). While carbon concentrations are enhanced in peralkaline/alkaline compositions (Ni and Keppler, 2013), CO_2 is highly insoluble in silicate magmas (e.g., Dixon et al., 1995), and will degas deep within the Earth's crust to form fluid phases (Section "Carbon reprecipitation at depth"). The majority of this CO_2 is expected to be degassed into the atmosphere or oceans, although magmatic carbon-bearing fluids, among other carbon sources, may contribute to the formation of hydrothermal solids (e.g., Bénézeth et al., 2013). An additional minor reservoir of crustal carbon is in rare low-melt-fraction volcanic rocks, such as carbonatites, nephelinites, and kimberlites (e.g., Jones et al., 2013).

In near-surface environments, reduced forms of carbon (i.e., C^0 and hydrocarbons) are attributed to biological processes, and are hence commonly referred to as simply 'organic carbon' (Derry, 2014). This carbon is present almost exclusively within sediments, such as deep-sea/lacustrine shales or coals, and is derived from organic material resistant to microbial processing (e.g., microbial membranes or plant lignin; Manning et al., 2013). Burial of organic material in marine environments is the second largest sink of atmospheric CO_2 after silicate weathering and carbonate mineral precipitation; the content of organic carbon in marine sediments is enhanced by fluvial transport of organic carbon from continents to oceans (Galy et al., 2008). At higher crustal pressures, reduced and dehydrated carbon in sediments takes the form of graphite (Hazen et al., 2013a), which is a key contributor to the electrical conductivity of continental crust (Glover, 1996). Graphite may also form within some igneous and metamorphic rocks as an accessory phase precipitated from reduced C-O-H fluids (e.g., Luque del Villar et al., 1998). Under specific circumstances, organic carbon in the crust will undergo thermal maturation to generate biogenically-derived hydrocarbons (e.g., Sephton and Hazen, 2013). Further thermal maturation will result in the decarboxylation and dehydrogenation of organic compounds, resulting in the gradual oxidation and aromatisation of organic hydrocarbons to conclude in graphite (see Section "Deep abiotic organic matter" for a full discussion on deep abiotic organics).

Carbon in the continental crust will be remobilized during metamorphism in various forms such as CO_2, CH_4, or more complex ionic species (e.g., Manning et al., 2013; Sverjensky et al., 2020; Section "Carbon movement within and between deep reservoirs"). Destabilization of solid carbon during metamorphism may result from a number of tectonic or volcanic processes that result in disequilibrium pressure-temperature conditions, including volcanism (e.g., Black and Gibson, 2019; Ganino and Arndt, 2009; Johnston et al., 2011; Mason et al., 2017), localized microbial and thermogenic breakdown to form CH_4 (Section "Metamorphic and magmatic processes of carbon mobilization"; e.g., Etiope et al., 2019; Etiope and Sherwood Lollar, 2013), and regional and contact metamorphism and metasomatism (Section "Metamorphic and magmatic processes of carbon mobilization"; Aiuppa et al., 2017; Ague, 2000; Ague and Nicolescu, 2014; Becker et al., 2008; Capriolo et al., 2021; Groppo et al., 2013, 2017; Halama and Bebout, 2021; Kerrick and Caldeira, 1998; Stewart and Ague, 2018; Svensen et al., 2004). As a result, the lengths of tectonic settings, in particular those of arcs and subduction zones, are believed to correlate with periods of icehouse-greenhouse activity on Earth (McKenzie et al., 2016; Gernon et al., 2022; Pall et al., 2018). Retrograde metamorphism may in turn consume mobile carbon in fluids to precipitate minerals such as carbonates and/or graphite (Section "Carbon reprecipitation at depth"; e.g., Hu et al., 2021; Piccoli et al., 2016, 2018, 2021; Scambelluri et al., 2016). Finally, solid carbon in carbonates will be mobilized by processes such as oceanic and atmospheric acidification (e.g., Doney et al., 2009; Eyssautier-Chuine et al., 2016) and reverse weathering (Isson and Planavsky, 2018).

Much like other elements in the continental crust, the concentration of carbon is assessed by determining the volumetric quantities of each lithology in the crust, and then further assigning each lithology with a carbon concentration characteristic of representative rocks exposed at the Earth's surface (see current Treatise chapter Derry, 2024, for a full review). In the context of continental carbon, sampling biases may introduce additional uncertainty: the uppermost crust is easiest to access, yet is also most prone to chemical weathering, which will increase carbon content over time as a result of secondary carbonate formation (Hartmann et al., 2012). In addition, both oxidized and reduced forms of carbon must be considered to provide a complete picture of continental carbon budgets. In the bulk continental crust, the proportion of reduced carbon relative to the total carbon budget is considered to range from 0.10 to 0.28, depending on the choice and proportions of characteristic crustal lithologies selected (Derry, 2014; Gao et al., 1998; Hartmann et al., 2012; Wedepohl, 1995; Yaroshevsky, 2006); for example, sediments typically have a greater proportion of reduced carbon than crystalline basement (e.g., Yaroshevsky, 2006).

A recent summary of the present-day carbon budget of the continental crust is provided by Hirschmann (2018). Literature values assessed by Hirschmann (2018) converge on values of $76 \pm 16 \times 10^{21}$ g C hosted in sedimentary rocks and $15 \pm 8 \times 10^{21}$ g C within crystalline rocks for a total of 91×10^{21} g C, and is based on previous estimates of crustal carbon budgets (e.g., Gao et al., 1998; Hayes and Waldbauer, 2006; Hunt, 1972; Wedepohl, 1995; Yaroshevsky, 2006). This budget is distributed across the solid exosphere, including carbon in oceanic domains (see following section), at a concentration of 27 ± 5 ppm (Hirschmann, 2018).

Oceanic crust and upper lithospheric mantle

At the present day, the total mass of carbon in oceanic crust and lithosphere is on the order of $\sim 1.0–1.5 \times 10^{22}$ g C (Hirschmann, 2018; Müller et al., 2022). The majority of this carbon (~60%) is stored within pelagic sediments, with the remainder comprising carbonate minerals in the oceanic basement and sub-oceanic lithospheric mantle (Hirschmann, 2018; Müller et al., 2022). Because seawater-rock interactions in the ocean do not only affect crustal sequences but also the uppermost part of the oceanic lithospheric mantle, this section presents an overview of the upper oceanic lithosphere affected by magmatic and hydrothermal processes at mid-ocean ridges.

Altered lithospheric mantle

Seawater percolates through permeable uppermost oceanic crust and lithospheric mantle where it may be exposed, e.g., at mid-ocean ridges or through faulting (e.g., Fisher, 2005). Carbonate minerals can form during serpentinization through the coupled hydration and carbonation of olivine to form serpentine minerals and carbonates (e.g., Power et al., 2013; Kelemen et al., 2011; Menzel et al., 2018). Ultramafic rocks can therefore have significant potential for rapid carbonate formation upon reaction with CO_2-bearing fluids (e.g., Kelemen et al., 2011; Kelemen and Matter, 2008; Matter and Kelemen, 2009). Significant natural carbon sequestration is expected where mantle peridotite is exposed to seawater at oceanic settings and subject to carbonation (Alt et al., 2013). Serpentinization and coupled carbonation of the oceanic lithosphere may therefore occur via a number of different tectonic processes: (a) widespread exposure and faulting of peridotite at (ultra-)slow spreading centers (Alt et al., 2013; Cannat et al., 2010; Dick et al., 2003; Kelemen et al., 2011; Merdith et al., 2020; White et al., 2001) and locally at the ridge axis at faster spreading centers and oceanic transform zones (Alt et al., 2013; Klein et al., 2024); (b) exposure of continental lithospheric mantle within magma-poor continent-ocean transitions (Albers et al., 2021; Grevemeyer et al., 2022; Liu et al., 2023; Sawyer et al., 1994; Schwarzenbach et al., 2013); c) faulting of oceanic plates during bending at the outer rise as they enter subduction zones (van Avendonk et al., 2011; Christensen and Ruff, 1988; Faccenda, 2014; Grevemeyer et al., 2018; Lefeldt et al., 2012; Ranero et al., 2003).

There is a higher concentration of carbon near exposed serpentinite seafloor as a consequence of seawater accessibility. While uppermost oceanic serpentinite is primarily inorganic carbon, deeper serpentinite (>50–100 m) principally hosts organic carbon, which is sourced from methanogenic microorganisms within serpentinites that thrive on the hydrogen gas byproduct of serpentinization (Schwarzenbach et al., 2013) and abiotic forms of organic matter (e.g., Sforna et al., 2018; Ménez, 2020). Most data on carbon concentrations in altered peridotite are obtained from seafloor drill samples, with the remainder determined from ophiolites (Kelemen and Manning, 2015). These altered peridotites have an average bulk concentration of 681 ± 45 ppm C (Kelemen and Manning, 2015), although concentrations from some settings may be as high as 17.1 wt% CO_2 (Albers et al., 2021). Carbonated serpentinites therefore host a minor yet not insignificant proportion of the overall oceanic lithosphere carbon budget, estimated as $\sim 0.2–0.3 \times 10^{21}$ g C (Merdith et al., 2020; Müller et al., 2022).

Altered oceanic crust

In the high-permeability upper crust, carbon, sourced from magmatic fluids and seawater, precipitates as the carbonate minerals calcite and aragonite within rocks and veins at low temperatures (<100 °C; Alt and Teagle, 1999). Most basaltic crust alteration will occur within the first few tens of millions of years after crust formation (Alt and Teagle, 1999; Coogan and Dosso, 2015; Coogan and Gillis, 2018; Coogan et al., 2016). The combination of pore infilling through carbonate mineral precipitation and gradual accumulation of sediment cover will limit subsequent circulation of water through oceanic crust over geological time, thereby decreasing carbon sequestration as the crust ages (Grevemeyer et al., 1999); overlying carbonate sediments may themselves be incorporated into the basaltic crust as recrystallized carbonate minerals to facilitate this process (Gillis and Coogan, 2011). High degrees of basalt alteration will also limit the availability of exposed fresh material required to precipitate carbonate minerals, thereby limiting further carbonate precipitation in aged crust (Albers et al., 2023). Another control on crustal carbonate formation is

bottom-water temperature, which promotes faster fluid-rock reactions resulting in carbonate precipitation (Coogan and Gillis, 2013; Gillis and Coogan, 2011).

Estimates of bulk oceanic crustal CO_2 concentration suggest a range of 0.18–0.22 wt% CO_2 (Alt and Teagle, 1999; Kelemen and Manning, 2015). Most CO_2 is concentrated in the uppermost 300 m of oceanic crust at an estimated mean concentration of 1.85 wt% (Müller and Dutkiewicz, 2018), which represents two-thirds of the total CO_2 in typically ~7 km-thick oceanic crust (Gillis and Coogan, 2011; Staudigel et al., 1989). Estimates of present-day oceanic crust carbon storage using these concentration estimates range from 2 to 4 $\times$ 10^{21} g C (Hirschmann, 2018; Kelemen and Manning, 2015; Müller and Dutkiewicz, 2018). At least a fraction of this carbon is present in the form of organic compounds (Shilobreeva et al., 2011).

Sediments

The key parameters to consider when assessing the carbon budget of pelagic oceanic sediments are the mass of present-day sediment and the amount of carbon present within said sediment. Both parameters are highly heterogeneous in the modern oceans (Conrad, 2013; Dutkiewicz et al., 2016; Hayes et al., 2021), and are assessed respectively through seafloor seismic reflection surveys and direct sampling through the ocean research drilling programs (Plank, 2014; Plank and Langmuir, 1998; Rea and Ruff, 1996). The principal controls on the thickness of sediment at any given point on the seafloor are (a) the distance of the point from the nearest passive continental margin, a measure of the sedimentary input to that point, and (b) the age of the oceanic crust, a measure of time over which sediment accumulation has occurred (Dutkiewicz et al., 2017; Olson et al., 2016). Large rivers will accelerate local oceanic sedimentation rates; for example, the Ganges river fan possesses a column of sediment of 7 km thickness at its maximum (Curray, 2014).

Carbon-bearing sediments can be subdivided into carbonate (predominantly $CaCO_3$) and organic carbon (e.g., Clift, 2017). Accumulation of significant thicknesses of oceanic sedimentary carbonate is a geological novelty on Earth (e.g., Gilbert et al., 2022). While metazoan carbonate biomineralization is known from the Ediacaran onwards (e.g., Grant, 1990; Wood, 2011), the onset of extensive neritic biomineralization during the Marine Mesozoic Resolution was the principal herald of widespread and significant marine carbonate production representative of present-day carbonate sedimentation in the oceans (Erba, 2006; Falkowski et al., 2004; Ridgwell, 2005).

Sedimentary carbon accumulation on oceanic crust is limited by the carbonate/calcite compensation depth (CCD), which marks the depth below which the rate of inorganic carbonate dissolution exceeds the rate of deposition (e.g., Broecker, 2008; Derry, 2022; Dutkiewicz et al., 2019; Ridgwell and Zeebe, 2005; van Andel, 1975). Within present-day oceans, the CCD corresponds to 4.5–5.0 km below sea level (Dutkiewicz et al., 2016; Zeebe, 2012). Terrestrial sediment fluxes (Derry, 2022; Walling and Fang, 2003), biological productivity (Kumar et al., 1995; Sarmiento et al., 2004), and sea-surface temperature and salinity (Dutkiewicz et al., 2016), all act in concert to affect carbonate deposition or dissolution, thereby controlling the position of the CCD. The parameterization of these factors permits the extrapolation of carbonate sediment thicknesses to all present-day ocean basins (Dutkiewicz et al., 2019). Furthermore, the thermal subsidence of ocean basins with age will mean that old oceanic crust will carry negligible sedimentary carbonate minerals, in contrast to shallow seafloor in regions of high biological productivity (Dutkiewicz et al., 2016, 2019; Plank, 2014). On the other hand, organic carbon is rapidly consumed by biological processes such as respiration (e.g., Higgins et al., 2009). Preservation of organic carbon in sediments therefore requires rapid deposition and burial, for example, beneath regions of high biological productivity or at deep sea fans where sedimentation rates are higher (Galy et al., 2007; Plank and Manning, 2019). Temperature during sediment burial additionally has a strong effect on organic carbon sediment preservation (Malinverno and Martinez, 2015). Finally, the weathering of silicate minerals and organic carbon in pelagic sediments will fix substantial CO_2 into carbonate minerals over geological time (Wallmann et al., 2008). At the present day, the mass of carbon within sediments is estimated to be on the order of 10 $\times$ 10^{21} g C (Dutkiewicz et al., 2019; Hirschmann, 2018; Yaroshevsky, 2006); pelagic sediments are therefore the largest reservoir of carbon on oceanic plates at the present day.

Deep abiotic organic matter

Carbon dioxide is generally considered as the dominant carbon species in the modern Earth (Fig. 1). However, as conditions become more reducing at depth, CH_4 and H_2, together with smaller hydrocarbons, become stable at the expense of CO_2 or other more oxidized carbon species within the stability field of graphite or diamond (Sverjensky et al., 2020). In the mantle, the transition from CO_2-dominated to CH_4-dominated regimes occurs at depths of 125–140 km (~4 GPa) in sub-continental domains, and at shallower depths of ~90 km (~2.5 GPa) in the sub-oceanic mantle. The chemical complexity of the fluid organics that could be present is exemplified by the wealth of organic matter found in the fluid inclusions of diamonds from the Urals placers from ~200 km depth, though their exact origin remains unknown (see Table 4 in Sobolev et al., 2019). They contain aliphatic hydrocarbons up to C17, cyclic hydrocarbons up to C15, oxygenated hydrocarbons, and heterocyclic compounds, together with nitrogenated and sulfonated compounds (plus CO_2 and H_2O). This is supported by experimental and theoretical work. Above 2 GPa, heating pure CH_4 at high temperature triggers its polymerization to higher alkanes (C3), with ethane the most abundant species (Kolesnikov et al., 2009). Theoretical simulations have shown that formic acid is thermodynamically more stable than the products of the water-gas shift reaction (CO_2 and H_2) above 3 GPa and at ~750–1150 °C (Stolte et al., 2021). This result is in good agreement with the spectroscopic signature of carboxylic functional groups coating diamond inclusions in the deeply subducted metamorphic rocks of the Lago di Cignana in the Western Alps at $P \geq 3.2$ GPa and $T \sim 600$ °C (Frezzotti, 2019), and with thermodynamic models suggesting that organic acids play an important role in diamond nucleation and growth in deep Earth

(Sverjensky et al., 2014; Sverjensky and Huang, 2015). Similarly, but at shallower depths, the graphite or other condensed carbon forms present in many crustal and mantle rocks such as those described at mid-ocean ridges of within subduction contexts — and now emplaced and incorporated in the continental crust — may not be of biotic origin (i.e., transformation of subducted biogenic organic matter), but instead has precipitated from deep carbonic fluids (e.g., Boutier et al., 2024b; Debret et al., 2022; Evans et al., 2002; Luque del Villar et al., 1998; Ménez et al., 2018) or from the interaction between reduced fluids and carbonates (Galvez et al., 2013; Malvoisin et al., 2012; Peng et al., 2021; Tao et al., 2018; Vitale Brovarone et al., 2017).

Expanding on the carboxylic acids, experimental work has shown that pressure expands miscibility gaps in C-O-H fluids, and immiscible fluids are generated at pressures in excess of 1.5 GPa (600–700 °C), with formic acid yielding both aqueous and dry methane and ethane fluids $\pm CO_2$ and $\pm H_2$ depending on the oxygen fugacity (Li, 2017). At higher pressures (up to 4.6 GPa) and lower temperatures (300–350 °C), aqueous Na- or Ca-acetate yields aqueous and mineral carbonate (as expected from the speciation of C(IV) at high pressure; Facq et al., 2014), soluble light alkanes (C1–C3), and immiscible hydrocarbons; the higher the pressure, the greater the amount of hydrocarbons and methane generated (see Huang et al., 2017; Huang et al., 2023 for details). At 350 °C and above, immiscible hydrocarbons tend to become aromatic, and may transform into polycyclic aromatic hydrocarbons and ultimately into graphite, depending on temperature and composition. Natural fluid inclusions from high-pressure metamorphic rocks support the immiscibility of CH_4, and potentially the immiscibility of other hydrocarbons in aqueous fluids at high pressure conditions (Giuntoli et al., 2024; Sverjensky et al., 2020; Vitale Brovarone et al., 2017).

As of today, the complexity of the fluid organics observed in deep fluid inclusions has been partly reproduced in experiments (McCollom, 2013), emphasizing that highly mobile and likely highly reactive hydrocarbons are stable at sub-lithospheric conditions, provided that the temperature is low enough to kinetically prevent the formation of graphite or diamond, as their compositions are mainly controlled by the local water activity and oxygen fugacity.

While lithospheric subsurface environments should be the exclusive realm of CO_2 as discussed in previous sections, there are numerous occurrences of CH_4 reported in vents, seeps, springs and aquifers at slow-spreading mid-ocean ridges (Abrajano et al., 1988; Andreani et al., 2023; Charlou et al., 2010; Etiope and Sherwood Lollar, 2013; Grozeva et al., 2020; Klein et al., 2019; Young et al., 2017), in ophiolites or peridotitic massifs and metamorphic complexes (Boutier et al., 2021, 2024b; Harada and Tsujimori, 2024; Herviou et al., 2021; Hu et al., 2021; Peng et al., 2021; Shi et al., 2005; Tao et al., 2018; Vitale Brovarone et al., 2017, 2020b), in alkaline igneous complexes (Potter and Longstaffe, 2007; Salvi and Williams-Jones, 1997), and in Precambrian basements (Etiope and Sherwood Lollar, 2013; Sherwood Lollar et al., 2008; Warr et al., 2021). Although CH_4 in these settings may be related to biotic processes such as thermogenic degassing, in many of these settings, reduced conditions are achieved through local fluid-rock interaction, in particular via aqueous alteration of Fe^{2+}-rich rocks, the most famous examples being the flames of the Chimera vents in Turkey and 'Los Fuegos Eternos' in the Philippines on continents, or black and white smokers at mid-oceanic ridges related to the process of olivine hydroxylation (serpentinization). Other localized anomalous deviances from lithospheric oxidation state are related to radiolytic dissociation of water in Precambrian basements (Sherwood Lollar et al., 2014), or the composition of fluids associated with alkaline intrusions (Potter and Longstaffe, 2007; Salvi and Williams-Jones, 1997). Methane in these settings is thought to form abiotically, even though successive biological reworking is likely (Young, 2019).

Natural occurrences of recognized abiotic organic volatiles of hydrothermal origin also include short-chain alkanes, and formic acid, the smallest organic acid. They have mainly been observed in geothermal systems or continental seeps within ophiolites and Precambrian shields, and at hydrothermal vents near mid-ocean ridges and subduction forearcs. These small abiotic organics have attracted a lot of attention over the last decades, in particular those formed at low temperature (below 400 °C), as they may provide a potential route to the emergence of life and/or support subsurface life (see Section "Carbon at the interface between the geosphere and biosphere").

The effectiveness of abiotic organic volatile generation at low temperatures remains a subject of controversy and debate. The mechanism of abiotic CH_4 synthesis is commonly assumed to be Fischer-Tropsch type reactions (FTT) between an oxidized carbon molecule (CO_2) and H_2, which is naturally produced by the serpentinization reaction occurring in ultrabasic rocks. As the ferrous iron of olivine (or pyroxene) is oxidized to form ferric hydrous minerals, water is reduced to form H_2, with catalytic support from Ni-, Fe-rich minerals. This H_2 in turn provides the ingredients for the FTT reaction. However, CH_4 formation is kinetically hindered at temperatures below 300–400 °C (McCollom, 2013). Understanding the detailed mechanism of the highly energetic H_2 and eventually CH_4 production by FTT reaction is of tremendous importance, as the serpentinization reaction is ubiquitous on Earth and likely on other planets, when hot water is in contact with ultramafic rocks, and might support life on other planetary bodies. The challenges are (i) the effectiveness of FTT reactions in an aqueous medium, as the Fischer-Tropsch reaction is restricted in its definition to the gaseous phase, (ii) the availability of CO that is the reactant form of C, (iii) the identification of a catalyst phase, and (iv) the potential distribution in mass of the expected alkane products according to the Shultz-Flory distribution.

Tens of experimental serpentinization studies, performed over decades, have therefore been attempted to identify the parameters that control the abiotic production of H_2, the subsequent FTT formation of CH_4, and eventually light hydrocarbons. A recent network analysis of >30 experimental studies (see Barbier et al., 2020; Huang et al., 2021a, Huang et al., 2021b for details) achieved an unbiased reading and interpretation of the literature and confirmed that H_2 is systematically and significantly formed in experiments, indicating that its production during serpentinization is well established. However, little or virtually no CH_4 is being produced in agreement with the kinetic/thermal control on CH_4 formation. The carbon budget of some experiments yielding high CH_4 production indicated some contamination, in total agreement with the very few studies that included labeled ^{13}C in the carbon source (Grozeva et al., 2017; McCollom et al., 2010). The FTT reaction is very unlikely to be the route to produce the large methane emissions observed in near-surface ultramafic bodies, unless most of the CH_4 present at those settings is related to hotter

and longer water-rock interactions in fluid inclusions (Andreani et al., 2023; Klein et al., 2019; McDermott et al., 2015). Similarly, abiotic production of CH_4 and potentially other light hydrocarbons in serpentinizing ultramafic rocks may be kinetically favored at higher pressure and temperature conditions, such as at subduction zones (Boutier et al., 2021; Vitale Brovarone et al., 2020a).

In continental ultramafic systems (ophiolites and peridotite massifs), Etiope and Whiticar (2019) reevaluated the origin of methane by taking into account the latest theory, experiments and analytical methods, e.g., CH_4 isotopologues, applied to a larger set of field data on vents, seeps and springs. They converged on a model of abiotic methane generation based the Sabatier reaction, which consists in a catalytic CO_2 hydrogenation in a water-free (or unsaturated) rock, at relatively low temperature, with metal-rich catalysts such as the magnetite or chromite found in many ultramafic rocks.

For oceanic contexts, the reader is referred to the recent detailed evaluation of abiotic organics in hydrothermally altered mantle-derived rocks of Andreani and Ménez (2019). In short, CH_4 observed at mid-oceanic deep-sea vents likely results from the entrapment and re-speciation at high temperature (>400 °C) of mantle-derived CO_2 within fluid inclusions or vesicles in mantle and magmatic rocks (e.g., Andreani et al., 2023; Klein et al., 2019; McDermott et al., 2015), the fluids later being released during hydrothermal processing of the oceanic rocks. Moreover, in the large amount of total organic carbon measured in some serpentinized abyssal peridotites, a fraction is very likely present as solid carbonaceous matter, potentially including an abiotic contribution. As a consequence, understanding the formation and diversity of abiotic organic material produced during the hydrothermal alteration of ultramafic rocks requires a paradigm shift, no longer centered on FTT reactions. One includes the potential (and possibly metastable) formation of organic carbon compounds with intermediate oxidation states, mediated by rock-forming minerals during hydrothermal reactions (see Seewald et al., 2006; Fig. 15.4 in Andreani and Ménez, 2019); such compounds may include formic acid, formaldehyde, methanol, methane, ethane, ethene, benzene and graphite and all the polycyclic aromatic hydrocarbons in between, which form from successive reversible redox, dehydrogenation and hydrogenation reactions. At temperatures below 400 °C, where the formation of methane and graphite is kinetically inhibited, a large variety of highly volatile and mobile single-carbon organic species can then become available in addition to CO_2 species in fluids within natural serpentinizing systems of highly variable pH and local H_2 levels. As of today, the liquid and solid forms of abiotic organic matter have often received much less attention in both experimental and natural studies. Occurrence of organic minerals related to hydrothermal alteration in mafic and ultramafic rocks has been seldom reported, e.g., karpatite ($C_{24}H_{12}$), which has the highest molecular weight among natural organic minerals (see review of polycyclic aromatic hydrocarbon minerals by Echigo and Kimata, 2010). Recent high-resolution investigations of closed micro-environments void of biotic contamination in fresh or metamorphic hydrothermally altered ultramafic samples highlighted that the presence of hydrothermally derived abiotic organic carbon trapped within the uppermost lithosphere occurs often as heavy and aromatic compounds that are chemically and structurally diverse and closely associated to phyllosilicates (e.g., Andreani et al., 2023; Ménez et al., 2018; Sforna et al., 2018). Similarly, as anticipated above, graphite in many metamorphic rocks may be of abiotic origin and result from organic geochemical pathways deviating from conventional metamorphic petrology assumptions (Boutier et al., 2024b; Debret et al., 2022).

Carbon movement within and between deep reservoirs

The global carbon cycle results from the interplay and interconnections among deep and surface processes, and the response time of various forms of carbon to their timescales (Lee et al., 2019). Deep carbon on Earth is mobilized through multiple processes such as tectonics, metamorphism, magmatism, or a combination of them, and may involve movements of solid or fluid carbon species. This section introduces the main plate tectonics processes mobilizing solid carbon and the related solid carbon fluxes, and then summarizes the main processes of carbon mobilization from solids to fluids and the associated fluxes of deep carbon in fluids.

Movements of carbon from the crust to the deep Earth

Subduction of crustal carbon

Subduction, the tectonic mechanism of returning oceanic lithosphere into the Earth at convergent settings, is the principal input of exospheric carbon into the deep Earth (Fig. 4). Processes resulting in the sequestration of carbon in oceanic plates will determine the quantity of carbon returned into the Earth's interior, which at the present day is predicted to be 82 ± 14 Mt. C yr^{-1} (where 1 Mt. $= 10^{12}$ g; Plank and Manning, 2019), alternatively 68–140 Mt. C yr^{-1} (Müller et al., 2022) or 107 ± 26 Mt. C yr^{-1} (see Section "Secular variation of surficial versus deep carbon reservoirs or steady state?"). The largest fraction of this carbon is represented by carbonate minerals, which account for about 80% of total subducted carbon (Plank and Manning, 2019, and references therein). The second largest input of solid carbon into subduction, accounting for about 20% of total carbon inputs, is reduced carbon (organic matter; graphitic carbon; graphite). The contribution of surface/subsurface hydrocarbons to deep carbon recycling is less constrained owing to the question as to if these compounds are transferred to depth at convergent margins or mobilized at shallow depths. Nevertheless, some experimental studies have assessed the potential transformation and stability of subducted hydrocarbons at convergent margins (Serovaiskii et al., 2019).

The overarching subducting carbon budget may be evaluated by characterizing the carbon concentrations within the different individual lithological components comprising the subducting slab that can be sampled, and combining these concentrations with the kinematic parameters of subduction (e.g., Dasgupta and Hirschmann, 2010; Kelemen and Manning, 2015; Plank and Manning, 2019). An adjacent methodology is to parameterize the controls on global carbon subduction at the present-day, and apply these

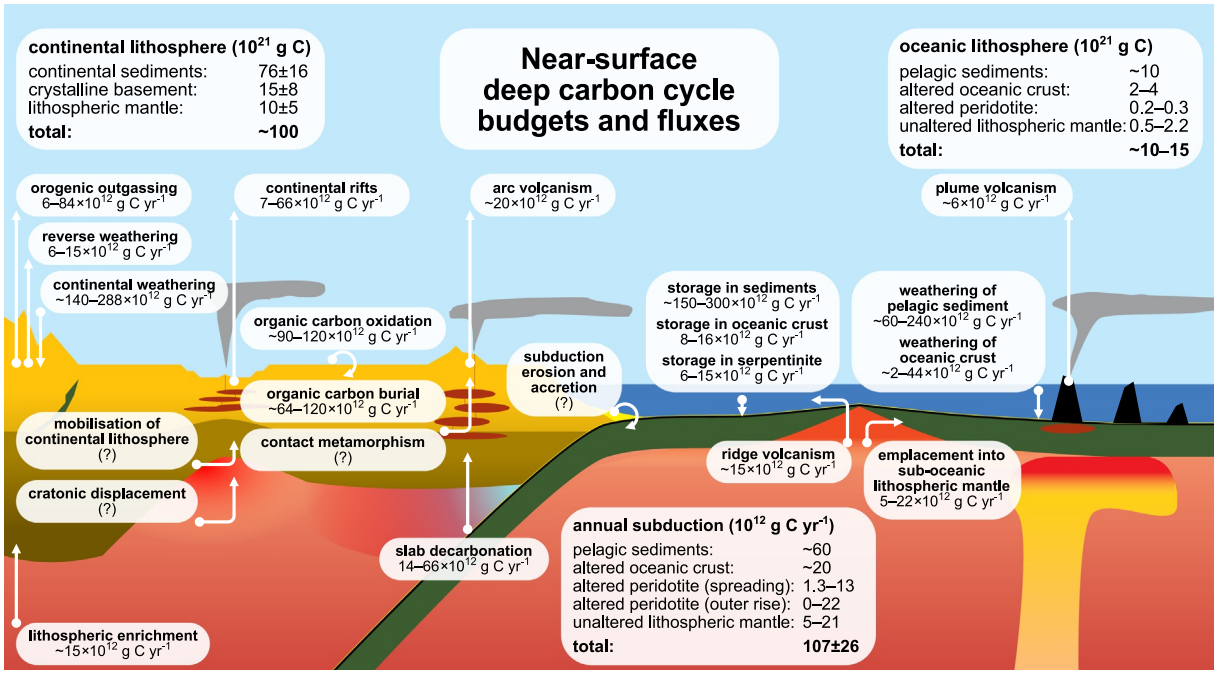

Fig. 4 Schematic diagram illustrating the budgets and fluxes of carbon within the near-surface deep carbon cycle. The continental lithosphere hosts ~100 × 10^{21} g carbon (Hirschmann, 2018; Gibson and McKenzie, 2023), which is obtained from enrichment of the sub-continental lithospheric mantle (Foley and Fischer, 2017) and weathering of continental crust (Gaillardet et al., 1999), and lost to the atmosphere through orogenic outgassing (Becker et al., 2008; Stewart and Ague, 2018; Stewart et al., 2019), reverse weathering (Isson and Planavsky, 2018; Isson et al., 2020), and magmatism. Volcanic outgassing at intraplate (rift and plume) and arc settings contributes to the mobilization of crustal and lithospheric carbon in continental settings (Bekaert et al., 2021; Brune et al., 2017; Hauri et al., 2019; Werner et al., 2019; Wong et al., 2019), which is enhanced through a number of additional unquantified lithospheric processes (Gorczyk and Gonzalez, 2019; Mason et al., 2017; Muirhead et al., 2020). In oceanic settings, the carbon budget is estimated to be ~10–15 × 10^{21} g (Hirschmann, 2018; Müller et al., 2022), which is subdivided between carbon-bearing sediments (Cartapanis et al., 2018; Clift, 2017; Dutkiewicz et al., 2019; Hayes et al., 2021; Hirschmann, 2018; Yaroshevsky, 2006), altered oceanic crust (Kelemen and Manning, 2015; Li et al., 2019; Merdith et al., 2019; Müller and Dutkiewicz, 2018; Müller et al., 2022), serpentinized peridotites (Alt et al., 2013; Merdith et al., 2020; Müller et al., 2022; Schwarzenbach et al., 2013), and sub-oceanic lithospheric mantle (Gibson and McKenzie, 2023; Keller et al., 2017; Müller et al., 2022). Carbon in oceanic lithosphere is obtained at mid-ocean ridges (Keller et al., 2017) and through weathering of pelagic sediments and oceanic crust (Coogan and Gillis, 2018; Wallmann et al., 2008); additional carbon is introduced into the oceans through mid-ocean ridge volcanism (Hauri et al., 2019; Le Voyer et al., 2019; Müller et al., 2022; Tucker et al., 2018). During subduction, the slab is decarbonated (Kelemen and Manning, 2015; Müller et al., 2022), dissolved (Ague and Nicolescu, 2014; Frezzotti et al., 2011; Piccoli et al., 2021), or reduced (Malvoisin et al., 2012; Galvez et al., 2013; Vitale Brovarone et al., 2017; Peng et al., 2021), and carbon is sequestered into the forearc (Barry et al., 2019; Debret et al., 2022; Fullerton et al., 2021) and in arc magmas (Johnston et al., 2011). Carbon exchange between continents and downgoing slabs may also occur as a result of subduction erosion and accretion (Clift and Vannucchi, 2004; Straub et al., 2020). Organic carbon burial across both oceans and continents is likely to balance organic carbon oxidation (Kump and Arthur, 1999). 10^{12} g C is equivalent to 1 Mt. C; 10^{21} g C is equivalent to 10^{9} Mt. C, or 10^{6} Gt C.

parameterizations to plate tectonic reconstruction models (e.g., Müller et al., 2022; Wong et al., 2019). As seafloor/subseafloor alteration processes account for a large fraction of carbon storage in the oceanic lithosphere, reviews of carbon ingassing at subduction zones traditionally categorize inputs into three principal lithological components, which are characterized by observations from ocean research drilling programs (e.g., Staudigel et al., 1989; Kelemen and Manning, 2015; Plank and Manning, 2019): carbon in serpentinized lithospheric mantle (Section "Altered lithospheric mantle"), basaltic oceanic crust (Section "Altered oceanic crust"), and carbon in the sediment overlying the basaltic crust (Section "Sediments"). The carbon sequestered within these subducting reservoirs in the lithosphere is sourced from the ocean itself, as the percolation of seawater into permeable oceanic lithosphere is the principal means of carbon deposition within the crust and uppermost mantle (Section 4.4.2). Contributions to the sedimentary component of subducting carbon come primarily from marine organisms in the form of carbonate shells and reduced organic carbon remains (Clift, 2017), although there is significant input from terrestrial sediments, predominantly at river estuaries and deltas where sedimentation rates are substantial (e.g., Dutkiewicz et al., 2016).

In addition to these three traditional reservoirs of subducting carbon, recent work has highlighted that a non-negligible fraction of carbon can be present in oceanic lithospheric mantle sections unaffected by seafloor/subseafloor alteration (see Section "Sub-oceanic lithospheric mantle"; Gibson and McKenzie, 2023; Keller et al., 2017; Müller et al., 2022). This sequestered carbon in unaltered oceanic lithosphere may be remobilized upon entering the Earth at subduction zones. However, as with quantifying the mass of the ocean lithospheric budget, there is substantial uncertainty as a result of the multiple controls on carbon emplacement at mid-ocean ridges (Keller et al., 2017). By selecting representative values for these multiple parameters, it is believed that sequestered carbon in the unaltered oceanic lithosphere may contribute 5–21 Mt. C yr^{-1} to the overall subducting carbon flux at the present day (Merdith et al., 2019; Müller et al., 2022).

Owing to the low production rate of oceanic peridotite, exposed oceanic lithosphere generated at magma-poor rifts and mid-ocean ridges has previously not been considered as a significant contributor toward the budget of subducting carbon (1–4% of all present-day oceanic crust, contributing ~1.3 Mt. C yr^{-1}; Alt et al., 2013; Kelemen and Manning, 2015). However, more recent estimates suggest that carbonated serpentinite from (ultra-)slow spreading ridges may contribute ~5–13 Mt. C yr^{-1} at the present day (Müller et al., 2022). Serpentinites formed during plate flexure are also believed to be substantial contributors of carbon owing to the formation of lithosphere-scale faulting and serpentinization (e.g., Ranero et al., 2003), itself a function of slab dip (Faccenda, 2014). Serpentinite carbonation as a result of outer-rise bending is therefore expected to contribute a substantial amount to the subducting carbon budget, although this value remains very unconstrained (0–22 Mt. C yr^{-1}; Kelemen and Manning, 2015; Müller et al., 2022). Instead, carbon uptake by basaltic oceanic crust as a result of weathering and alteration is believed to be a greater store of carbon at the mid-ocean ridge environment, contributing ~20 Mt. C yr^{-1} toward total fluxes of subducted carbon (Kelemen and Manning, 2015; Li et al., 2019; Merdith et al., 2019; Müller et al., 2022; Müller and Dutkiewicz, 2018).

Quantifying the subduction flux of carbon-bearing sediments is also complex. As established in Section 4.4.2.3, factors such as the age of subducting plate, distance from continents, and biological productivity will directly control the amount of sedimentary carbon accumulated on the plate (Dutkiewicz et al., 2016, 2019; Plank, 2014). Furthermore, sediment subduction may be hindered by accretion on the overriding plate, which appears to be substantial at slow subduction rates (<6–7 cm yr^{-1}; Clift and Vannucchi, 2004). If considering subduction fluxes over geological time, prior to the Marine Mesozoic Revolution, sedimentary carbonate is not considered to be a significant contributor to subduction zones (Edmond and Huh, 2003; Müller et al., 2022), although the radiative evolution of biomineralizing metazoans from the Cambrian onwards may have significantly affected the exospheric carbon cycle in the absence of carbonate sediment subduction (Walton and Shorttle, 2024). Similarly, the fluxes of subducted organic carbon have changed over geological time following major variations of surface organic carbon production such as the Cambrian explosion (Giuliani et al., 2022). In the modern oceans, organic carbon constitutes a mass fraction ranging from 0.5 to 1.5 wt% in carbonate-free oceanic sediments (Malinverno and Martinez, 2015). However, the quantities of subducted organic carbon through geological time are currently unknown and are assumed to constitute a very minor fraction of total subducting carbon through geological time, reflecting values typical of deep sea sediments distal to continents (<0.5 wt%; Müller et al., 2022). Nevertheless, recent work has shown that latitude-dependent variations in the compositions of subducted sediments, possibly related to latitudinal variations in the primary production of phytoplankton and organic matter burial, may impart a strong control on the redox state of arc magmas (Hu et al., 2024). The GLOSS-II composition, representative of 'average' subducted sediment, has 3.07 ± 0.23 wt% carbon, but in practice sedimentary compositions will be substantially variable depending on depth and environment of deposition (Plank, 2014). Furthermore, different subduction systems will subduct variable proportions of carbonate to organic carbon (Clift, 2017). At the present day, seafloor sediment is believed to be the greatest contributor to the overall subducted carbon budget, of which ~20% is organic carbon (~60 Mt. C yr^{-1}; Clift, 2017; Müller et al., 2022; Wong et al., 2019).

Subduction erosion

In contrast (but not antithetical) to the process of sediment accretion on continental crust is the erosion of the upper plate forearc during subduction (e.g., Clift and Vannucchi, 2004; Stern, 2011, 2020; Straub et al., 2020), which is believed to be the most significant process destroying continental crust (e.g., Clift et al., 2009b,a). The principal evidence for continental erosion arises from the subsidence of some convergent margin forearcs (e.g., Ranero and von Huene, 2000; Vannucchi et al., 2001). In addition, despite potential for blending with geochemical signatures for slab components and crustal contaminants (e.g., Straub et al., 2020), it is possible to identify signatures of eroded crust in arc magmas (e.g., Stern, 2020; Straub et al., 2015). Estimates of present-day subduction erosion typically range from 30 to 150 km^3 Myr^{-1} per km length of subduction zone (e.g., Clift, 2017; Straub et al., 2020; Vannucchi et al., 2016); it is therefore likely that erosion of the overriding plate can contribute toward the carbon budget of subduction. However, it is difficult to determine the contributions of this contribution beyond qualitative assessment. It is known that the rate of material transfer during erosion depends on several factors, including the topography and sediment cover of the subducting plate, high convergence rates, and subduction channel fluid dynamics (Clift and Vannucchi, 2004; Straub et al., 2020; Vannucchi et al., 2012). Furthermore, eroded convergent margins typically have overlying plates exposing igneous arc basement, which bears less carbon than other lithologies (Clift, 2017; Yaroshevsky, 2006); the lithology of the overriding plate will be a further contributor to the overall carbon budget of subduction erosion. Further characterization of the subduction erosion process, and therefore also of volume and mass fluxes of eroded overlying crust at subduction zones, will be required in order to completely capture the quantities of carbon contributed to subduction from this process.

Movements of carbon from depth to the crust

Tectonic movements of solid carbon from the deep Earth to the surface

At convergent margins, tectonic or mechanical movements of solid carbon from mantle depths to the crust or within the crust are primarily controlled by off-scraping or diapirism of downgoing slab material or eroded mantle wedge material (see reviews by Klein and Behn, 2021; Plank and Manning, 2019). Carbon-bearing subducted materials, especially subducted sediments but also large volumes of subducted oceanic igneous and mantle rocks, can be removed from the downgoing slab, reducing the amount of subducted carbon reaching the convective mantle. A dominant fraction of this material is removed from the downgoing slab at trenches to form accretionary prisms (Tewksbury-Christle et al., 2021), At greater depths within the forearc to arc region, the fate of

this material is uncertain; subducted sediments may be removed from the slab to form diapirs that partially melt or do not melt as they rise into the mantle wedge, and be emplaced at the base of the crust (Behn et al., 2011; Ducea et al., 2022; Kelemen and Behn, 2016), or be exhumed as tectonic slices or mélanges along the plate boundary to form orogenic complexes (Agard et al., 2009; Guillot et al., 2009). The fluxes of solid carbon associated with these tectonic or mechanical movements of deep rocks toward the surface are largely unknown. It has been suggested that off-scraping of sediments at trenches may remove a fraction of subducted sediments as high as 35% of global subducted sediments (Straub et al., 2020). Nevertheless, the ultimate amount of solid carbon being mobilized through tectonic or mechanical processes varies from one subduction zone to another, or even subduction zone sub-segments relative to adjacent sub-segments, based on the specific tectonic setting, the type and amounts of subducted sediments, and the thermal regimes controlling the contextual mobilization of carbon through metamorphic or magmatic degassing (Plank and Manning, 2019).

Metamorphic and magmatic processes of carbon mobilization

The mobilization of carbon from solids to fluids requires changing conditions and is strongly dependent upon the closed or open system behavior of the considered systems. Rock chemistry, changes in pressure and/or temperature conditions, changing redox, and/or on the presence and nature of fluids are the main parameters controlling the mobilization of carbon from the main solid carbon phases, namely carbonate minerals, organic matter, diamond (Fig. 5), and fluids and melts. Such conditions can be achieved through multiple processes and at various geological contexts. These processes are summarized in the following sections.

Mobilization of carbon from carbonate minerals

The three main processes mobilizing carbon from carbonate minerals are decarbonation reactions, carbonate dissolution, and melting. In the forearc to subarc regions of subduction zones as well as in the continental crust, decarbonation and dissolution are the most important processes, whereas carbonate melting is expected to take place at greater depths in the mantle, or during anatexis in the lower crust.

Decarbonation is the process of carbonate breakdown through carbonate-silicate reactions in response to rising temperature. Also referred to as 'Urey reactions' (Urey, 1952), decarbonation can be summarized by the generic reaction:

$$MCO_3 + SiO_2 \rightarrow MSiO_3 + CO_2$$

where M represents a divalent cation, most typically Ca^{2+} or Mg^{2+}.

Examples of decarbonation reactions are common in metamorphic rocks in metasedimentary, metamafic, and ultramafic rocks, and involve a broad range of carbonate (calcite, dolomite, ankerite) and silicate (quartz, serpentine, and many others) reactants (Baumgartner and Valley, 2001; Epstein et al., 2020; Ferry, 1991; Cook-Kollars et al., 2014; Collins et al., 2015; Stewart et al., 2019; Vitale Brovarone et al., 2018; Fig. 6a). Decarbonation is effective in regional and contact metamorphic settings. Besides the characteristic calc-silicate products, decarbonation reactions are also identified by shifts in the carbon isotopic composition of the residual carbonate fraction; residual carbonate is ^{12}C-enriched due to the positive $\Delta Carb\text{-}CO_2$ (e.g., Baumgartner and Valley, 2001; Bottinga, 1969; Epstein et al., 2020; Cook-Kollars et al., 2014; Collins et al., 2015). Decarbonation reactions do not require the presence of an aqueous fluid to produce carbon-bearing fluids. Nevertheless, the presence of aqueous fluids, for example during infiltration of external fluids or in response to local dehydration reactions, has been shown to enhance decarbonation reactions (Ferry, 1991; Gorman et al., 2006; Menzel et al., 2020; Vitale Brovarone et al., 2018). Decarbonation is believed to contribute substantially to metamorphic carbon degassing at convergent margins (Gorman et al., 2006; Kelemen and Manning, 2015; Kerrick and Connolly, 2001), with collisional metamorphism producing higher CO_2 fluxes relative to subduction metamorphism, and cumulative fluxes as high as about 6–84 Mt. C yr^{-1} (Stewart et al., 2019; Fig. 4). Experimental studies and thermodynamic modeling results predict decarbonation reactions and the formation of CO_2-enriched fluids to be particularly efficient at subarc depths in subducting slabs (Gorman et al., 2006; Gonzalez et al., 2016). At shallower depths, contact metamorphism at convergent margins may also substantially contribute to carbon degassing (Aiuppa et al., 2017).

In addition to decarbonation reactions, carbonate dissolution also contributes to the mobilization of deep carbon from solid to fluid phases. Carbonate dissolution has only recently been added to the inventory of processes contributing to deep carbon budgets and fluxes (Ague and Nicolescu, 2014; Facq et al., 2014; Frezzotti et al., 2011; Kelemen and Manning, 2015). The lack of previous assessments was related to the only recent establishment of values for the dielectric constant of water at high-pressure conditions (Sverjensky et al., 2014). Carbonate dissolution may be effective at mobilizing carbon into aqueous fluids in the absence of silicate minerals, i.e., when decarbonation reactions cannot take place. Carbonate solubility is dependent upon pressure, temperature, and redox conditions (Fig. 6b,c). Experimental studies on aragonite solubility demonstrated that, under oxidized conditions, the speciation of carbonic fluids produced by carbonate dissolution is strongly dependent upon the pressure and temperature conditions, with bicarbonate ions dominating at pressure < 3 GPa to at least 400 °C and carbonate ions at higher pressure and temperature conditions (Facq et al., 2014). CO_2 was found to be present in appreciable amounts below 2–3 GPa (Li, 2017). Reduced conditions, instead, have been shown to boost carbonate mineral solubility in aqueous fluids, with methane controlling the speciation of carbonic aqueous fluids resulting from carbonate dissolution (Lazar et al., 2014) (Fig. 6c). Natural examples of carbonate dissolution are documented in metamorphic terranes such as the Cyclades (Ague and Nicolescu, 2014) and Corsica (Piccoli et al., 2016, 2021).

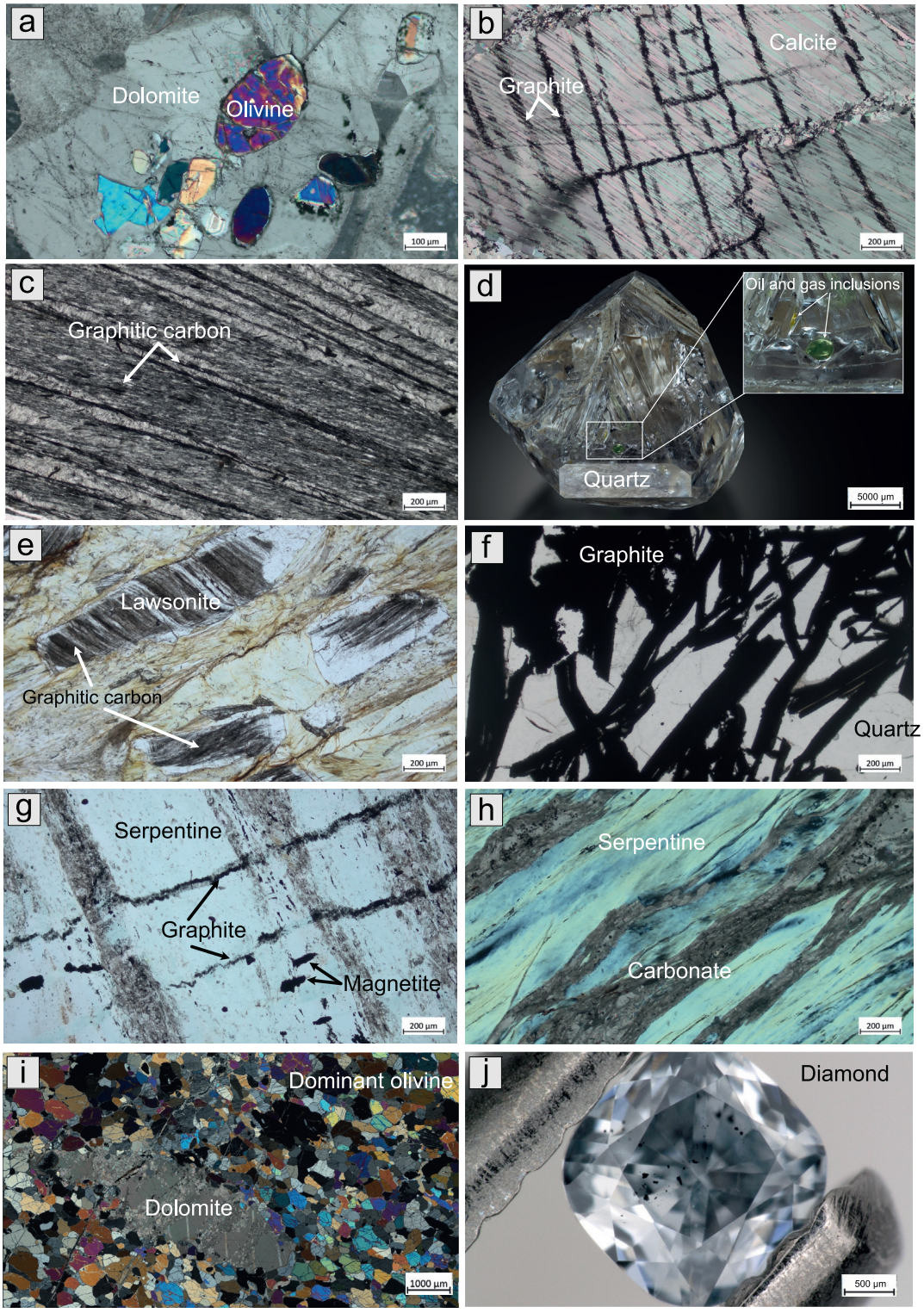

Fig. 5 Photomicrographs of natural deep carbon forms. (a) Olivine-bearing dolomite marble, Hida belt, Japan (Harada and Tsujimori, 2024). Olivine formation indicates the reaction between silicates and dolomite to produce olivine + CO_2 with increasing temperature. (b) Calcite crystals being partially converted to graphite during the infiltration of reduced fluids. Note the preferential reaction along grain boundaries and carbonate twin planes and cleavage. Samples from the Belvidere Mountain Complex, Northern Vermont (Boutier et al., 2024b). (c) Graphitic carbon in metapelitic rocks from the Wepawaug Schist, Connecticut, USA (Ague, 2003; Zhang et al., 2018a,b). Based on carbon stable isotopes, the graphitic carbon is interpreted to represent metamorphosed biogenic organic material (Zhang et al., 2018a,b). (d) Hydrocarbon oil and gas inclusions in hydrothermal quartz from Porretta Terme, Northern Apennines, Italy (Olivieri and Miglioli, 2021). The hydrocarbon oils and gases are interpreted to have formed through thermogenic processes during burial and heating of biogenic organic matter (Tassi et al., 2022). (e) Example of leaching of graphitic carbon during fluid infiltration in graphitic schists (Vitale Brovarone et al., 2020b). Note the presence of abundant graphitic carbon included in lawsonite, and the absence of it in the surrounding matrix. (f) Fluid-deposited graphite-quartz vein, Amitsoq graphite mine, Southwestern Greenland (Bondam, 1992; Fratelli, 2023). Sample provided by GreenRoc Strategic Materials plc. (g) Discordant graphite veins in high-pressure serpentinite, Balangero, Western Italian Alps (Vitale Brovarone et al., 2017). (h) Network of discordant carbonate veins in serpentinite, Alpine Corsica, France. (i) Dolomite formation in metasomatized garnet peridotite from the Ulten zone, Italy (Sapienza et al., 2009; Consuma et al., 2020). (j) Blue boron-bearing diamond, with dark inclusions of ferropericlase [(Mg,Fe)O], olivine [$(Mg,Fe)_2SiO_4$] and nyerereite [$Na_2Ca(CO_3)_2$] studied in Smith et al. (2018). This *gem* weighs 0.03 carats and its depth of formation resulted to be at least 430 km in the transition zone. (a) Photo credits Orlando Olivieri. (j) Photo credit Evan M. Smith/GIA.

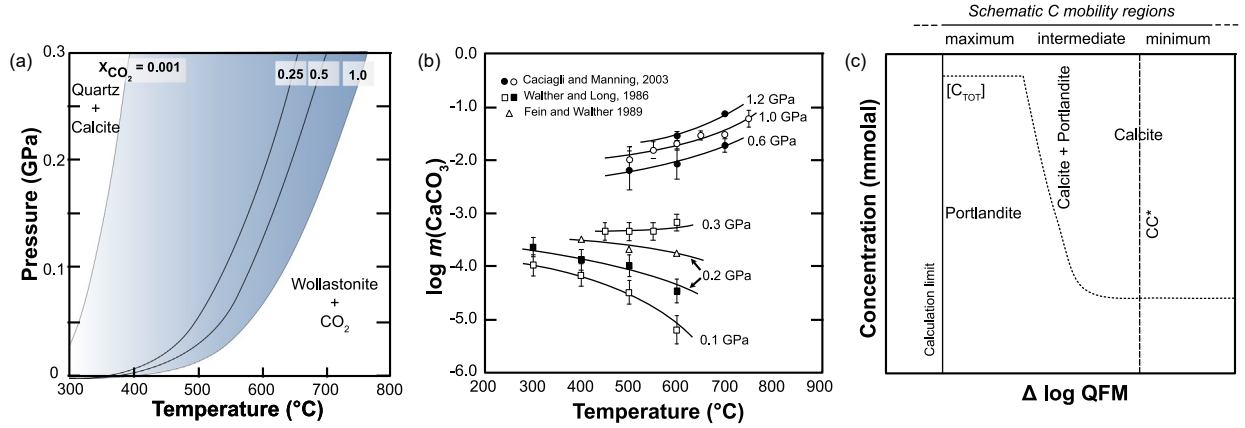

Fig. 6 Processes of carbon degassing from carbonate minerals. In all subfigures, $[C_{TOT}]$ is total carbon concentration (dotted lines) and $[Ca_{TOT}]$ is total calcium concentration (solid lines). (a) Pressure-temperature diagram showing the topology of decarbonation reactions (carbonate-silicate reactions) for varying H_2O-CO_2 ratios, here shown as XCO_2. The classical reaction calcite + quartz = wollastonite + CO_2 is shown as an example. (b) High-pressure determinations of calcite solubility in H_2O. Solubilities in molality. Experimental data from Caciagli and Manning (2003), Fein and Walther (1989), and Walther and Long (1986). (c) Schematic diagram showing carbonate solubility variations as a function of fO_2, expressed as Δ log relative to the quartz-fayalite-magnetite buffer (QFM). Vertical dashed line: cc* calcium carbonate solubility transition point. Defined as the fO_2 at which $[Ca_{TOT}]$ is 1% greater than $[Ca_{TOT}]$ at the hematite-magnetite buffer relative to the $[Ca_{TOT}]$ plateau within the calcium carbonate + portlandite field. At fO_2 values greater than *cc**, $[Ca_{TOT}]$ is approximately constant; below *cc**, $[Ca_{TOT}]$ increases as fO_2 decreases. The schematic diagram illustrates the higher solubility ($[C_{TOT}]$) and carbon mobility of calcium carbonate under reducing conditions. Vertical shaded rectangle: calcite + portlandite + fluid stability field (metastable in *C*). Vertical solid line: limit of calculation, where $X(H_2O) = 0.9$. (a) Modified after Stewart EM, Ague JJ, Ferry JM, Schiffries CM, Tao R-B, Isson TT, and Planavsky NJ (2019) Carbonation and decarbonation reactions: Implications for planetary habitability. *American Mineralogist* 104(10): 1369–1380. https://doi.org/10.2138/am-2019-6884. (b) Modified after Manning CE, Shock EL, and Sverjensky DA (2013) The chemistry of carbon in aqueous fluids at crustal and upper-mantle conditions: Experimental and theoretical constraints. *Reviews in Mineralogy and Geochemistry*, 75(1): 109–148. https://doi.org/10.2138/rmg.2013.75.5. (c) Modified after Lazar C, Zhang C, Manning CE, and Mysen BO (2014) Redox effects on calcite-portlandite-fluid equilibria at forearc conditions: Carbon mobility, methanogenesis, and reduction melting of calcite†. *American Mineralogist* 99(8–9): 1604–1615. https://doi.org/10.2138/am.2014.4696.

An increasing body of literature has documented examples of natural carbonate reduction at various metamorphic settings (Boutier et al., 2024b; Galvez et al., 2013; Tao et al., 2018; Peng et al., 2021; Vitale Brovarone et al., 2017; Wang et al., 2022) (Fig. 5b). Although at least some of these cases can be explained by carbonate dissolution in aqueous fluids under reducing conditions, the immiscibility of H_2 in metamorphic fluids under a vast pressure-temperature range may promote carbonate-H_2 reactions in the absence of an initial aqueous fluid. In this instance, the term carbonate hydrogenation should be preferred. A simple example of carbonate reduction is.

$$CaCO_3 + 4H_2 \rightarrow Ca(OH)_2 + CH_4 + H_2O$$

where the breakdown of carbonate is promoted by hydrogenation. Carbonate reduction and hydrogenation are documented in subduction zone metamorphic rocks as a consequence of fluid-rock interactions such as serpentinization (Boutier et al., 2024b; Peng et al., 2021; Vitale Brovarone et al., 2020a), or during prograde or early retrograde metamorphism of weakly altered oceanic crustal rocks (Wang et al., 2022). The same processes are also expected to occur at mantle pressures and temperatures (Scott et al., 2004). Fluxes of carbon through these processes are largely unquantified. Fluxes of CH_4 produced through metamorphic decarbonation reactions of ultramafic and mafic rocks are estimated at 1.5 Mt. CH_4 yr^{-1} (Vitale Brovarone et al., 2017) and up to about 11 Mt. CH_4 yr^{-1} (Zhang et al., 2023).

Mobilization of carbon from organic matter, graphite, and diamond

During diagenesis and low-temperature (<300 °C) metamorphism, organic matter undergoes a series of chemical reactions that progressively release heteroatoms such as hydrogen, sulfur, nitrogen, and oxygen, in addition to carbon. Following laboratory experimental results and observations in natural settings, this process results in the carbonization and – at higher temperature – graphitization of organic matter (Vandenbroucke and Largeau, 2007) (Fig. 7a). With progressive loss of heteroatoms during carbonization (or kerogen transformation) and graphitization, carbon is released in the fluid in the form of hydrocarbon oils and gasses (Buseck and Beyssac, 2014; Tissot and Welte, 1984; Vandenbroucke and Largeau, 2007), promoting the formation of a progressively purer and more structured organic matter, or graphitic carbon (Fig. 5c) (Beyssac and Rumble, 2014). Light hydrocarbon gasses produced during this process are referred to as thermogenic gasses and, as well as for oils, are referred to as biotic in origin (Fig. 5d) (i.e., formed through the transformation of biogenic matter; Etiope, 2015). Studies conducted in low-grade metamorphic terranes suggest that thermogenic degassing is efficient up to about 300 °C, whereas at higher temperatures the contribution of this process is considered negligible (Mullis et al., 1994; Tarantola et al., 2007). Thermogenic degassing is primarily controlled by temperature and does not require an external agent such as aqueous fluids. Such conditions are expected during diagenesis in

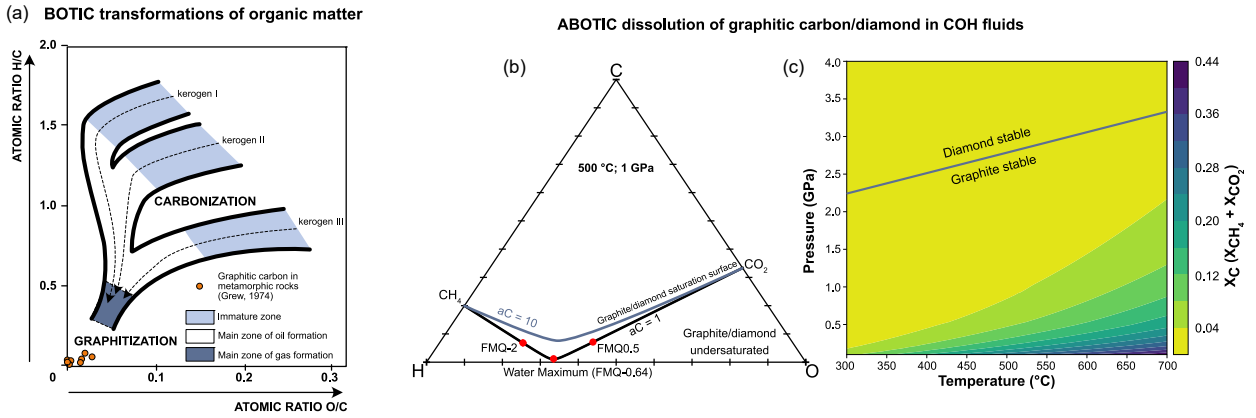

Fig. 7 Processes of carbon degassing from organic matter and graphitic carbon. (a) Biotic pathways of solid organic carbon mobilization to form hydrocarbon oils and gasses. Van Krevelen diagram showing the transformation pathways for kerogens and mobilization of carbon as biotic hydrocarbon oils and gasses during carbonization and successive graphitization. Kerogen types I, II, and III derive from lacustrine algae, marine micro-organisms, and terrestrial plants, respectively, from. The immature zone represents conditions prior to the release of large amounts of oil and gas hydrocarbons. The diagram also shows compositional data of graphitic carbon from selected metamorphic rocks from Grew (1974). (b-c) Abiotic pathways of solid organic carbon mobilization in aqueous fluids. Diagrams calculated with the Thermotopes-COH software (Boutier et al., 2024a). (b) C-O-H thermodynamic model at 500 °C and 1 GPa. The lower part of the diagram, below the carbon saturation curve, corresponds to carbon undersaturated conditions (no graphite/graphitic carbon/diamond stable). See Holloway (1984) and Connolly and Cesare (1993) for details. The subfigure also shows the predicted fluid compositions for carbon-saturated systems at water-maximum conditions (ΔFMQ = –0.64 at the model conditions), ΔFMQ = –2, and ΔFMQ = +0.5 for a carbon activity (aC) equal to one (graphite stable). Note the higher carbon concentrations in more reduced or more oxidized carbon-saturated fluids relative to the so-called water maximum. The carbon saturation curve for a less graphitic carbon form is also shown and calculated with aC equal to 10. Note the higher solubility for aC > 1, corresponding to less graphitic carbon forms less crystalline than graphite. (c) Pressure-temperature diagram showing total dissolved (X_C), calculated by summing the molar fractions of CH_4 and CO_2 (XCH_4 and XCO_2, respectively), for a graphite/diamond-saturated fluid at water maximum. At these conditions, CH_4 and CO_4 have the same concentration. Other C-bearing fluid species are in negligible concentrations. It can be seen that the solubility of graphite/diamond increases with temperature and decreases with pressure. (a) Modified from Buseck PR and Beyssac O (2014) From organic matter to graphite: Graphitization. *Elements* 10(6): 421–426. https://doi.org/10.2113/gselements.10.6.421, after Vandenbroucke M and Largeau C (2007) Kerogen origin, evolution and structure. *Organic Geochemistry* 38(5): 719–833. https://doi.org/10.1016/j.orggeochem.2007.01.001.

sedimentary basins, or during prograde metamorphism in the shallow forearc of subduction zones margins, in accretionary prisms, and in contact metamorphic aureoles hosted in organic-rich sedimentary rocks. The contribution of thermogenic degassing of hydrocarbons induced by igneous intrusions may release carbonic fluids in amounts high enough to affect global climate conditions. For example, it has been proposed that the end-Triassic mass extinction and initial Eocene global warming may have been caused by voluminous intrusions of mantle-derived melts in organic-rich sedimentary basins at large igneous provinces (Capriolo et al., 2021; Svensen et al., 2004).

Beyond the conditions favorable to extensive thermogenic degassing, the contribution of reduced solid carbon materials to geological carbon degassing may be minimal in closed systems (Connolly, 1995; Pattison, 2006), even though high-temperature thermogenic degassing may still be present (Boutier et al., 2024b). At those conditions, graphitic carbon solubility becomes the dominant mechanism of carbon mobilization from organic carbon solids to fluids, especially in open systems flushed by metamorphic aqueous fluids (Fig. 5e) (Tumiati et al., 2020, 2022; Vitale Brovarone et al., 2020b; Zhang et al., 2018b). The carbon-rich gasses produced by aqueous dissolution of graphitic carbon should be considered abiotic in origin (Fig. 7), even though – in the absence of carbonate minerals, see below – their carbon isotope composition may reflect a biotic origin.

The solubility of graphitic carbon in aqueous metamorphic fluids depends on the redox state, on the pressure and temperature conditions, and on their physicochemical properties (e.g., crystallinity). The amount of carbon that can be dissolved from organic materials to aqueous fluids is higher for strongly oxidized or strongly reduced conditions, and is minimized for intermediate redox conditions at the so-called "water maximum" of carbon-saturated C-O-H fluids (Fig. 7b) (Connolly and Cesare, 1993; Holloway, 1984). Pressure decreases the solubility of graphitic carbon, whereas temperature has an opposite effect (Fig. 7c). Crystalline organic matter is less soluble than amorphous organic matter (Fig. 7b) (Toffolo et al., 2023 and references therein; Tumiati et al., 2020, and references therein; Vitale Brovarone et al., 2020b). Experimental work has shown that the solubility of organic matter, from amorphous to graphitic carbon forms, is dependent on both the structure of the considered material and its surficial properties (Toffolo et al., 2023). Increasing temperature during prograde metamorphism promotes the progressive crystallization of organic matter, increasing its solubility. In subduction zones, increasing pressure during prograde metamorphism may, depending upon thermal regimes, counterbalance this effect (Fig. 7c). Compared to a pure C-O-H system, the presence of silicate minerals can increase the solubility of graphitic carbon in aqueous fluids by up to 30%, as a consequence of a decrease in water activity probably related to organic species containing Si-O-C and Si-O-Mg bonds (Tumiati et al., 2017).

Experimental work has demonstrated that, for graphite-aragonite-water equilibria at fH_2 = FMQ (equivalent to fO_2 expressed as ΔFMQ = +0.61 log units) at subarc conditions, the largest fraction of dissolved CO_2 derives from graphite solubility, whereas carbonate dissolution at the investigated conditions produces bicarbonate ions mostly (Tumiati et al., 2022). In turn, the isotope

composition of the experimentally produced, graphite-derived CO_2 reflected carbonate-CO_2 equilibria, with implications on the interpretation of volcanic gas compositions and their slab source materials.

As discussed for carbonate minerals, interactions between organic matter and H_2-rich fluids may promote the mobilization of carbon from solid phases to light hydrocarbons in fluids. Experimental results obtained at pressure-temperature conditions consistent with subduction zone and upper mantle settings indicate that graphite hydrogenation to form CH_4 may be a very efficient process (Peña-Alvarez et al., 2021). Experiments of diamond hydrogenation showed similarly fast, yet slightly lower reaction rates compared to graphite (Peña-Alvarez et al., 2021). Natural examples of graphite hydrogenations are also documented (Vitale Brovarone et al., 2017).

Carbon reprecipitation at depth

Not all the carbon being mobilized from metamorphic and metasomatic processes is degassed to Earth's surface. Precipitation of carbonate minerals, graphite, organic compounds, or diamonds from geological fluids or melts is a common process taking place at virtually any depth geological setting. Carbon saturation, redox, pressure/temperature variations and fluid-rock chemistry are some of the key parameters controlling the precipitation of carbon minerals from fluids or melts. At least some diamonds are thought to represent precipitates from deep/ultradeep carbonic fluids (Smith et al., 2016; Stachel et al., 2017; Thomassot et al., 2007). Voluminous or trace amounts of graphite form from percolating fluids and their interactions with rocks and/or other fluids and in rocks and geological contexts spanning mafic and ultramafic rocks at convergent and divergent margins (Luque et al., 2014), and virtually any rock types at various metamorphic, magmatic, and hydrothermal settings within the crust (Fig. 5f,g) (Boutier et al., 2024b; Galvez et al., 2013; Luque et al., 2014; Rumble et al., 1986; Tao et al., 2018). This also extends to other forms of condensed carbon materials, precipitation of which may serve as a carbon source for microbial pathways in the deep subsurface (Debret et al., 2022; Ménez et al., 2018). Carbonate precipitation in upper mantle rocks has been documented in multiple settings. Carbonate veins and carbonation processes, i.e., pervasive replacement of silicate rocks by carbonate minerals, recycling deep carbon in fluids are ubiquitous in crustal and mantle rocks, as demonstrated by natural and experimental data (Fig. 5h,i) (Consuma et al., 2020; Bouilhol et al., 2022; Hu et al., 2021; Kelemen et al., 2011; Menzel et al., 2018; Okamoto et al., 2021; Peng et al., 2021; Piccoli et al., 2016; Sieber et al., 2018). The so-called cold nose of the forearc mantle wedge of many subduction zones represents a characteristic zone of intense reprecipitation of dissolved carbon through carbonation processes (e.g., De Obeso et al., 2022; Kelemen et al., 2022; Menzel et al., 2018, 2024). In the forearc region of Costa Rica, carbon and noble gas data from hot springs indicate that a large fraction — as high as 91% — of carbon in fluids released from devolatilization reactions in the subducting slab reprecipitate as carbonate minerals in the crust before reaching the surface (Barry et al., 2019). Within the biosphere, microbial activity may also contribute to the modulation of carbon degassing through the precipitation of carbonate minerals or organic biomass (see Section "Carbon at the interface between the geosphere and biosphere").

Movements of deep carbon in melts

Carbon in intraplate magmatism

Partial melting in the asthenospheric (convecting) mantle is an inescapable consequence of the presence of CO_2 and H_2O (Fig. 8). Nominally anhydrous minerals can store small amounts of H_2O, which results in a decrease of their melting temperature from 10 °C to ~100 °C; the more H_2O, the lower the melting temperature (Bell and Rossman, 1992; Bolfan-Casanova, 2005; Demouchy and Bolfan-Casanova, 2016; Green, 1973; Hirschmann et al., 2009). In contrast, carbon and CO_2 are insoluble in mantle minerals at asthenospheric conditions, but can be stored as carbonate minerals in relative oxidizing conditions. Accordingly, various constraints from experimental petrology have long shown that, independently of its concentration in the system, carbon stored as carbonates decreases the solidus of mantle rocks by several hundred degrees (Dasgupta, 2018; Green, 1973; Wallace and Green, 1988; Falloon and Green, 1989; Hammouda and Keshav, 2015).

Geochemical surveys have identified intermingled depleted and enriched mantle regions with H_2O and CO_2 contents ranging from a few ppm to a few wt% (tentative average: 50–250 ppm, Hirschmann, 2010; Marty, 2012; Le Voyer et al., 2017; Shimizu et al., 2019). This is thus expected to produce minute amounts of partial melts in the asthenosphere, of the order of 0.1 vol% to several vol %. Possible variations in pressure and temperature in the asthenospheric mantle are not expected to prevent the presence of incipient melts. Oxidation state could however preclude incipient melting if carbon is present as diamonds rather than oxidized carbon (i.e., carbonate minerals). Oxygen fugacity conditions in the convective upper mantle are however broadly oxidizing enough to enable incipient melting from 50 km down to 200–300 km depth (Brey et al., 1983; Gaillard et al., 2015; Kushiro, 1975; Moussallam et al., 2019; Rohrbach and Schmidt, 2011; Stagno et al., 2013; Wyllie et al., 1983; White and Wyllie, 1992; Zhang et al., 2024). At greater depths, diamonds are expected to prevail, preventing the occurrence of melting (Rohrbach and Schmidt, 2011; Stagno et al., 2013).

Pressure and temperature variations in the asthenosphere are, however, expected to significantly affect the chemical nature and volume fraction of melts produced by CO_2-H_2O-bearing peridotite melting. High-pressure and low-temperature melting tends to produce low-SiO_2 carbon-rich melts (i.e., carbonatites), whereas low-pressure and high-temperature melting tends to produce silicate melts (i.e., basalts). In between, all intermediate compositions are possible (Brey et al., 2008; Dasgupta et al., 2007, 2013b; Gudfinnsson and Presnall, 2005; Massuyeau et al., 2015, 2021). Fig. 9 illustrates this variability in melt composition versus depth for a 'normal' mantle (140 ppm CO_2; 240 ppm H_2O; mantle potential temperature = 1350 °C; see Massuyeau et al., 2021). The

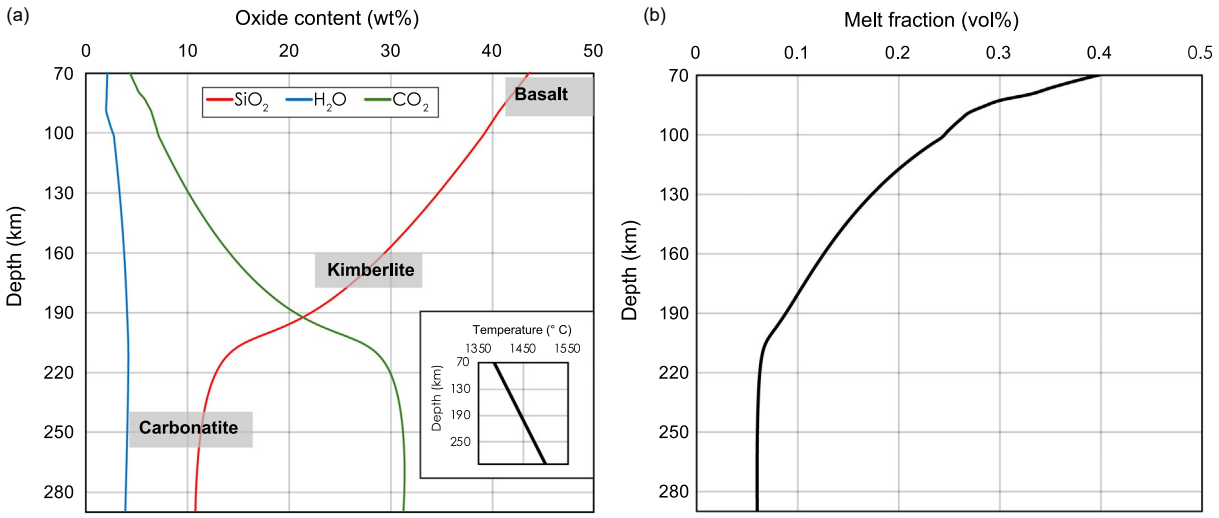

Fig. 8 Composition (a) and volume (b) of magmatic liquids equilibrated in the ambient convective upper mantle in terms of SiO_2, CO_2 and H_2O, as calculated with MAGLAB (Massuyeau et al., 2021). The inset represents the adiabatic profile used for the calculations, considering a normal mantle with 140 ppm CO_2 and 240 ppm H_2O.

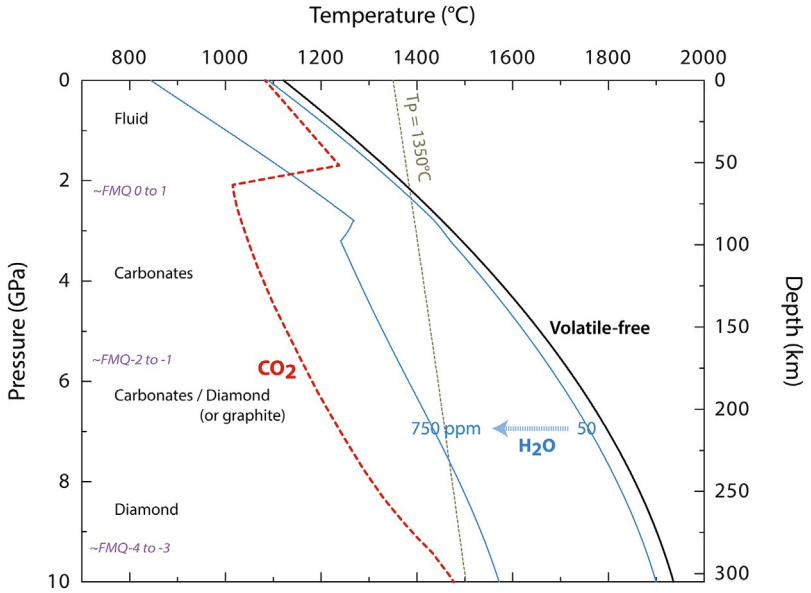

Fig. 9 Comparison of solidus curves for a bulk peridotite composition in volatile-free (bold black line), H_2O-bearing (thin blue line), and CO_2-bearing (dashed red line) systems, presented in a temperature and pressure/depth diagram. Dry solidus after Hirschmann (2000); H_2O-bearing solidus after Hirschmann et al. (2009) for 50 and 750 ppm H_2O; CO_2-bearing solidus from Dasgupta (2013, 2018). The solid mantle adiabatic pressure-temperature path corresponds to a potential temperature of 1350 °C. fO_2 variations versus depth as well as the nature of the various carbon-bearing phases (fluid-carbonate-diamond/graphite) are indicated on the left part of the figure.

melt compositions transition relatively abruptly from carbonatites to basalts in response to small variations in pressure and temperature (Dasgupta et al., 2007, 2013b; Stagno and Frost, 2010). This reflects the strongly non-ideal mixing properties between molten carbonate minerals and molten silicate minerals, which often results in liquid-liquid immiscibility (Brooker and Kjarsgaard, 2011; Freestone and Hamilton, 1980; Massuyeau et al., 2015; Nabyl et al., 2020; Novella et al., 2014). Immiscibility between silicate and carbonate melts is a popular mechanism to explain the formation of many carbonatites found at the surface (Nabyl et al., 2020; Yaxley et al., 2022). It has often been described in experiments conducted at moderate pressure and in variably fractionated, low-temperature alkaline melts (e.g., Nabyl et al., 2020; Weidendorfer et al., 2017). Yet, at asthenospheric pressure-temperature conditions, such immiscibility has only been observed during experimental simulations of partial melting of eclogite or pelitic rocks (Hammouda, 2003; Kiseeva et al., 2012; Litasov and Ohtani, 2010; Thomsen and Schmidt, 2008; Yaxley and Brey, 2004), whereas peridotite melting does not seem to produce immiscible carbonate-silicate melts. Indeed, increasing pressure and water content

tends to decrease the non-ideal carbonate-silicate mixing, enabling the formation of intermediate melt compositions, such as the famous kimberlites, which are in equilibrium with mantle peridotites at depth of 120–250 km (i.e., pressure of 4–8 GPa; Massuyeau et al., 2021; Stamm and Schmidt, 2017).

The chemical composition of these intraplate magmas are diverse, and range from low to high SiO_2 contents, which seemingly reflects the interruption of the adiabatic melting regime at variable depths as illustrated in Fig. 9 (Gudfinnsson and Presnall, 2005; Massuyeau et al., 2021; Tappe et al., 2007). This interruption at variable depth is controlled by the thickness of the (non-convective) lithosphere, which ranges from >200 km beneath cratons, where kimberlites are found, to ~60 km in some oceanic domains, where basanites or alkali basalts are extracted from the convective asthenosphere. Therefore, the combination of the CO_2-driven mantle melting regime and the variable thickness of the lithospheric lids provides a simple explanation of the variability of melt compositions found in intraplate domains.

These melts are produced by adiabatic incipient melting of the asthenosphere and constitute ~0.1 to several vol% of the mantle, depending on the bulk concentrations of CO_2-H_2O and the potential temperature. On top of these thermochemical variables, melt accumulation and mantle compaction processes can affect melt behavior in the mantle (Grégoire et al., 2006; Havlin et al., 2013; Keller et al., 2017; Massuyeau et al., 2021; Soltanmohammadi et al., 2018). These accumulation/migration processes are driven by the peculiar CO_2 mantle melting regimes, which produce a range of melt densities (Agee, 2008; Dobson et al., 1996; Jing and Karato, 2011; Massuyeau et al., 2023; Lange and Carmichael, 1987; Ritter et al., 2020; Sakamaki et al., 2006; Suzuki et al., 1995), viscosities (Behrens and Schulze, 2003; Dingwell, 2007; Dingwell et al., 2022; Dobson et al., 1996; Giordano et al., 2008; Kushiro, 1976; Ritter et al., 2021; Sakamaki et al., 2013; Whittington et al., 2009), and mantle permeabilities (Grégoire et al., 2006; Keller et al., 2017), inducing variable melt buoyancies along the melting column and contributing to volatile redistribution (Bekaert et al., 2021; Dasgupta, 2013; Gaillard et al., 2019; Schettino and Poli, 2020). In many cases however, calculated melt mobilities are lower than 1 cm yr^{-1}, which implies that they are less mobile than the convective mantle itself. It is only in regions where melt fractions are higher than the 'normal' mantle (due to higher CO_2-H_2O or higher potential temperatures) that melt mobility could exceed mantle convection rates (Gaillard et al., 2019) and thus lead to migration/accumulation/extraction processes. In most cases, however, one expects that such incipient melts do not reach the surface and remain trapped at the lithosphere-asthenosphere boundary, causing metasomatism of the lithosphere (see Section "Sub-continental lithospheric mantle").

We do not have in situ analyses of these CO_2-driven melting processes, but electrical and seismic geophysical observations have been used to interpret in near real-time the formation and interconnection of these incipient melts in the asthenosphere (Chantel et al., 2016; Gardés et al., 2020; Hammouda and Laporte, 2000; Kawakatsu et al., 2009; Kawakatsu and Utada, 2017; Laumonier et al., 2017; Minarik and Watson, 1995; Massuyeau et al., 2021; Rychert et al., 2020; Schmerr, 2012; Selway and O'Donnell, 2019; Selway et al., 2019; Sifré et al., 2014; Yoshino et al., 2010, 2018). The interpretation of remote sensing geophysical data is not unequivocal as several geological processes could explain one geophysical proxy. The recently discovered 'petit-spots,' a new class of volcanoes, might represent some leakage of these asthenospheric melts, permitted by the bending and stretching of the oceanic lithosphere prior to enter into subduction (Hirano et al., 2006; Hirano and Machida, 2022). These melts are very CO_2-rich and may indicate incipient melts trapped at the lithosphere-asthenosphere boundary. The seminal question is then how broadly distributed those melts are. This requires the analysis of constraints from experimental petrology, mantle geochemistry, geophysics and an understanding of the occurrence of petit-spots. Hammouda et al. (2021) suggested a global layer of such incipient melts at the lithosphere-asthenosphere boundary, but mantle heterogeneities with carbon-depleted and carbon-enriched regions might speak for local melt enrichments.

Carbon in arc basalts

At subduction zones, arc volcanism transfers some CO_2 from the slab to the Earth's surface. Hydrous silicate melts, which are formed in the mantle wedge, can transport carbon as dissolved carbonate minerals in basaltic melts or in supercritical fluids. Due to large uncertainties and large observed variations in CO_2 fluxes at arcs (Aiuppa et al., 2019; Mason et al., 2017), few estimates of the average CO_2 content of primary arc magmas are available. Outgassing rates of CO_2 at volcanic arcs are indeed highly variable, with the greatest CO_2 emitters involving an overwhelming contribution from thermally destabilized sedimentary carbonate rocks (Aiuppa et al., 2019; Iacono-Marziano et al., 2009; Mason et al., 2017). In a review paper, Plank and Manning (2019) suggested that up to 1 wt% CO_2 could be dissolved and transported in primary arc basalts. This is c. 10 times greater than the average CO_2 contents of primary mid-ocean-ridge basalts. This estimate is indirect as it is based on C/S ratio measured in volcanic gasses, with sulfur (i.e., mostly SO_2 outgassing) being affected by complex processes during transcrustal magma transport (e.g., Mungall et al., 2015). In spite of these unknown, it appears that arc magmas have higher CO_2 concentrations than mid ocean ridge basalts; in terms of total CO_2 fluxes however, emissions from mid-ocean ridges and arcs are, within uncertainties, equivalent (Kelemen and Manning, 2015; Fig. 4). Below we analyze the dynamic of carbon transfer throughout the plumbing system of arc volcanoes.

The solubility of carbon in molten basalts is low and it increases broadly linearly with pressure so that it reaches ~1 wt% at pressure equivalent to the base of the continental crust (~1 GPa, corresponding to 30 km depth; Iacono-Marziano et al., 2012). As most other volatile components (i.e., water, sulfur and halogens) are much more soluble in silicate melts than CO_2, CO_2 is the first volatile component released by magma during their transcrustal journey. Considering furthermore that most rising melt remains locked in the crust and evolves as intrusive bodies, this implies that a large portion of magmatic CO_2 in arcs is outgassed at great depth and must exist as supercritical fluids in the crust. Variation in melt compositions can affect CO_2 solubility and thus the depth of fluid saturations (Iacovino et al., 2021; Wieser et al., 2022). Alkaline primary melts dissolve more CO_2 and thus reach fluid-saturation at shallower depth. If primary arc basalts contain 1 wt% CO_2, depending on melt compositions they will start

forming a supercritical CO_2-rich fluid phase at depths ranging from 30 to 10 km as they ascend through the crust. These CO_2-rich deep fluids rise through the crust in a way that can be decoupled from the magmatic flow (Edmonds et al., 2022). Thus, CO_2 can be released from stagnant melts in the crust (non-eruptive), which is not the case of other magmatic volatile components bar noble gasses. It is thus difficult to estimate and model the global emissions of CO_2 by arc volcanoes since these emissions start from the deep crust, yield surficial fluxes that are very diffused (Chiodini et al., 2005; Werner et al., 2019), and can originate from a combination of intrusive/extrusive events (Edmonds et al., 2022). Using remote satellite data compiled in the period 2005–2015, Fischer et al. (2019) have shown that non-eruptive CO_2 degassing by volcanoes largely exceeds that emitted during volcanic eruptions (30 times more) at planetary scale. This survey also suggests that a significant portion of subducted carbon remains stored in the arc lithosphere, possibly in the form of metasomatic carbonates or at shallower levels, in aquifers. Finally, as suggested by Iacono-Marziano et al. (2009), intrusion of magma in crustal reservoirs hosted by sedimentary carbonate rocks can lead to melt-carbonate interactions massively producing CO_2; Mason et al. (2017) and Aiuppa et al. (2019) provide regional and global evidence for the importance of this mechanism, which adds some complexity in our analyses of the volcanic CO_2 emissions at a planetary scale.

Diamonds as clues on deep and super-deep carbon movements

Diamond is the highest-pressure form of solid carbon and is stable over a depth range of hundreds of kilometers from the upper mantle down to the transition zone and into the lower mantle (Day et al., 2023, and references therein). Diamonds are classified in two very different categories: lithospheric, which formed beneath the cratonic areas between 120 and 130 and 200–220 km depth and sub-lithospheric (also called super-deep diamonds), which formed at depths greater than 280–300 km and down to at least 700–800 km depth within the lower mantle or along the subducting slabs (Nestola et al., 2023; Timmerman et al., 2023). From the above (see Section "Carbon throughout the Earth's mantle"), it is evident that diamonds can form within very different geological environments from the upper to the lower mantle and can therefore have peridotitic and eclogitic origin (and much rarely websteritic; Stachel et al., 2022a). These precious stones are therefore unique minerals that can provide crucial information regarding the movements of carbon within the deep Earth in space and time.

Diamonds may experience long vertical journeys through the Earth's interior, from the deep mantle to the surface, as documented by ultra-deep diamonds recovered at the Earth's surface (Nestola et al., 2018). They can also move horizontally for thousands of kilometers, likely transported on the 'shoulders' of tectonic plates. For example, diamonds emplaced within the North Australian Craton and now found within the Meratus Mountains in Southeast Borneo, Indonesia, testify to horizontal movements of lithospheric carbon in diamonds for thousands of kilometers (Kueter et al., 2016). Lastly, eclogitic diamonds related to subduction zones demonstrate the transfer of carbon from the crust to hundreds of kilometers downwards into the mantle within subducting slabs (Lorenzon et al., 2023).

The possibility of tracking the movements of diamonds within and among different geological environments inside the Earth with diamond ages would represent an unprecedented tool to retrieve key missing tiles of solid carbon geodynamics between 120 and 130 and 700–780 km depth range (Gu et al., 2022; Nestola et al., 2018; Thomson et al., 2016).

Diamonds over (geological) time

Most (if not all) carbon reaching depths greater than 150 km, temperatures above 1320 °C, and oxygen fugacity below −1.8 log units relative to the FMQ buffer within the Earth's mantle precipitate as diamonds (Stagno and Frost, 2010). Diamond precipitation is thought to happen through oxidation or reduction of carbon-bearing species like CO_2 and/or CH_4 carried by fluids and/or melts that interact with the surrounding rocks (Day et al., 2023). This well-accepted formation process is likely occurring at present within the mantle, even if no diamonds are presently being erupted to the Earth's surface. There are no doubts that every day, new diamonds are being produced within the Earth's mantle, but they are unable to reach the surface because deep, kimberlitic eruptions have not occurred on our planet since at least ∼30 Ma (Batumike et al., 2008). Kimberlites are rare, mafic volcanic rocks erupted directly from deep regions of the mantle; these rocks are able to transport diamonds to the Earth's surface and this is why they are intensely explored on cratonic areas worldwide. The reason why kimberlites are no longer erupted is not certain, with recent work suggesting that kimberlitic eruptions are promoted by specific slab flux and subduction angles of tectonic plates (Mather et al., 2023). These authors reconstructed the slab dip angles of subduction segments for the past 170 million years to understand pulses in kimberlitic eruptions, concluding that high subduction rates promote the return flow of fertile mantle, which in turn increases partial melting and magma generation within the deep mantle (Mather et al., 2023). This geodynamical model could help predict when kimberlite eruptions restart on the Earth and, consequently, when new diamonds will be possibly sampled and transported to the Earth's surface. The youngest kimberlite erupted only about 12,000 years ago (Igwisi Hills volcanoes, Tanzania; Brown et al., 2012), but unfortunately did not transport any diamonds. It cannot be excluded that this young kimberlitic volcanic activity can indicate a reactivation of these global geological processes. Although the age of kimberlitic events is known, constraining the age of diamonds in them remains a major scientific challenge.

Diamond ages are constrained through numerous analytical approaches, and span between 3.5 Ga and 220–140 Ma (for a review, see Smit et al., 2022; Fig. 10a); this demonstrates that diamonds have formed over most of the life of our planet. In particular, peridotitic lithospheric diamonds are the oldest known diamonds, while lithospheric eclogitic diamonds are generally not older than 3.0 Ga (Fig. 10; Shirey and Richardson, 2011; Smit et al., 2022). Unfortunately, just a few super-deep diamonds have

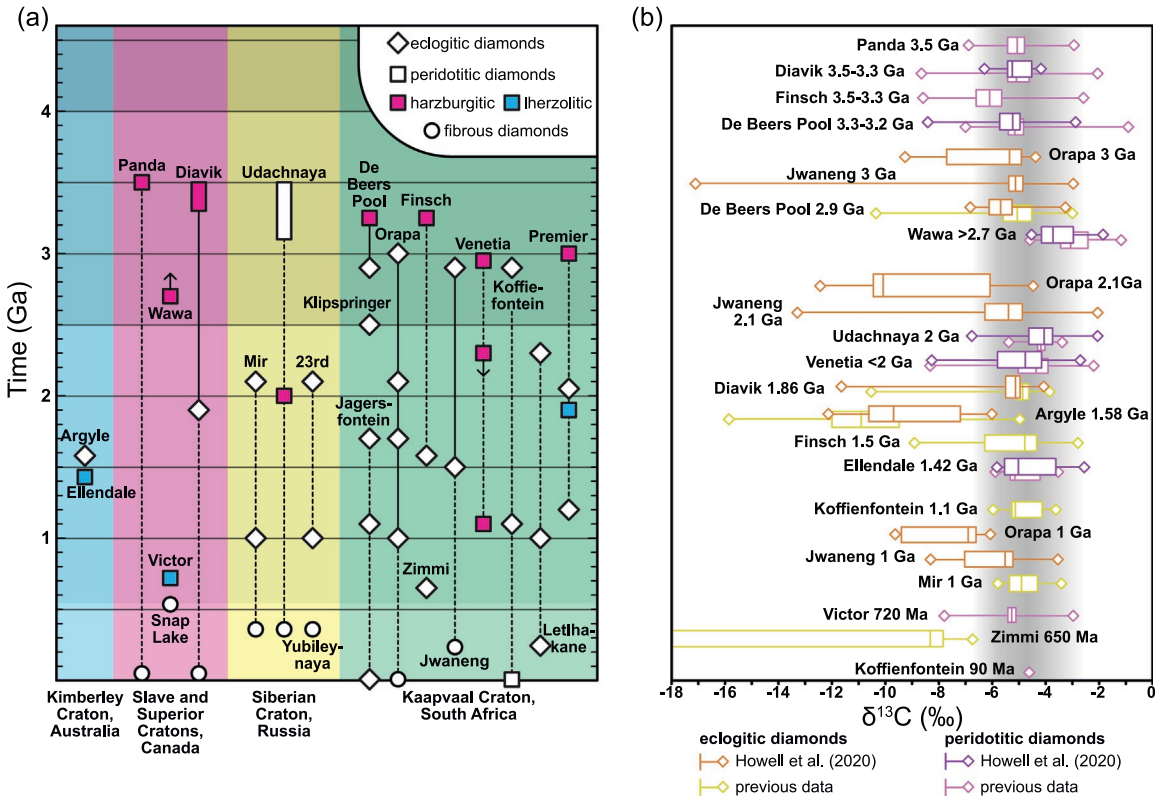

Fig. 10 Diagrams concerning diamond age and isotopic composition. (a) Illustration showing the historical occurrence of diamond growth events on Earth (Fig. 1 in Howell et al., 2020). Diamond symbols represent eclogitic diamond growth events; square symbols represent peridotitic diamond growth events, with additional color differentiation for harzburgitic diamonds (magenta) and lherzolitic diamonds (blue); circle symbols represent fibrous growth events, which constrain the age of the corresponding kimberlite eruption. (b) Box plot showing $\delta^{13}C$ data recorded from diamonds (Fig. 7 in Howell et al., 2020). Redrawn after Howell D, Stachel T, Stern RA, Pearson DG, Nestola F, Hardman MF, Harris JW, Jaques AL, Shirey SB, Cartigny P, Smit KV, Aulbach S, Brenker FE, Jacob DE, Thomassot E, Walter MJ, and Navon O (2020) Deep carbon through time: Earth's diamond record and its implications for carbon cycling and fluid speciation in the mantle. *Geochimica et Cosmochimica Acta* 275: 99–122. https://doi.org/10.1016/j.gca.2020.02.011.

been dated as of today, and based on the existing data, the oldest specimens are not older than 650–700 Ma (Timmerman et al., 2023), therefore appearing to be much younger than the oldest lithospheric diamonds.

Fluxes of deep carbon in diamonds

Once the possibility for deep carbon in diamonds to move vertically and horizontally in the deep Earth is proven, an estimate of how much carbon can be transported by the movement of diamond can be determined. Firstly, it is important to consider that most diamonds (between 98% and 99%) are lithospheric (Stachel and Harris, 2008). This percentage can significantly vary among world localities, as recently reported by Curtolo et al. (2023) who, on a basis of 1069 specimens, show a percentage of lithospheric diamonds of ~95.4% for all reported Canadian diamonds. Only a few localities (Juina, Brazil; Walter et al., 2011; Kankan, Guinea, Stachel et al., 2000a) appear to contain an extremely high amount of super-deep diamonds. All things considered, it can be assumed that 98% is a representative percentage for lithospheric diamonds worldwide, leaving super-deep diamonds to account for the remaining 2%.

Garber et al. (2018), combining seismological, mineralogical and petrological constraints, buoyancy and electrical conductivity data from natural samples, and mass balance constraints for global carbon, proposed diamonds to account for 2 vol% of lithosphere. This most recent estimate can therefore be considered reasonable as it is in broad agreement with other authors reporting 3 vol% (Anand et al., 2004) or 1 vol% (e.g., Peltonen et al., 2002). With the 2 vol% of lithospheric diamonds, Garber et al. (2018) calculated the mass of carbon as diamond being 10^{18} kg (assuming the present-day conditions) for cratonic roots with a shape of an inverted cone with 1000 km base and 50 km height. The authors state that if such roots are similar at the global scale, then the total mass of carbon as diamond would result in about 10^{16} t (10^{22} g), in agreement with estimates of the SCLM carbon budget (Hirschmann, 2018; see Section "Sub-continental lithospheric mantle").

With respect to the quantification proposed by Garber et al. (2018), we can consider that such mass of diamond would only refer to lithospheric diamonds. In addition to this, an additional 2% of super-deep diamonds should be considered, which would

correspond to further 2×10^{14} t, resulting in a final 1.02×10^{16} t worldwide. This amount corresponds to 2% of overall carbon on the planet, or alternatively ~1–10% of carbon in the present-day mantle (Garber et al., 2018: McDonough and Sun, 1995; Dasgupta and Hirschmann, 2010).

Diamonds and their solid carbon inclusions

Laboratory experiments definitively show that a few carbonate minerals can be stable at pressure and temperature conditions at which diamonds form, such as magnesite, aragonite, a few polymorphs of calcite, dolomite, Na-carbonates (e.g., Cerantola et al., 2023; Litasov et al., 2020; Tao et al., 2014, and references therein). Diamonds and their inclusions can provide important information as for these solid carbon phases actually exist in the deep Earth.

In both lithospheric and sub-lithospheric diamonds, common inclusions of carbonate minerals such as calcite, magnesite and dolomite have been reported (Brenker et al., 2007; Stachel et al., 2022a). However, other, more rare carbonates have been identified in both lithospheric and sublithospheric diamonds including aragonite (Smith et al., 2022); siderite (Stachel et al., 2000b); nyerereite, $Na_2Ca(CO_3)_2$ (Howell et al., 2012); huntite, $CaMg_3(CO_3)_4$ (Agrosì et al., 2019); nahcolite, $NaHCO_3$ (Kaminsky et al., 2009); eitelite $Na_2Mg(CO_3)_2$ (Kaminsky et al., 2013).

Other carbon-bearing mineral inclusions have also been identified in diamonds in addition to carbonate minerals; these include carbide minerals such as cohenite, Fe_3C (Smith et al., 2016); moissanite, SiC (Kaminsky, 2012); haxonite, $(Fe,Ni)_{23}C_6$ (Kaminsky, 2012). Both carbonate minerals and carbide minerals, however, are not common inclusions in diamonds (they are actually extremely rare) and thus they possibly do not represent a significant fraction of the solid carbon related to diamonds.

Diamonds as trackers of global carbon recycling and geobiological evolution

One of the most intriguing and geologically significant aspects in studying diamonds is the clear evidence that in some instances they show a biotic signature with respect to their carbon isotopic composition (i.e., $\delta^{13}C$), displaying values consistent with a biogenically-derived organic carbon source. A very recent and extensive review on the carbon isotopic compositions as a function of the different regions of diamond formation is provided by Stachel et al. (2022b). These authors report carbon isotopic compositions for 4307 worldwide diamonds, of which 3474 are of known paragenesis (mainly peridotitic versus eclogitic, with the websteritic fraction being extremely limited), and with $\delta^{13}C$ ranging from −41‰ to +2.5‰ (VPDB).

The carbon isotope composition of the mantle, obtained by studying carbonatites, kimberlitic carbonates, mantle xenoliths and volcanic CO_2, is $\delta^{13}C = -5‰$ (Deines, 2002). Most of the 1700 peridotitic diamonds in Stachel et al. (2022b) show $\delta^{13}C$ varying between −2‰ and − 8‰ with the modal abundance centered at −5‰. On the other hand, 1204 eclogitic diamonds analyzed by these authors show a much greater variability: while 50% of these diamonds also show an average value of −5‰ similar to the peridotitic types, the remaining 50% show a variable $\delta^{13}C$ ranging from −10‰ to −41‰, the minimum value mentioned above.

Stachel et al. (2022b) also investigated 209 super-deep diamonds. From this group of diamonds, the so-called asthenospheric-transition zone diamonds (formed between 250 and 660 km depth; 55 samples) show a variability in $\delta^{13}C$ between −28‰ and +0.7‰ with two modes at about −10‰ and −20‰; the 'lower-mantle' diamonds (formed at depth greater than 660 km, 154 samples) show a strong mode at $\delta^{13}C = -5‰$ and a second, weaker mode at about −25‰ (mainly due to the Brazilian diamonds from the Juina locality). The analysis by Stachel et al. (2022b) indicates that peridotitic lithospheric and lower mantle diamonds share the same mantle carbon source. Eclogitic lithospheric diamonds and asthenospheric-transition zone diamonds also share similar values of $\delta^{13}C$ but in this case in addition to values of −5‰ they are also characterized by much lower values of $\delta^{13}C$. It appears clear that in order to search for diamonds showing a biogenic-like signature, we must look among eclogitic and asthenosphere-transition zone diamonds.

The presence of ^{12}C-enriched carbon in diamonds has been an issue debated for many years. Seafloor sediments have been long considered as the most favored crustal carbon source given the similar $\delta^{13}C$ values to surficial sedimentary carbonate minerals ($\delta^{13}C \approx 0‰$) or organic matter ($\delta^{13}C < -20‰$). While sedimentary carbonate and graphitized organic carbon can potentially be retained in slabs and buried to significant depth (Duncan and Dasgupta, 2017), they cannot explain the combined carbon and nitrogen isotopic characteristics of eclogitic diamond. Diamonds formed from organic matter, in which carbon and nitrogen are coupled, should retain the positive $\delta^{15}N$ values of organic matter in subducting sediments (Li et al., 2019); however, most (>60%) ^{13}C-depleted eclogitic diamonds show $\delta^{15}N < 0$ (Cartigny et al., 2014). Furthermore, some eclogitic diamonds display extreme negative $\delta^{15}N$ values, which has not been observed in subducting sediments. Therefore, the leading hypothesis is that the diamonds characterized by ^{12}C-enriched carbon are related to the presence of subducted biotic organic carbon in altered oceanic crust (see Walter et al., 2011, and references therein). This view has been recently supported by Li et al. (2019), who not only show that the altered igneous portion of oceanic crust has a total carbon content similar to that of subducted sediments, but that the $\delta^{13}C$ range of normal and biogenic carbonate and organic matter in altered oceanic crust (from −24‰ to +11‰) is similar to the range observed in diamonds (−41‰ to +3‰). In addition, altered oceanic crusts shows has nitrogen with a highly variable $\delta^{15}N$, assimilated as ammonium ions, into secondary clay minerals during alteration (Li et al., 2019). Clay minerals formed by low temperature (<100 °C) alteration generally show positive $\delta^{15}N$ values and are isotopically similar to organic matter. On the other hand, clay minerals that form by alteration at higher temperatures (>250 °C) show $\delta^{15}N$ as low as −16‰ and are related to the generation of ammonium ions by abiotic N_2 reduction. From these observations, Li et al. (2019) reported three possible carbon and nitrogen reservoirs with distinct isotopic signatures within altered oceanic crust that could mix with the mantle signature ($\delta^{13}C = -5‰$; $\delta^{15}N = -4‰$) to produce the isotopic signatures reflected by most eclogitic and websteritic diamonds. These three reservoirs are: (C1) 'normal carbonate' (negligible organic matter) + ^{15}N-enriched (sedimentary-like) clay ($\delta^{13}C = 0‰$; $\delta^{15}N = 16‰$);

(C2) 'biogenic carbonate' (±OM) + ^{15}N-enriched clay ($\delta^{13}C = -30‰$; $\delta^{15}N = 16‰$); (C3) no carbonate or OM but ^{15}N-depleted clay ($\delta^{15}N < -12‰$).

Howell et al. (2020) performed a large in situ study of the carbon isotope composition of diamond through time. They analyzed 88 peridotitic and 56 eclogitic diamond fragments, with formation ages ranging from the Paleoarchean (maximum age: 3.5 Ga) to the Mesoproterozoic (minimum age: 1.0 Ga; Fig. 10b). This global diamond record revealed no systematic variation with time in the mantle carbon isotope record over 3 billion years, with the modal $\delta^{13}C$ of peridotitic diamonds at $-5 \pm 2‰$ since the earliest diamond growth at 3.5 Ga. This study also revealed a tail toward ^{13}C-depleted carbon in eclogitic diamonds, with its first occurrence in the record from 3.0 Ga onwards, showing no signs of systematic variation through time (Fig. 10b). As reported by the authors, if the low $\delta^{13}C$ carbon signature is related to a biogenic carbon contribution in altered oceanic crust (Li et al., 2019), this would indicate that this contribution has been consistent from at least 3.0 Ga.

Walter et al. (2011) investigated a suite of super-deep diamonds from Juina (Brazil) with $\delta^{13}C$ sometimes variable between about −20‰ and −25‰. These authors clearly state that the carbon from which these diamonds formed "may have been deposited originally within oceanic crust at the seafloor" and that the low values of their $\delta^{13}C$ would indicate a recycled organic source of carbon (Cartigny, 2005). In detail, based on the mineral inclusions found within these diamonds, Walter et al. (2011) indicate that they must have been formed within the lower mantle and suggest that "the carbon was transported as carbonate, some of which would have been isotopically light, having originated as organic carbon".

Walter et al. (2011) is one of the first studies showing that super-deep diamonds could have a ^{12}C-enriched carbon source. The same applies for some worldwide blue diamonds studied by Smith et al. (2018) containing boron and ^{12}C-enriched carbon, which track a surficial and possibly organic carbon source. Doucet et al. (2021) reported similar diamonds related to subduction processes and characterized by carbon organic sources. However, a typical problem when super-deep diamonds are investigated is the determination of their age. At the moment, only a few studies reported the age of super-deep diamonds showing ^{12}C-enriched carbon. Walter et al. (2011) report possible ages for their subduction-related super-deep diamonds close to 100 Ma (Bulanova et al., 2010) and in general it would appear that super-deep diamonds are younger than lithospheric diamonds (Smit et al., 2022). This still remains to be fully understood and a definitive answer will be provided once more super-deep diamond ages will be available.

Secular variation of surficial versus deep carbon reservoirs or steady state?

There has been significant discussion on whether the shallow Earth deep carbon cycle is balanced, i.e., if total subduction fluxes are accounted for by total volcanic degassing (Kelemen and Manning, 2015; Plank and Manning, 2019; Wong et al., 2019; Müller et al., 2022). An analysis of carbon flux balance for inputs to and output from the mantle suggest a steady state regime for the modern era, albeit with large uncertainties. Plank and Manning (2019) concluded that the highly variable speciation and quantity of subducted carbon, the diversity of pressure-temperature paths along slabs, and the possible crustal contamination by various sediments render the assessment of carbon inputs to versus outputs from the mantle highly dependent of the global geodynamic configurations. Connections between the Wilson cycles and global mantle carbon inputs/outputs are thus expected, with some links with the surficial and deep carbon reservoirs formed across the history of planet Earth. As briefly discussed in Section "Origins of deep carbon" Gaillard et al. (2022a) concluded that the mass of surface carbon formed in the early Hadean, once the magma ocean solidified, was identical, within uncertainties, to the present-day mass of surface carbon. This may rather indicate a steady state regime for the inputs to and output from the mantle back to 4.5 Ga. Nevertheless, secular variations in the distribution and amounts of different forms of carbon, such as organic and inorganic carbon, are well documented. To list only a few notable examples, the Great Oxidation Event has imparted substantial redox changes in both surface and deep environments, affecting the stability of different carbon forms; the Cambrian explosion led to a remarkable increase in the productivity of organic carbon (Husson and Peters, 2017); lastly, the Marine Mesozoic Revolution may have marked an unprecedented change in the deposition and accumulation of inorganic carbon in marine carbonates (e.g., Müller et al., 2022; Ridgwell, 2005). Although these secular variations may have not impacted the global fluxes of carbon inputs and outputs, and may have been promoted by deep-Earth processes (Eguchi et al., 2020), their chemical fingerprints can be traced through geological time in the rock record (e.g., Kump et al., 2011; Giuliani et al., 2022).

Modern Earth carbon ingassing and outgassing of the mantle is summarized in Fig. 11. Following Plank and Manning (2019), we select recent published carbon flux values for subducted slab lithological components. In addition, we review recent estimates of carbon outgassing fluxes at tectonic settings. To obtain a total carbon in/outgassing flux, we perform Monte Carlo simulations to obtain a median estimate and uncertainty interval. We randomly select an individual carbon flux estimate from each flux subcategory shown in Fig. 11 (e.g., selecting one of the three subducting oceanic crust carbon estimates), and subsequently randomly sample a carbon flux value from the error range of that estimate (i.e., the range denoted by the error bars in Fig. 11), assuming that the uncertainty is uniformly distributed within that range. An individual estimate for total in/outgassing is thereby obtained from the sum of each individual sampled flux value contributing to carbon in/outgassing. The in/outgassing fluxes presented in Fig. 11 are median values ±2 standard deviations ($n = 100{,}000$).

On a first order we note that our values for in/outgassing are broadly in concordance with Plank and Manning (2019), in that there is rough parity within 2 standard deviations between ingassing and outgassing. However, the ingassing flux we present (107 ± 26 Mt. C yr^{-1}) is slightly larger than the outgassing flux (70 ± 36 Mt. C yr^{-1}). We attribute this to several reasons. Firstly, there is significant uncertainty in all fluxes presented in Fig. 11, thereby complicating an appropriate comparison. We also note that

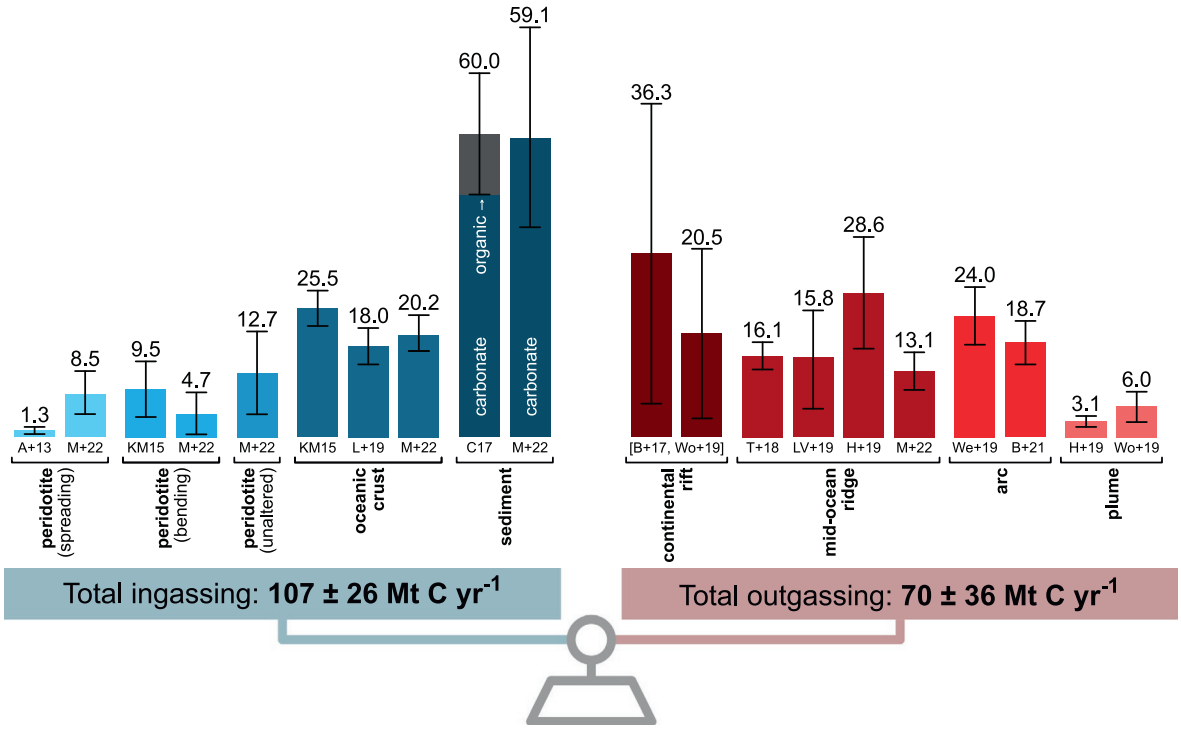

Fig. 11 Figure illustrating the carbon flux balance into (left) and out of (right) the mantle, following Plank and Manning (2019). All values shown are in Mt. C yr^{-1}, and represent the selected value as illustrated by the solid bars. The error bars show uncertainty in the estimate. The total input and output fluxes (±2 standard deviations) are determined by Monte Carlo error propagation assuming uniform uncertainties in individual values and by randomly selecting an estimate within each contribution (see Section "Secular variation of surficial versus deep carbon reservoirs or steady state?" for further details). References, in order of first appearance from left to right: A+13: Alt et al. (2013); M+22: Müller et al. (2022); KM15: Kelemen and Manning (2015); L+19: Li et al. (2019); C17: Clift (2017); [B+17, Wo+19]: the two models of Brune et al. (2017) combined with present-day average rift degassing flux of Wong et al. (2019); H+19: Hauri et al. (2019); T+18: Tucker et al. (2018); LV+19: Le Voyer et al. (2019); We+19: Werner et al. (2019); B+21: Bekaert et al. (2021); H+19: Hauri et al. (2019).

several fluxes are introduced or are revised relative to Plank and Manning (2019), such as the role of peridotite, which is now divided into three categories based on the circumstances of peridotite carbonation. In particular we highlight the introduction of sub-oceanic lithospheric mantle as a reservoir for oceanic carbon, which has only recently been quantified (Keller et al., 2017; Müller et al., 2022). We also consider the large, uncertain rift fluxes of Wong et al. (2019), which are substituted for the intraplate diffuse fluxes of Plank and Manning, but do not account for the degassing of individual rift-related volcanoes in these settings. We also note that estimates of fluxes of solid carbon exhumed in metamorphic rocks is essentially unquantified (Plank and Manning, 2019). Finally, we note that there are several processes during subduction that are not considered here, such as sequestration of carbon into the forearc slab, mantle and crust as carbonate and/or reduced carbon (Barry et al., 2019; Debret et al., 2022; Fullerton et al., 2021; Hu et al., 2021; Piccoli et al., 2019; Vitale Brovarone et al., 2017), which will affect the carbon that is outgassed during volcanism. It therefore remains an open question as to whether the balance between subduction and outgassing remains at parity at the present day (e.g., Kelemen and Manning, 2015), and how this balance may be sustained (if at all) through geological time (e.g., Müller et al., 2022; Wong et al., 2019).

Concluding remarks

Efforts from a broad range of scientific disciplines have provided a substantial contribution to the understanding of carbon reservoirs and movements in the deep Earth. However, despite deep carbon being the largest carbon reservoir on Earth, it remains the least understood. This can be depicted by the large uncertainties in deep carbon reservoirs and fluxes (see Fig. 4), which stems from a partial understanding of the range and distribution of deep forms of carbon and related processes. Considering the two most striking peculiarities of our planet, life and subduction, fundamental questions remain on how, to what extent, and since when life has influenced deep carbon. What is the response time of deep carbon to major surface biogeochemical changes? Can carbon isotope signatures classically interpreted as biotic (or contaminated by biotic carbon materials) be explained by purely abiotic processes? How much and how diverse are the abiotic organics potentially formed in the interior of planet Earth, thereby potentially rejuvenating Gold's theory (Gold, 1992)? Would the answer challenge our models on when the first biogenic carbon reached the convective mantle? To what degree does the lack of a sound quantification of diffuse carbon degassing at the Earth's surface affect

our models of deep carbon inputs and outputs? The current diversification of geobiological approaches to deep carbon studies still suffers from a jungle of semantic obstacles regarding the types of carbon and its origins. Simple terms such as organic/inorganic carbon, abiotic, biotic, or biogenic carbon are used in multiple ways and with very diverse meanings among emerging communities. In turn, this growing diversification of geo-biological disciplines represents a fundamental milestone in the understanding of deep carbon, and how it has been shaping the coevolution of Earth and life since at least 3.8 Ga. It also offers an opportunity to question processes on other planetary bodies, as the James Webb Space Telescope continues to reveal new, detailed observations of exoplanets and their intrinsic processes.

Acknowledgments

This chapter builds on the significant increase in knowledge gained under the auspices of the Deep Carbon Observatory decadal program. The authors thank J. Ague, D. Sverjensky, S. Tumiati I. Martinez, and G. Siron, for stimulating discussions, and A. Turchyn for editorial handling. T. Tsujimori and S. Bernstein are thanked for providing samples. This work is part of the project that has received funding from the European Research Council (ERC) under the European Union's Horizon 2020 research and innovation program to AVB (Grant Agreement No. 864045, acronym DeepSeep), DG (Grant No. 948972-COEVOLVE-ERC-2020-STG), FN (Gtant Agreement No. 307322), and MGP (Grant Agreement No. 101041620 INHERIT). A MUR FARE (acronym DRYNK) grant to AVB and grant and MUR PRIN2022 (Grant Agreement. 20224YR3AZ; acronym HYDECARB) to AVB and DG are also acknowledged. FG acknowledges the GASTON project (ANR-18-CE31-0021). This work has received partial support by funding from the European Union's Horizon Europe research and innovation program under the Marie Skłodowska-Curie grant agreement No 101154017 project SUBCARB to BDP.

References

Abdulla HA, Burdige DJ, and Komada T (2018) Accumulation of deaminated peptides in anoxic sediments of Santa Barbara Basin. *Geochimica et Cosmochimica Acta* 223: 245–258. https://doi.org/10.1016/j.gca.2017.11.021.

Abrajano TA, Sturchio NC, Bohlke JK, Lyon GL, Poreda RJ, and Stevens CM (1988) Methane-hydrogen gas seeps, Zambales Ophiolite, Philippines: Deep or shallow origin? *Chemical Geology* 71(1): 211–222. https://doi.org/10.1016/0009-2541(88)90116-7.

Agard P, Yamato P, Jolivet L, and Burov E (2009) Exhumation of oceanic blueschists and eclogites in subduction zones: Timing and mechanisms. *Earth-Science Reviews* 92(1): 53–79. https://doi.org/10.1016/j.earscirev.2008.11.002.

Agee CB (2008) Static compression of hydrous silicate melt and the effect of water on planetary differentiation. *Earth and Planetary Science Letters* 265(3): 641–654. https://doi.org/10.1016/j.epsl.2007.11.010.

Agrosì G, Tempesta G, Mele D, Caggiani MC, Mangone A, Della Ventura G, Cestelli-Guidi M, Allegretta I, Hutchison MT, Nimis P, and Nestola F (2019) Multiphase inclusions associated with residual carbonate in a transition zone diamond from Juina (Brazil). *Lithos* 350–351: 105279. https://doi.org/10.1016/j.lithos.2019.105279.

Ague JJ (2000) Release of CO_2 from carbonate rocks during regional metamorphism of lithologically heterogeneous crust. *Geology* 28(12): 1123–1126. https://doi.org/10.1130/0091-7613(2000)28<1123:ROCFCR>2.0.CO;2.

Ague JJ (2003) Fluid infiltration and transport of major, minor, and trace elements during regional metamorphism of carbonate rocks, Wepawaug Schist, Connecticut, USA. *American Journal of Science* 303(9): 753–816.

Ague JJ and Nicolescu S (2014) Carbon dioxide released from subduction zones by fluid-mediated reactions. *Nature Geoscience* 7(5): 355–360. https://doi.org/10.1038/ngeo2143.

Aiuppa A, Fischer TP, Plank T, Robidoux P, and Di Napoli R (2017) Along-arc, inter-arc and arc-to-arc variations in volcanic gas CO_2/S_T ratios reveal dual source of carbon in arc volcanism. *Earth-Science Reviews* 168: 24–47. https://doi.org/10.1016/j.earscirev.2017.03.005.

Aiuppa A, Fischer TP, Plank T, and Bani P (2019) CO_2 flux emissions from the Earth's most actively degassing volcanoes, 2005–2015. *Scientific Reports* 9(1): 5442. https://doi.org/10.1038/s41598-019-41901-y.

Albers E, Bach W, Pérez-Gussinyé M, McCammon C, and Frederichs T (2021) Serpentinization-driven H_2 production from continental break-up to mid-ocean ridge spreading: Unexpected high rates at the West Iberia Margin. *Frontiers in Earth Science* 9. https://doi.org/10.3389/feart.2021.673063.

Albers E, Jöns S, Gerdes A, Klügel A, Beier C, Kasemann SA, and Bach W (2023) Timing of carbon uptake by oceanic crust determined by rock reactivity. *Geology* 51(9): 875–879. https://doi.org/10.1130/G51238.1.

Alcott LJ, Walton C, Planavsky NJ, Shorttle O, and Mills BJW (2024) Crustal carbonate build-up as a driver for Earth's oxygenation. *Nature Geoscience* 1–7. https://doi.org/10.1038/s41561-024-01417-1.

Alt JC and Teagle DAH (1999) The uptake of carbon during alteration of ocean crust. *Geochimica et Cosmochimica Acta* 63(10): 1527–1535. https://doi.org/10.1016/S0016-7037(99)00123-4.

Alt JC, Schwarzenbach EM, Früh-Green GL, Shanks WC, Bernasconi SM, Garrido CJ, Crispini L, Gaggero L, Padrón-Navarta JA, and Marchesi C (2013) The role of serpentinites in cycling of carbon and sulfur: Seafloor serpentinization and subduction metamorphism. *Lithos* 178: 40–54. https://doi.org/10.1016/j.lithos.2012.12.006.

Anand M, Taylor LA, Misra KC, Carlson WD, and Sobolev NV (2004) Nature of diamonds in Yakutian eclogites: Views from eclogite tomography and mineral inclusions in diamonds. *Lithos* 77(1): 333–348. https://doi.org/10.1016/j.lithos.2004.03.026.

Andreani M and Ménez B (2019) New perspectives on abiotic organic synthesis and processing during hydrothermal alteration of the oceanic lithosphere. In: Orcutt BN, Daniel I, and Dasgupta R (eds.) *Deep Carbon: Past to Present*, pp. 447–479. Cambridge University Press. https://www.cambridge.org/core/books/deep-carbon/new-perspectives-on-abiotic-organic-synthesis-and-processing-during-hydrothermal-alteration-of-the-oceanic-lithosphere/A5D606A890244645BD109DDA6059349C.

Andreani M, Montagnac G, Fellah C, Hao J, Vandier F, Daniel I, Pisapia C, Galipaud J, Lilley MD, Früh Green GL, Borensztajn S, and Ménez B (2023) The rocky road to organics needs drying. *Nature Communications* 14(1). https://doi.org/10.1038/s41467-023-36038-6. Article 1.

Armstrong K, Frost DJ, McCammon CA, Rubie DC, and Boffa Ballaran T (2019) Deep magma ocean formation set the oxidation state of Earth's mantle. *Science* 365(6456): 903–906. https://doi.org/10.1126/science.aax8376.

Aulbach S and Stagno V (2016) Evidence for a reducing Archean ambient mantle and its effects on the carbon cycle. *Geology* 44(9): 751–754. https://doi.org/10.1130/G38070.1.

Aulbach S, Massuyeau M, and Gaillard F (2017) Origins of cratonic mantle discontinuities: A view from petrology, geochemistry and thermodynamic models. *Lithos* 268–271: 364–382. https://doi.org/10.1016/j.lithos.2016.11.004.

Aulbach S, Massuyeau M, Garber JM, Gerdes A, Heaman LM, Viljoen K, and s. (2020) Ultramafic carbonated melt- and auto-metasomatism in mantle eclogites: Compositional effects and geophysical consequences. *Geochemistry, Geophysics, Geosystems* 21(5): e2019GC008774. https://doi.org/10.1029/2019GC008774.

Badro J (2014) Spin transitions in mantle minerals. *Annual Review of Earth and Planetary Sciences* 42: 231–248. https://doi.org/10.1146/annurev-earth-042711-105304.

Bajgain SK, Mookherjee M, and Dasgupta R (2021) Earth's core could be the largest terrestrial carbon reservoir. *Communications Earth & Environment* 2(1): 1–10. https://doi.org/10.1038/s43247-021-00222-7.

Ballhaus C (1995) Is the upper mantle metal-saturated? *Earth and Planetary Science Letters* 132(1): 75–86. https://doi.org/10.1016/0012-821X(95)00047-G.

Ballhaus C and Ronald Frost B (1994) The generation of oxidized CO_2-bearing basaltic melts from reduced CH_4-bearing upper mantle sources. *Geochimica et Cosmochimica Acta* 58(22): 4931–4940. https://doi.org/10.1016/0016-7037(94)90222-4.

Ballmer MD, Lourenço DL, Hirose K, Caracas R, and Nomura R (2017) Reconciling magma-ocean crystallization models with the present-day structure of the Earth's mantle. *Geochemistry, Geophysics, Geosystems* 18(7): 2785–2806. https://doi.org/10.1002/2017GC006917.

Barbier S, Huang F, Andreani M, Tao R, Hao J, Eleish A, Prabhu A, Minhas O, Fontaine K, Fox P, and Daniel I (2020) A review of H_2, CH_4, and hydrocarbon formation in experimental serpentinization using network analysis. *Frontiers in Earth Science* 8. https://www.frontiersin.org/articles/10.3389/feart.2020.00209.

Barboni M, Boehnke P, Keller B, Kohl IE, Schoene B, Young ED, and McKeegan KD (2017) Early formation of the Moon 4.51 billion years ago. *Science Advances* 3(1): e1602365. https://doi.org/10.1126/sciadv.1602365.

Bar-On YM, Phillips R, and Milo R (2018) The biomass distribution on Earth. *Proceedings of the National Academy of Sciences* 115(25): 6506–6511. https://doi.org/10.1073/pnas.1711842115.

Barry PH, de Moor JM, Giovannelli D, Schrenk M, Hummer DR, Lopez T, Pratt CA, Segura YA, Battaglia A, Beaudry P, Bini G, Cascante M, d'Errico G, di Carlo M, Fattorini D, Fullerton K, Gazel E, González G, Halldórsson SA, et al. (2019) Forearc carbon sink reduces long-term volatile recycling into the mantle. *Nature* 568(7753): 487. https://doi.org/10.1038/s41586-019-1131-5.

Barry PH, De Moor JM, Chiodi A, Aguilera F, Hudak MR, Bekaert DV, Turner SJ, Curtice J, Seltzer AM, Jessen GL, Osses E, Blamey JM, Amenábar MJ, Selci M, Cascone M, Bastianoni A, Nakagawa M, Filipovich R, Bustos E, et al. (2022) The helium and carbon isotope characteristics of the Andean convergent margin. *Frontiers in Earth Science* 10. https://doi.org/10.3389/feart.2022.897267.

Batumike JM, Griffin WL, Belousova EA, Pearson NJ, O'Reilly SY, and Shee SR (2008) LAM-ICPMS U–Pb dating of kimberlitic perovskite: Eocene–Oligocene kimberlites from the Kundelungu Plateau, D.R. Congo. *Earth and Planetary Science Letters* 267(3): 609–619. https://doi.org/10.1016/j.epsl.2007.12.013.

Baumgartner LP and Valley JW (2001) Stable isotope transport and contact metamorphic fluid flow. *Reviews in Mineralogy and Geochemistry* 43(1): 415–467. https://doi.org/10.2138/gsrmg.43.1.415.

Becker JA, Bickle MJ, Galy A, and Holland TJB (2008) Himalayan metamorphic CO_2 fluxes: Quantitative constraints from hydrothermal springs. *Earth and Planetary Science Letters* 265(3): 616–629. https://doi.org/10.1016/j.epsl.2007.10.046.

Behn MD, Kelemen PB, Hirth G, Hacker BR, and Massonne H-J (2011) Diapirs as the source of the sediment signature in arc lavas. *Nature Geoscience* 4(9): 641–646. https://doi.org/10.1038/ngeo1214.

Behrens H and Schulze F (2003) Pressure dependence of melt viscosity in the system $NaAlSi_3O$,-$CaMgSi_2O_6$. *American Mineralogist* 88(8–9): 1351–1363. https://doi.org/10.2138/am-2003-8-919.

Bekaert DV, Turner SJ, Broadley MW, Barnes JD, Halldórsson SA, Labidi J, Wade J, Walowski KJ, and Barry PH (2021) Subduction-driven volatile recycling: A global mass balance. *Annual Review of Earth and Planetary Sciences* 49(1): 37–70. https://doi.org/10.1146/annurev-earth-071620-055024.

Bell DR and Rossman GR (1992) Water in Earth's mantle: The role of nominally anhydrous minerals. *Science* 255(5050): 1391–1397. https://doi.org/10.1126/science.255.5050.1391.

Bénézeth P, Stefánsson A, Gautier Q, and Schott J (2013) Mineral solubility and aqueous speciation under hydrothermal conditions to 300 °C – The carbonate system as an example. *Reviews in Mineralogy and Geochemistry* 76(1): 81–133. https://doi.org/10.2138/rmg.2013.76.4.

Berner RA (1994) GEOCARB II: A revised model of atmospheric CO_2 over phanerozoic time. *American Journal of Science; (United States)* 294(1). https://doi.org/10.2475/ajs.294.1.56.

Berner RA (2004) *The Phanerozoic Carbon Cycle: CO_2 and O_2*. USA: Oxford University Press.

Beyssac O and Rumble D (2014) Graphitic carbon: A ubiquitous, diverse, and useful geomaterial. *Elements* 10(6): 415–420. https://doi.org/10.2113/gselements.10.6.415.

Black BA and Gibson SA (2019) Deep carbon and the life cycle of large igneous provinces. *Elements* 15(5): 319–324. https://doi.org/10.2138/gselements.15.5.319.

Blomgren VJ, Crossey LJ, Karlstrom KE, Fischer TP, and Darrah TH (2019) Hot spring hydrochemistry of the Rio Grande rift in northern New Mexico reveals a distal geochemical connection between Valles Caldera and Ojo Caliente. *Journal of Volcanology and Geothermal Research* 387: 106663. https://doi.org/10.1016/j.jvolgeores.2019.106663.

Bojanova DP, De Anda VY, Haghnegahdar MA, Teske AP, Ash JL, Young ED, Baker BJ, LaRowe DE, and Amend JP (2023) Well-hidden methanogenesis in deep, organic-rich sediments of Guaymas Basin. *The ISME Journal* 17(11): 1828–1838. https://doi.org/10.1038/s41396-023-01485-y.

Bolfan-Casanova N (2005) Water in the Earth's mantle. *Mineralogical Magazine* 69(3): 229–257. https://doi.org/10.1180/0026461056930248.

Bondam J (1992) Graphite occurrences in Greenland: A review. In: *Grønlands Geologiske Undersøgelse. Open file series 92/06*.

Bottinga Y (1969) Calculated fractionation factors for carbon and hydrogen isotope exchange in the system calcite-carbon dioxide-graphite-methane-hydrogen-water vapor. *Geochimica et Cosmochimica Acta* 33(1): 49–64. https://doi.org/10.1016/0016-7037(69)90092-1.

Bouilhol P, Debret B, Inglis EC, Warembourg M, Grocolas T, Rigaudier T, Villeneuve J, and Burton KW (2022) Decoupling of inorganic and organic carbon during slab mantle devolatilisation. *Nature Communications* 13(1): 308. https://doi.org/10.1038/s41467-022-27970-0.

Boulard E, Guyot F, and Fiquet G (2020) High-pressure transformations and stability of Ferromagnesite in the Earth's mantle. In: *Carbon in Earth's Interior*, pp. 105–113. American Geophysical Union (AGU). https://doi.org/10.1002/9781119508229.ch11.

Boutier A, Vitale Brovarone A, Martinez I, Sissmann O, and Mana S (2021) High-pressure serpentinization and abiotic methane formation in metaperidotite from the Appalachian subduction, northern Vermont. *Lithos* 396–397: 106190. https://doi.org/10.1016/j.lithos.2021.106190.

Boutier A, Martinez I, Daniel I, Tumiati S, Siron G, and Vitale Brovarone A (2024a) Thermotopes-COH—A software for carbon isotope modeling and speciation of COH fluids. *Computers & Geosciences* 105533. https://doi.org/10.1016/j.cageo.2024.105533.

Boutier A, Martinez I, Sissmann O, Agostini S, Daniel I, Van Baalen M, Mana S, and Vitale Brovarone A (2024b) Complexity of graphite formation in response to metamorphic methane generation and transformation in an orogenic ultramafic body. *Geochimica et Cosmochimica Acta* 364: 166–183. https://doi.org/10.1016/j.gca.2023.10.028.

Bräuer K, Kämpf H, Niedermann S, and Strauch G (2018) Monitoring of helium and carbon isotopes in the western Eger Rift area (Czech Republic): Relationships with the 2014 seismic activity and indications for recent (2000–2016) magmatic unrest. *Chemical Geology* 482: 131–145. https://doi.org/10.1016/j.chemgeo.2018.02.017.

Brenker FE, Vollmer C, Vincze L, Vekemans B, Szymanski A, Janssens K, Szaloki I, Nasdala L, Joswig W, and Kaminsky F (2007) Carbonates from the lower part of transition zone or even the lower mantle. *Earth and Planetary Science Letters* 260(1): 1–9. https://doi.org/10.1016/j.epsl.2007.02.038.

Brey G, Brice WR, Ellis DJ, Green DH, Harris KL, and Ryabchikov ID (1983) Pyroxene-carbonate reactions in the upper mantle. *Earth and Planetary Science Letters* 62(1): 63–74. https://doi.org/10.1016/0012-821X(83)90071-7.

Brey GP, Bulatov VK, Girnis AV, and Lahaye Y (2008) Experimental melting of carbonated peridotite at 6–10 GPa. *Journal of Petrology* 49(4): 797–821. https://doi.org/10.1093/petrology/egn002.

Broadley MW, Ballentine CJ, Chavrit D, Dallai L, and Burgess R (2016) Sedimentary halogens and noble gases within Western Antarctic xenoliths: Implications of extensive volatile recycling to the sub continental lithospheric mantle. *Geochimica et Cosmochimica Acta* 176: 139–156. https://doi.org/10.1016/j.gca.2015.12.013.

Broadley MW, Bekaert DV, Piani L, Füri E, and Marty B (2022) Origin of life-forming volatile elements in the inner Solar System. *Nature* 611(7935): 245–255. https://doi.org/10.1038/s41586-022-05276-x.

Brodholt J and Badro J (2017) Composition of the low seismic velocity E′ layer at the top of Earth's core. *Geophysical Research Letters* 44(16): 8303–8310. https://doi.org/10.1002/2017GL074261.

Broecker WS (2008) A need to improve reconstructions of the fluctuations in the calcite compensation depth over the course of the Cenozoic. *Paleoceanography* 23(1). https://doi.org/10.1029/2007PA001456.

Brooker RA and Kjarsgaard BA (2011) Silicate–Carbonate Liquid Immiscibility and Phase Relations in the System SiO_2–Na_2O–Al_2O_3–CaO–CO_2 at 0.1–2.5 GPa with Applications to Carbonatite Genesis. *Journal of Petrology* 52(7–8): 1281–1305. https://doi.org/10.1093/petrology/egq081.

Brown RJ, Manya S, Buisman I, Fontana G, Field M, Niocaill CM, Sparks RSJ, and Stuart FM (2012) Eruption of kimberlite magmas: Physical volcanology, geomorphology and age of the youngest kimberlitic volcanoes known on earth (the Upper Pleistocene/Holocene Igwisi Hills volcanoes, Tanzania). *Bulletin of Volcanology* 74(7): 1621–1643. https://doi.org/10.1007/s00445-012-0619-8.

Brune S, Williams SE, and Müller RD (2017) Potential links between continental rifting, CO_2 degassing and climate change through time. *Nature Geoscience* 10(12): 941–946. https://doi.org/10.1038/s41561-017-0003-6.

Brune S, Kolawole F, Olive J-A, Stamps DS, Buck WR, Buiter SJH, Furman T, and Shillington DJ (2023) Geodynamics of continental rift initiation and evolution. *Nature Reviews Earth and Environment* 1–19. https://doi.org/10.1038/s43017-023-00391-3.

Bulanova GP, Walter MJ, Smith CB, Kohn SC, Armstrong LS, Blundy J, and Gobbo L (2010) Mineral inclusions in sublithospheric diamonds from Collier 4 kimberlite pipe, Juina, Brazil: Subducted protoliths, carbonated melts and primary kimberlite magmatism. *Contributions to Mineralogy and Petrology* 160(4): 489–510. https://doi.org/10.1007/s00410-010-0490-6.

Burdige DJ (2005) Burial of terrestrial organic matter in marine sediments: A re-assessment. *Global Biogeochemical Cycles* 19(4). https://doi.org/10.1029/2004GB002368.

Buseck PR and Beyssac O (2014) From Organic Matter to Graphite: Graphitization. *Elements* 10(6): 421–426. https://doi.org/10.2113/gselements.10.6.421.

Caciagli NC and Manning CE (2003) The solubility of calcite in water at 6–16 kbar and 500–800 °C. *Contributions to Mineralogy and Petrology* 146(3): 275–285. https://doi.org/10.1007/s00410-003-0501-y.

Canfield DE and Des Marais DJ (1991) Aerobic sulfate reduction in microbial mats. *Science* 251(5000): 1471–1473. https://doi.org/10.1126/science.11538266.

Cannat M, Fontaine F, and Escartín J (2010) Serpentinization and associated hydrogen and methane fluxes at slow spreading ridges. In: *Diversity of Hydrothermal Systems on Slow Spreading Ocean Ridges*, pp. 241–264. American Geophysical Union (AGU). https://doi.org/10.1029/2008GM000760.

Cappelli L, Wallace PA, Randazzo A, Kamau PM, Njoroge RW, Otieno V, Tubula MS, Mariita NO, Mangi P, and Fontijn K (2023) Diffuse soil CO_2 emissions at rift volcanoes: Structural controls and total budget of the Olkaria Volcanic Complex (Kenya) case study. *Journal of Volcanology and Geothermal Research* 107929. https://doi.org/10.1016/j.jvolgeores.2023.107929.

Capriolo M, Marzoli A, Aradi LE, Ackerson MR, Bartoli O, Callegaro S, Dal Corso J, Ernesto M, Gouvêa Vasconcellos EM, De Min A, Newton RJ, and Szabó C (2021) Massive methane fluxing from magma–sediment interaction in the end-Triassic Central Atlantic Magmatic Province. *Nature Communications* 12(1): 5534. https://doi.org/10.1038/s41467-021-25510-w.

Cartapanis O, Galbraith ED, Bianchi D, and Jaccard SL (2018) Carbon burial in deep-sea sediment and implications for oceanic inventories of carbon and alkalinity over the last glacial cycle. *Climate of the Past* 14(11): 1819–1850. https://doi.org/10.5194/cp-14-1819-2018.

Cartigny P (2005) Stable isotopes and the origin of diamond. *Elements* 1(2): 79–84. https://doi.org/10.2113/gselements.1.2.79.

Cartigny P, Palot M, Thomassot E, and Harris JW (2014) Diamond formation: A stable isotope perspective. *Annual Review of Earth and Planetary Sciences* 42: 699–732. https://doi.org/10.1146/annurev-earth-042711-105259.

Casagli A, Frezzotti ML, Peccerillo A, Tiepolo M, and De Astis G (2017) (Garnet)-spinel peridotite xenoliths from Mega (Ethiopia): Evidence for rejuvenation and dynamic thinning of the lithosphere beneath the southern Main Ethiopian Rift. *Chemical Geology* 455: 231–248. https://doi.org/10.1016/j.chemgeo.2016.11.001.

Cerantola V, Sahle CJ, Petitgirard S, Wu M, Checchia S, Weis C, Di Michiel M, Vaughan GBM, Collings IE, Arató R, Wilke M, Jones AP, Hanfland M, and Tse JS (2023) Tetracarbonates in silicate melts may be at the origin of a deep carbon reservoir in the deep Earth. *Communications Earth & Environment* 4(1): 1–8. https://doi.org/10.1038/s43247-023-00722-8.

Chantel J, Manthilake G, Andrault D, Novella D, Yu T, and Wang Y (2016) Experimental evidence supports mantle partial melting in the asthenosphere. *Science Advances* 2(5): e1600246. https://doi.org/10.1126/sciadv.1600246.

Chariton S, McCammon C, Vasiukov DM, Stekiel M, Kantor A, Cerantola V, Kupenko I, Fedotenko T, Koemets E, Hanfland M, Chumakov AI, and Dubrovinsky L (2020) Seismic detectability of carbonates in the deep Earth: A nuclear inelastic scattering study. *American Mineralogist* 105(3): 325–332. https://doi.org/10.2138/am-2020-6901.

Charlou JL, Donval JP, Konn C, OndréAs H, Fouquet Y, Jean-Baptiste P, and Fourré E (2010) High production and fluxes of H_2 and CH_4 and evidence of abiotic hydrocarbon synthesis by serpentinization in ultramafic-hosted hydrothermal systems on the Mid-Atlantic Ridge. In: *Diversity Of Hydrothermal Systems On Slow Spreading Ocean Ridges*, pp. 265–296. American Geophysical Union (AGU). https://doi.org/10.1029/2008GM000752.

Chen H and Jacobson SA (2022) Impact induced atmosphere-mantle exchange sets the volatile elemental ratios on primitive Earths. *Earth and Planetary Science Letters* 594: 117741. https://doi.org/10.1016/j.epsl.2022.117741.

Chen C, Liu Y, Feng L, Foley SF, Zhou L, Ducea MN, and Hu Z (2018) Calcium isotope evidence for subduction-enriched lithospheric mantle under the northern North China Craton. *Geochimica et Cosmochimica Acta* 238: 55–67. https://doi.org/10.1016/j.gca.2018.06.038.

Chiodini G, Granieri D, Avino R, Caliro S, Costa A, and Werner C (2005) Carbon dioxide diffuse degassing and estimation of heat release from volcanic and hydrothermal systems. *Journal of Geophysical Research: Solid Earth* 110(B8). https://doi.org/10.1029/2004JB003542.

Christensen DH and Ruff LJ (1988) Seismic coupling and outer rise earthquakes. *Journal of Geophysical Research: Solid Earth* 93(B11): 13421–13444. https://doi.org/10.1029/JB093iB11p13421.

Clift PD (2017) A revised budget for Cenozoic sedimentary carbon subduction. *Reviews of Geophysics* 55(1): 97–125. https://doi.org/10.1002/2016RG000531.

Clift PD, Schouten H, and Vannucchi P (2009a) Arc-continent collisions, sediment recycling and the maintenance of the continental crust. *Geological Society, London, Special Publications* 318(1): 75–103. https://doi.org/10.1144/SP318.3.

Clift PD and Vannucchi P (2004) Controls on tectonic accretion versus erosion in subduction zones: Implications for the origin and recycling of the continental crust. *Reviews of Geophysics* 42(2). https://doi.org/10.1029/2003RG000127.

Clift PD, Vannucchi P, and Morgan JP (2009b) Crustal redistribution, crust–mantle recycling and Phanerozoic evolution of the continental crust. *Earth-Science Reviews* 97(1): 80–104. https://doi.org/10.1016/j.earscirev.2009.10.003.

Collins NC, Bebout GE, Angiboust S, Agard P, Scambelluri M, Crispini L, and John T (2015) Subduction zone metamorphic pathway for deep carbon cycling: II. Evidence from HP/UHP metabasaltic rocks and ophicarbonates. *Chemical Geology* 412: 132–150.

Colman DR, Poudel S, Stamps BW, Boyd ES, and Spear JR (2017) The deep, hot biosphere: Twenty-five years of retrospection. *Proceedings of the National Academy of Sciences* 114(27): 6895–6903. https://doi.org/10.1073/pnas.1701266114.

Connolly JAD (1995) Phase diagram methods for graphitic rocks and application to the system C–O–H–FeO–TiO_2–SiO_2. *Contributions to Mineralogy and Petrology* 119(1): 94–116. https://doi.org/10.1007/BF00310720.

Connolly JAD and Cesare B (1993) C-O-H-S fluid composition and oxygen fugacity in graphitic metapelites. *Journal of Metamorphic Geology* 11(3): 379–388. https://doi.org/10.1111/j.1525-1314.1993.tb00155.x.

Conrad CP (2013) The solid Earth's influence on sea level. *Geological Society of America Bulletin* 125(7–8): 1027–1052. https://doi.org/10.1130/B30764.1.

Consuma G, Braga R, Giovanardi T, Bersani D, Konzett J, Lugli F, Mazzucchelli M, and Tropper P (2020) In situ Sr isotope analysis of mantle carbonates: Constraints on the evolution and sources of metasomatic carbon-bearing fluids in a paleo-collisional setting. *Lithos* 354–355: 105334. https://doi.org/10.1016/j.lithos.2019.105334.

Coogan LA and Dosso SE (2015) Alteration of ocean crust provides a strong temperature dependent feedback on the geological carbon cycle and is a primary driver of the Sr-isotopic composition of seawater. *Earth and Planetary Science Letters* 415: 38–46. https://doi.org/10.1016/j.epsl.2015.01.027.

Coogan LA and Gillis KM (2013) Evidence that low-temperature oceanic hydrothermal systems play an important role in the silicate-carbonate weathering cycle and long-term climate regulation. *Geochemistry, Geophysics, Geosystems* 14(6): 1771–1786. https://doi.org/10.1002/ggge.20113.

Coogan LA and Gillis KM (2018) Low-temperature alteration of the seafloor: Impacts on ocean chemistry. *Annual Review of Earth and Planetary Sciences* 46: 21–45. https://doi.org/10.1146/annurev-earth-082517-010027.

Coogan LA, Parrish RR, and Roberts NMW (2016) Early hydrothermal carbon uptake by the upper oceanic crust: Insight from in situ U-Pb dating. *Geology* 44(2): 147–150. https://doi.org/10.1130/G37212.1.

Cook-Kollars J, Bebout GE, Collins NC, Angiboust S, and Agard P (2014) Subduction zone metamorphic pathway for deep carbon cycling: I. Evidence from HP/UHP metasedimentary rocks, Italian Alps. *Chemical Geology* 386: 31–48.

Correale A, Pelorosso B, Rizzo AL, Coltorti M, Italiano F, Bonadiman C, and Giacomoni PP (2019) The nature of the West Antarctic Rift System as revealed by noble gases in mantle minerals. *Chemical Geology* 524: 104–118. https://doi.org/10.1016/j.chemgeo.2019.06.020.

Cottrell E, Kelley KA, Hauri EH, and Le Voyer M (2019) *Mantle Carbon Contents for Mid-Ocean Ridge Segments (1.0) [dataset]*. Interdisciplinary Earth Data Alliance (IEDA). https://doi.org/10.1594/IEDA/111333.

Curray JR (2014) The Bengal depositional system: From rift to orogeny. *Marine Geology* 352: 59–69. https://doi.org/10.1016/j.margeo.2014.02.001.

Curtolo A, Novella D, Logvinova A, Sobolev NV, Davies RM, Day MC, Pamato MG, and Nestola F (2023) Petrology and geochemistry of Canadian diamonds: An up-to-date review. *Earth-Science Reviews* 246: 104588. https://doi.org/10.1016/j.earscirev.2023.104588.

Dasgupta R (2013) Ingassing, storage, and outgassing of terrestrial carbon through geologic time. *Reviews in Mineralogy and Geochemistry* 75(1): 183–229. https://doi.org/10.2138/rmg.2013.75.7.

Dasgupta R (2018) Volatile-bearing partial melts beneath oceans and continents–Where, how much, and of what compositions? *American Journal of Science* 318(1): 141–165. https://doi.org/10.2475/01.2018.06.

Dasgupta R and Hirschmann MM (2006) Melting in the Earth's deep upper mantle caused by carbon dioxide. *Nature* 440(7084): 659–662. https://doi.org/10.1038/nature04612.

Dasgupta R and Hirschmann MM (2010) The deep carbon cycle and melting in Earth's interior. *Earth and Planetary Science Letters* 298(1): 1–13. https://doi.org/10.1016/j.epsl.2010.06.039.

Dasgupta R, Hirschmann MM, and Smith ND (2007) Partial melting experiments of peridotite + CO_2 at 3 GPa and genesis of Alkalic Ocean Island Basalts. *Journal of Petrology* 48(11): 2093–2124. https://doi.org/10.1093/petrology/egm053.

Dasgupta R, Chi H, Shimizu N, Buono AS, and Walker D (2013a) Carbon solution and partitioning between metallic and silicate melts in a shallow magma ocean: Implications for the origin and distribution of terrestrial carbon. *Geochimica et Cosmochimica Acta* 102: 191–212. https://doi.org/10.1016/j.gca.2012.10.011.

Dasgupta R, Mallik A, Tsuno K, Withers AC, Hirth G, and Hirschmann MM (2013b) Carbon-dioxide-rich silicate melt in the Earth's upper mantle. *Nature* 493(7431): 211–215. https://doi.org/10.1038/nature11731.

Day MC, Pamato MG, Novella D, and Nestola F (2023) Imperfections in natural diamond: The key to understanding diamond genesis and the mantle. *La Rivista del Nuovo Cimento* 46(7): 381–471. https://doi.org/10.1007/s40766-023-00045-6.

de Obeso JC, Kelemen PB, Leong JM, Menzel MD, Manning CE, Godard M, Cai Y, Bolge L, Party ODPP, and 1 S. (2022) Deep Sourced Fluids for Peridotite Carbonation in the Shallow Mantle Wedge of a Fossil Subduction Zone: Sr and C Isotope Profiles of OmanDP Hole BT1B. *Journal of Geophysical Research: Solid Earth* 127(1): e2021JB022704. https://doi.org/10.1029/2021JB022704.

Debret B, Ménez B, Walter B, Bouquerel H, Bouilhol P, Mattielli N, Pisapia C, Rigaudier T, and Williams HM (2022) High-pressure synthesis and storage of solid organic compounds in active subduction zones. *Science Advances* 8(37): eabo2397. https://doi.org/10.1126/sciadv.abo2397.

Deines P (2002) The carbon isotope geochemistry of mantle xenoliths. *Earth-Science Reviews* 58(3): 247–278. https://doi.org/10.1016/S0012-8252(02)00064-8.

del Giorgio PA and Duarte CM (2002) Respiration in the open ocean. *Nature* 420(6914): 379–384. https://doi.org/10.1038/nature01165.

Delpech G, Scott JM, Grégoire M, Moine BN, Li D, Liu J, Pearson DG, van der Meer QHA, Waight TE, Michon G, Guillaume D, O'Reilly SY, Cottin J-Y, and Giret A (2023) The subantarctic lithospheric mantle. In: Martin AP and van der Wal W (eds.) *The Geochemistry and Geophysics of the Antarctic Mantle*. Geological Society of London. https://doi.org/10.1144/M56-2020-13.

Demouchy S and Bolfan-Casanova N (2016) Distribution and transport of hydrogen in the lithospheric mantle: A review. *Lithos* 240–243: 402–425. https://doi.org/10.1016/j.lithos.2015.11.012.

Derry LA (2014) Organic Carbon Cycling and the Lithosphere. In: *Treatise on Geochemistry*, pp. 239–249. Elsevier. https://doi.org/10.1016/B978-0-08-095975-7.01014-7.

Derry LA (2022) Carbonate weathering, CO_2 redistribution, and Neogene CCD and pCO_2 evolution. *Earth and Planetary Science Letters* 597: 117801. https://doi.org/10.1016/j.epsl.2022.117801.

Dick HJB, Lin J, and Schouten H (2003) An ultraslow-spreading class of ocean ridge. *Nature* 426(6965): 405–412. https://doi.org/10.1038/nature02128.

Dingwell DB (2007) Properties of rocks and minerals—Diffusion, viscosity, and flow of melts. In: Price GD (ed.) *Treatise on Geophysics, Volume 2: Mineral Physics*, pp. 419–436. Elsevier.

Dingwell DB, Hess K-U, Wilding MC, Brooker RA, Di Genova D, Drewitt JWE, Wilson M, and Weidendorfer D (2022) The glass transition and the non-Arrhenian viscosity of carbonate melts. *American Mineralogist* 107(6): 1053–1064. https://doi.org/10.2138/am-2021-7752.

Dixon JE, Stolper EM, and Holloway JR (1995) An experimental study of water and carbon dioxide solubilities in mid-ocean ridge basaltic liquids. Part I: Calibration and solubility models. *Journal of Petrology* 36(6): 1607–1631. https://doi.org/10.1093/oxfordjournals.petrology.a037267.

Dobson DP, Jones AP, Rabe R, Sekine T, Kurita K, Taniguchi T, Kondo T, Kato T, Shimomura O, and Urakawa S (1996) In-situ measurement of viscosity and density of carbonate melts at high pressure. *Earth and Planetary Science Letters* 143(1): 207–215. https://doi.org/10.1016/0012-821X(96)00139-2.

Doney SC, Fabry VJ, Feely RA, and Kleypas JA (2009) Ocean acidification: The other CO_2 problem. *Annual Review of Marine Science* 1: 169–192. https://doi.org/10.1146/annurev.marine.010908.163834.

Doucet LS, Li Z-X, and Gamal El Dien H (2021) Oceanic and super-deep continental diamonds share a transition zone origin and mantle plume transportation. *Scientific Reports* 11(1): 16958. https://doi.org/10.1038/s41598-021-96286-8.

Ducea MN, Saleeby J, Morrison J, and Valencia VA (2005) Subducted carbonates, metasomatism of mantle wedges, and possible connections to diamond formation: An example from California. *American Mineralogist* 90(5–6): 864–870. https://doi.org/10.2138/am.2005.1670.

Ducea MN, Currie CA, Balica C, Lazar I, Mallik A, Petrescu L, and Vlasceanu M (2022) Diapirism of carbonate platforms subducted into the upper mantle. *Geology* 50(8): 929–933. https://doi.org/10.1130/G50000.1.

Duncan MS and Dasgupta R (2017) Rise of Earth's atmospheric oxygen controlled by efficient subduction of organic carbon. *Nature Geoscience* 10(5): 387–392. https://doi.org/10.1038/ngeo2939.

Dunne JP, Sarmiento JL, and Gnanadesikan A (2007) A synthesis of global particle export from the surface ocean and cycling through the ocean interior and on the seafloor. *Global Biogeochemical Cycles* 21(4). https://doi.org/10.1029/2006GB002907.

Dutkiewicz A, O'Callaghan S, and Müller RD (2016) Controls on the distribution of deep-sea sediments. *Geochemistry, Geophysics, Geosystems* 17(8): 3075–3098. https://doi.org/10.1002/2016GC006428.

Dutkiewicz A, Müller RD, Wang X, O'Callaghan S, Cannon J, and Wright NM (2017) Predicting sediment thickness on vanished ocean crust since 200 Ma. *Geochemistry, Geophysics, Geosystems* 18(12): 4586–4603. https://doi.org/10.1002/2017GC007258.

Dutkiewicz A, Müller RD, Cannon J, Vaughan S, and Zahirovic S (2019) Sequestration and subduction of deep-sea carbonate in the global ocean since the Early Cretaceous. *Geology* 47(1): 91–94. https://doi.org/10.1130/G45424.1.

Dziewonski AM and Anderson DL (1981) Preliminary reference Earth model. *Physics of the Earth and Planetary Interiors* 25(4): 297–356. https://doi.org/10.1016/0031-9201(81)90046-7.

Echigo T and Kimata M (2010) Crystal chemistry and genesis of organic minerals: A review of oxalate and polycyclic aromatic hydrocarbon minerals. *The Canadian Mineralogist* 48(6): 1329–1357. https://doi.org/10.3749/canmin.48.5.1329.

Edmond JM and Huh Y (2003) Non-steady state carbonate recycling and implications for the evolution of atmospheric PCO_2. *Earth and Planetary Science Letters* 216(1): 125–139. https://doi.org/10.1016/S0012-821X(03)00510-7.

Edmonds M, Liu EJ, and Cashman KV (2022) Open-vent volcanoes fuelled by depth-integrated magma degassing. *Bulletin of Volcanology* 84(3): 28. https://doi.org/10.1007/s00445-021-01522-8.

Eguchi J, Seales J, and Dasgupta R (2020) Great Oxidation and Lomagundi events linked by deep cycling and enhanced degassing of carbon. *Nature Geoscience* 13(1): 71–76. https://doi.org/10.1038/s41561-019-0492-6.

Epstein GS, Bebout GE, Angiboust S, and Agard P (2020) Scales of fluid-rock interaction and carbon mobility in the deeply underplated and HP-Metamorphosed Schistes Lustrés, Western Alps. *Lithos* 354: 105229.

Erba E (2006) The first 150 million years history of calcareous nannoplankton: Biosphere–geosphere interactions. *Palaeogeography, Palaeoclimatology, Palaeoecology* 232(2–4): 237–250. https://doi.org/10.1016/j.palaeo.2005.09.013.

Etiope G (2015) *Natural Gas Seepage: The Earth's Hydrocarbon Degassing*. Springer International Publishing. https://doi.org/10.1007/978-3-319-14601-0.

Etiope G and Sherwood Lollar B (2013) Abiotic methane on Earth. *Reviews of Geophysics* 51(2): 276–299. https://doi.org/10.1002/rog.20011.

Etiope G and Whiticar MJ (2019) Abiotic methane in continental ultramafic rock systems: Towards a genetic model. *Applied Geochemistry* 102: 139–152. https://doi.org/10.1016/j.apgeochem.2019.01.012.

Etiope G, Ciotoli G, Schwietzke S, and Schoell M (2019) Gridded maps of geological methane emissions and their isotopic signature. *Earth System Science Data* 11(1): 1–22. https://doi.org/10.5194/essd-11-1-2019.

Evans KA, Bickle MJ, Skelton ADL, Hall M, and Chapman H (2002) Reductive deposition of graphite at lithological margins in East Central Vermont: A Sr, C and O isotope study. *Journal of Metamorphic Geology* 20(8): 781–798. https://doi.org/10.1046/j.1525-1314.2002.00403.x.

Eyssautier-Chuine S, Marin B, Thomachot-Schneider C, Fronteau G, Schneider A, Gibeaux S, and Vazquez P (2016) Simulation of acid rain weathering effect on natural and artificial carbonate stones. *Environmental Earth Sciences* 75(9): 748. https://doi.org/10.1007/s12665-016-5555-z.

Faccenda M (2014) Water in the slab: A trilogy. *Tectonophysics* 614: 1–30. https://doi.org/10.1016/j.tecto.2013.12.020.

Facq S, Daniel I, Montagnac G, Cardon H, and Sverjensky DA (2014) In situ Raman study and thermodynamic model of aqueous carbonate speciation in equilibrium with aragonite under subduction zone conditions. *Geochimica et Cosmochimica Acta* 132: 375–390. https://doi.org/10.1016/j.gca.2014.01.030.

Falkowski PG, Katz ME, Knoll AH, Quigg A, Raven JA, Schofield O, and Taylor FJR (2004) The evolution of modern eukaryotic phytoplankton. *Science* 305(5682): 354–360. https://doi.org/10.1126/science.1095964.

Falkowski PG, Fenchel T, and Delong EF (2008) The microbial engines that drive Earth's biogeochemical cycles. *Science* 320(5879): 1034–1039. https://doi.org/10.1126/science.1153213.

Falloon TJ and Green DH (1989) The solidus of carbonated, fertile peridotite. *Earth and Planetary Science Letters* 94(3): 364–370. https://doi.org/10.1016/0012-821X(89)90153-2.

Fei Y and Brosh E (2014) Experimental study and thermodynamic calculations of phase relations in the Fe–C system at high pressure. *Earth and Planetary Science Letters* 408: 155–162. https://doi.org/10.1016/j.epsl.2014.09.044.

Fein JB and Walther JV (1989) Calcite solubility and speciation in supercritical NaCl-HCl aqueous fluids. *Contributions to Mineralogy and Petrology* 103(3): 317–324. https://doi.org/10.1007/BF00402918.

Ferry JM (1991) Dehydration and decarbonation reactions as a record of fluid infiltration. *Reviews in Mineralogy and Geochemistry* 26(1): 351–393.

Fischer TP, Burnard P, Marty B, Hilton DR, Füri E, Palhol F, Sharp ZD, and Mangasini F (2009) Upper-mantle volatile chemistry at Oldoinyo Lengai volcano and the origin of carbonatites. *Nature* 459(7243): 77–80. https://doi.org/10.1038/nature07977.

Fischer TP, Arellano S, Carn S, Aiuppa A, Galle B, Allard P, Lopez T, Shinohara H, Kelly P, Werner C, Cardellini C, and Chiodini G (2019) The emissions of CO_2 and other volatiles from the world's subaerial volcanoes. *Scientific Reports* 9(1): 1–11. https://doi.org/10.1038/s41598-019-54682-1.

Fischer RA, Cottrell E, Hauri E, Lee KKM, and Le Voyer M (2020) The carbon content of Earth and its core. *Proceedings of the National Academy of Sciences* 117(16): 8743–8749. https://doi.org/10.1073/pnas.1919930117.

Fischer-Gödde M and Kleine T (2017) Ruthenium isotopic evidence for an inner Solar System origin of the late veneer. *Nature* 541(7638): 525–527. https://doi.org/10.1038/nature21045.

Fisher AT (2005) Marine hydrogeology: Recent accomplishments and future opportunities. *Hydrogeology Journal* 13(1): 69–97. https://doi.org/10.1007/s10040-004-0400-y.

Flament N, Bodur ÖF, Williams SE, and Merdith AS (2022) Assembly of the basal mantle structure beneath Africa. *Nature* 603(7903): 846–851. https://doi.org/10.1038/s41586-022-04538-y.

Foley SF (2008) Rejuvenation and erosion of the cratonic lithosphere. *Nature Geoscience* 1(8). https://doi.org/10.1038/ngeo261. Article 8.

Foley SF (2011) A reappraisal of redox melting in the Earth's mantle as a function of tectonic setting and time. *Journal of Petrology* 52(7–8): 1363–1391. https://doi.org/10.1093/petrology/egq061.

Foley SF (2021) Redox melting in the mantle. In: *Magma Redox Geochemistry*, pp. 93–113. American Geophysical Union (AGU). https://doi.org/10.1002/9781119473206.ch5.

Foley SF and Fischer TP (2017) An essential role for continental rifts and lithosphere in the deep carbon cycle. *Nature Geoscience* 10(12): 897–902. https://doi.org/10.1038/s41561-017-0002-7.

Foley SF, Yaxley GM, Rosenthal A, Buhre S, Kiseeva ES, Rapp RP, and Jacob DE (2009) The composition of near-solidus melts of peridotite in the presence of CO_2 and H_2O between 40 and 60 kbar. *Lithos* 112: 274–283. https://doi.org/10.1016/j.lithos.2009.03.020.

Folk RL (1980) *Petrology of Sedimentary Rocks*. Hemphill Publishing Company.

Fratelli G (2023) *Amitsoq Graphite Deposit, South Greenland: Petrological and Geochemical Study of Competing Carbon and Hydrogen Storage Processes*. University of Bologna. Master Thesis, 68 pp.

Freestone IC and Hamilton DL (1980) The role of liquid immiscibility in the genesis of carbonatites? An experimental study. *Contributions to Mineralogy and Petrology* 73(2): 105–117. https://doi.org/10.1007/BF00371385.

Freude C and Blaser M (2016) Carbon isotope fractionation during catabolism and anabolism in acetogenic bacteria growing on different substrates. *Applied and Environmental Microbiology* 82(9): 2728–2737. https://doi.org/10.1128/AEM.03502-15.

Frezzotti ML (2019) Diamond growth from organic compounds in hydrous fluids deep within the Earth. *Nature Communications* 10(1): 4952. https://doi.org/10.1038/s41467-019-12984-y.

Frezzotti ML, Selverstone J, Sharp ZD, and Compagnoni R (2011) Carbonate dissolution during subduction revealed by diamond-bearing rocks from the Alps. *Nature Geoscience* 4(10): 703–706. https://doi.org/10.1038/ngeo1246.

Frondini F, Caliro S, Cardellini C, Chiodini G, Morgantini N, and Parello F (2008) Carbon dioxide degassing from Tuscany and Northern Latium (Italy). *Global and Planetary Change* 61(1): 89–102. https://doi.org/10.1016/j.gloplacha.2007.08.009.

Frost DJ and McCammon CA (2008) The redox state of Earth's mantle. *Annual Review of Earth and Planetary Sciences* 36: 389–420. https://doi.org/10.1146/annurev.earth.36.031207.124322.

Fryer P, Wheat CG, Williams T, Kelley C, Johnson K, Ryan J, Kurz W, Shervais J, Albers E, Bekins B, Debret B, Deng J, Dong Y, Eickenbusch P, Frery E, Ichiyama Y, Johnston R, Kevorkian R, Magalhaes V, et al. (2020) Mariana serpentinite mud volcanism exhumes subducted seamount materials: Implications for the origin of life. *Philosophical Transactions of the Royal Society A: Mathematical, Physical and Engineering Sciences* 378(2165): 20180425. https://doi.org/10.1098/rsta.2018.0425.

Fu S, Yang J, and Lin J-F (2017) Abnormal elasticity of single-crystal magnesiosiderite across the spin transition in Earth's lower mantle. *Physical Review Letters* 118(3): 036402. https://doi.org/10.1103/PhysRevLett.118.036402.

Fuchs G (2011) Alternative pathways of carbon dioxide fixation: Insights into the early evolution of life? *Annual Review of Microbiology* 65: 631–658. https://doi.org/10.1146/annurev-micro-090110-102801.

Fullerton KM, Schrenk MO, Yücel M, Manini E, Basili M, Rogers TJ, Fattorini D, Di Carlo M, d'Errico G, Regoli F, Nakagawa M, Vetriani C, Smedile F, Ramírez C, Miller H, Morrison SM, Buongiorno J, Jessen GL, Steen AD, et al. (2021) Effect of tectonic processes on biosphere–geosphere feedbacks across a convergent margin. *Nature Geoscience* 14(5): 301–306. https://doi.org/10.1038/s41561-021-00725-0.

Gaillard F, Scaillet B, Pichavant M, and Iacono-Marziano G (2015) The redox geodynamics linking basalts and their mantle sources through space and time. *Chemical Geology* 418: 217–233. https://doi.org/10.1016/j.chemgeo.2015.07.030.

Gaillard F, Sator N, Gardés E, Guillot B, Massuyeau M, Sifré D, Hammouda T, and Richard G (2019) The link between the physical and chemical properties of carbon-bearing melts and their application for geophysical imaging of Earth's mantle. In: Orcutt BN, Daniel I, and Dasgupta R (eds.) *Deep Carbon: Past to Present*, pp. 163–187. Cambridge University Press. https://hal.science/hal-02360784.

Gaillard F, Bouhifd MA, Füri E, Malavergne V, Marrocchi Y, Noack L, Ortenzi G, Roskosz M, and Vulpius S (2021) The diverse planetary ingassing/outgassing paths produced over billions of years of magmatic activity. *Space Science Reviews* 217(1): 22. https://doi.org/10.1007/s11214-021-00802-1.

Gaillard F, Bernadou F, Roskosz M, Bouhifd MA, Marrocchi Y, Iacono-Marziano G, Moreira M, Scaillet B, and Rogerie G (2022a) Redox controls during magma ocean degassing. *Earth and Planetary Science Letters* 577: 117255. https://doi.org/10.1016/j.epsl.2021.117255.

Gaillard F, Malavergne V, Bouhifd MA, and Rogerie G (2022b) A speciation model linking the fate of carbon and hydrogen during core – magma ocean equilibration. *Earth and Planetary Science Letters* 577: 117266. https://doi.org/10.1016/j.epsl.2021.117266.

Gaillardet J, Dupré B, Louvat P, and Allègre CJ (1999) Global silicate weathering and CO_2 consumption rates deduced from the chemistry of large rivers. *Chemical Geology* 159(1): 3–30. https://doi.org/10.1016/S0009-2541(99)00031-5.

Galvez ME, Beyssac O, Martinez I, Benzerara K, Chaduteau C, Malvoisin B, and Malavieille J (2013) Graphite formation by carbonate reduction during subduction. *Nature Geoscience* 6(6): 473–477. https://doi.org/10.1038/ngeo1827.

Galvez ME, Fischer WW, Jaccard SL, and Eglinton TI (2020) Materials and pathways of the organic carbon cycle through time. *Nature Geoscience* 13(8): 535–546. https://doi.org/10.1038/s41561-020-0563-8.

Galy V, France-Lanord C, Beyssac O, Faure P, Kudrass H, and Palhol F (2007) Efficient organic carbon burial in the Bengal fan sustained by the Himalayan erosional system. *Nature* 450: 407.

Galy V, Beyssac O, France-Lanord C, and Eglinton T (2008) Recycling of graphite during Himalayan erosion: A geological stabilization of carbon in the crust. *Science* 322(5903): 943–945. https://doi.org/10.1126/science.1161408.

Ganino C and Arndt NT (2009) Climate changes caused by degassing of sediments during the emplacement of large igneous provinces. *Geology* 37(4): 323–326. https://doi.org/10.1130/G25325A.1.

Gao S, Luo T-C, Zhang B-R, Zhang H-F, Han Y, Zhao Z-D, and Hu Y-K (1998) Chemical composition of the continental crust as revealed by studies in East China. *Geochimica et Cosmochimica Acta* 62(11): 1959–1975. https://doi.org/10.1016/S0016-7037(98)00121-5.

Garber JM, Maurya S, Hernandez J-A, Duncan MS, Zeng L, Zhang HL, Faul U, McCammon C, Montagner J-P, Moresi L, Romanowicz BA, Rudnick RL, and Stixrude L (2018) Multidisciplinary constraints on the abundance of diamond and eclogite in the Cratonic lithosphere. *Geochemistry, Geophysics, Geosystems* 19(7): 2062–2086. https://doi.org/10.1029/2018GC007534.

Gardés E, Laumonier M, Massuyeau M, and Gaillard F (2020) Unravelling partial melt distribution in the oceanic low velocity zone. *Earth and Planetary Science Letters* 540: 116242. https://doi.org/10.1016/j.epsl.2020.116242.

Garnero EJ, McNamara AK, and Shim S-H (2016) Continent-sized anomalous zones with low seismic velocity at the base of Earth's mantle. *Nature Geoscience* 9(7): 481–489. https://doi.org/10.1038/ngeo2733.

Gernon TM, Hincks TK, Merdith AS, Rohling EJ, Palmer MR, Foster GL, Bataille CP, and Müller RD (2021) Global chemical weathering dominated by continental arcs since the mid-Palaeozoic. *Nature Geoscience* 14(9). https://doi.org/10.1038/s41561-021-00806-0. Article 9.

Gernon TM, Barr R, Fitton JG, Hincks TK, Keir D, Longman J, Merdith AS, Mitchell RN, and Palmer MR (2022) Transient mobilization of subcrustal carbon coincident with Palaeocene–Eocene Thermal Maximum. *Nature Geoscience* 15(7). https://doi.org/10.1038/s41561-022-00967-6. Article 7.

Gibson SA and McKenzie D (2023) On the role of Earth's lithospheric mantle in global volatile cycles. *Earth and Planetary Science Letters* 602: 117946. https://doi.org/10.1016/j.epsl.2022.117946.

Gibson SA, Rooks EE, Day JA, Petrone CM, and Leat PT (2020) The role of sub-continental mantle as both "sink" and "source" in deep Earth volatile cycles. *Geochimica et Cosmochimica Acta* 275: 140–162. https://doi.org/10.1016/j.gca.2020.02.018.

Giggenbach WF (1996) Chemical Composition of Volcanic Gases. In: Scarpa R and Tilling RI (eds.) *Monitoring and Mitigation of Volcano Hazards*, pp. 221–256. Springer. https://doi.org/10.1007/978-3-642-80087-0_7.

Gilbert PUPA, Bergmann KD, Boekelheide N, Tambutté S, Mass T, Marin F, Adkins JF, Erez J, Gilbert B, Knutson V, Cantine M, Hernández JO, and Knoll AH (2022) Biomineralization: Integrating mechanism and evolutionary history. *Science Advances* 8(10): eabl9653. https://doi.org/10.1126/sciadv.abl9653.

Gillis KM and Coogan LA (2011) Secular variation in carbon uptake into the ocean crust. *Earth and Planetary Science Letters* 302(3): 385–392. https://doi.org/10.1016/j.epsl.2010.12.030.

Giordano D, Russell JK, and Dingwell DB (2008) Viscosity of magmatic liquids: A model. *Earth and Planetary Science Letters* 271(1): 123–134. https://doi.org/10.1016/j.epsl.2008.03.038.

Giovannelli D, Barry PH, Bekaert DV, Chiodi A, Cordone A, Jessen GL, Lloyd KG, de Moor JM, Morrison SM, Schrenk MO, and Brovarone AV (2021) Subsurface life can modify volatile cycling on a planetary scale. *Journal of the Italian Astronomical Society* 92(2): 60. http://sait.oat.ts.astro.it/MSAIt920221/PDF/2021MmSAI..2...60G.pdf.

Giovannelli D, Barry PH, de Moor JM, Jessen GL, Schrenk MO, and Lloyd KG (2022) Sampling across large-scale geological gradients to study geosphere–biosphere interactions. *Frontiers in Microbiology* 13. https://doi.org/10.3389/fmicb.2022.998133.

Giuliani A, Drysdale RN, Woodhead JD, Planavsky NJ, Phillips D, Hergt J, Griffin WL, Oesch S, Dalton H, and Davies GR (2022) Perturbation of the deep-Earth carbon cycle in response to the Cambrian Explosion. *Science Advances* 8(9): eabj1325. https://doi.org/10.1126/sciadv.abj1325.

Giuntoli F, Menegon L, Siron G, Cognigni F, Leroux H, Compagnoni R, Rossi M, and Vitale Brovarone A (2024) Methane-hydrogen-rich fluid migration may trigger seismic failure in subduction zones at forearc depths. *Nature Communications* 15(1). https://doi.org/10.1038/s41467-023-44641-w. Article 1.

Glover PWJ (1996) Graphite and electrical conductivity in the lower continental crust: A review. *Physics and Chemistry of the Earth* 21(4): 279–287. https://doi.org/10.1016/S0079-1946(97)00049-9.

Gold T (1992) The deep, hot biosphere. *Proceedings of the National Academy of Sciences* 89(13): 6045–6049. https://doi.org/10.1073/pnas.89.13.6045.

Gonzalez CM and Gorczyk W (2017) Decarbonation in an intracratonic setting: Insight from petrological-thermomechanical modeling. *Journal of Geophysical Research: Solid Earth* 122(8): 5992–6013. https://doi.org/10.1002/2017JB014051.

Gonzalez CM, Gorczyk W, and Gerya TV (2016) Decarbonation of subducting slabs: Insight from petrological–thermomechanical modeling. *Gondwana Research* 36: 314–332. https://doi.org/10.1016/j.gr.2015.07.011.

Gorczyk W and Gonzalez CM (2019) CO_2 degassing and melting of metasomatized mantle lithosphere during rifting – Numerical study. *Geoscience Frontiers* 10(4): 1409–1420. https://doi.org/10.1016/j.gsf.2018.11.003.

Gorman PJ, Kerrick DM, Connolly J, and a. D. (2006) Modeling open system metamorphic decarbonation of subducting slabs. *Geochemistry, Geophysics, Geosystems* 7(4). https://doi.org/10.1029/2005GC001125.

Grant SW (1990) Shell structure and distribution of Cloudina, a potential index fossil for the terminal Proterozoic. *American Journal of Science* 290-A: 261–294.

Green DH (1973) Experimental melting studies on a model upper mantle composition at high pressure under water-saturated and water-undersaturated conditions. *Earth and Planetary Science Letters* 19(1): 37–53. https://doi.org/10.1016/0012-821X(73)90176-3.

Grégoire M, Moine BN, O'Reilly SY, Cottin JY, and Giret A (2000) Trace Element Residence and Partitioning in Mantle Xenoliths Metasomatized by Highly Alkaline, Silicate- and Carbonate-rich Melts (Kerguelen Islands, Indian Ocean). *Journal of Petrology* 41(4): 477–509. https://doi.org/10.1093/petrology/41.4.477.

Grégoire M, Rabinowicz M, and Janse AJA (2006) Mantle mush compaction: A key to understand the mechanisms of concentration of kimberlite melts and initiation of swarms of kimberlite dykes. *Journal of Petrology* 47(3): 631–646. https://doi.org/10.1093/petrology/egi090.

Grevemeyer I, Kaul N, Villinger H, and Weigel W (1999) Hydrothermal activity and the evolution of the seismic properties of upper oceanic crust. *Journal of Geophysical Research: Solid Earth* 104(B3): 5069–5079. https://doi.org/10.1029/1998JB900096.

Grevemeyer I, Ranero CR, and Ivandic M (2018) Structure of oceanic crust and serpentinization at subduction trenches. *Geosphere* 14(2): 395–418. https://doi.org/10.1130/GES01537.1.

Grevemeyer I, Ranero CR, Papenberg C, Sallares V, Bartolomé R, Prada M, Batista L, and Neres M (2022) The continent-to-ocean transition in the Iberia Abyssal Plain. *Geology* 50(5): 615–619. https://doi.org/10.1130/G49753.1.

Grew ES (1974) Carbonaceous material in some metamorphic rocks of New England and other areas. *The Journal of Geology* 82(1): 50–73.

Grewal DS, Dasgupta R, Sun C, Tsuno K, and Costin G (2019) Delivery of carbon, nitrogen, and sulfur to the silicate Earth by a giant impact. *Science Advances* 5(1): eaau3669. https://doi.org/10.1126/sciadv.aau3669.

Groppo C, Rolfo F, Castelli D, and Connolly JAD (2013) Metamorphic CO_2 production from calc-silicate rocks via garnet-forming reactions in the CFAS–H_2O–CO_2 system. *Contributions to Mineralogy and Petrology* 166(6): 1655–1675. https://doi.org/10.1007/s00410-013-0947-5.

Groppo C, Rolfo F, Castelli D, and Mosca P (2017) Metamorphic CO_2 production in collisional orogens: Petrological constraints from phase diagram modeling of Himalayan, scapolite-bearing, calc-silicate rocks in the NKC(F)MAS(T)-HC system. *Journal of Petrology* 58(1): 53–83. https://doi.org/10.1093/petrology/egx005.

Grozeva NG, Klein F, Seewald JS, and Sylva SP (2017) Experimental study of carbonate formation in oceanic peridotite. *Geochimica et Cosmochimica Acta* 199: 264–286. https://doi.org/10.1016/j.gca.2016.10.052.

Grozeva NG, Klein F, Seewald JS, and Sylva SP (2020) Chemical and isotopic analyses of hydrocarbon-bearing fluid inclusions in olivine-rich rocks. *Philosophical Transactions of the Royal Society A: Mathematical, Physical and Engineering Sciences* 378(2165): 20180431. https://doi.org/10.1098/rsta.2018.0431.

Gu T, Pamato MG, Novella D, Alvaro M, Fournelle J, Brenker FE, Wang W, and Nestola F (2022) Hydrous peridotitic fragments of Earth's mantle 660 km discontinuity sampled by a diamond. *Nature Geoscience* 15(11): 950–954. https://doi.org/10.1038/s41561-022-01024-y.

Gudfinnsson GH and Presnall DC (2005) Continuous gradations among primary carbonatitic, kimberlitic, melilititic, basaltic, picritic, and komatiitic melts in equilibrium with garnet lherzolite at 3–8 GPa. *Journal of Petrology* 46(8): 1645–1659. https://doi.org/10.1093/petrology/egi029.

Guerrero-Cruz S, Vaksmaa A, Horn MA, Niemann H, Pijuan M, and Ho A (2021) Methanotrophs: Discoveries, environmental relevance, and a perspective on current and future applications. *Frontiers in Microbiology* 12. https://doi.org/10.3389/fmicb.2021.678057.

Guillot S, Hattori K, Agard P, Schwartz S, and Vidal O (2009) Exhumation Processes in Oceanic and Continental Subduction Contexts: A Review. In: Lallemand S and Funiciello F (eds.) *Subduction Zone Geodynamics*, pp. 175–205. Springer. https://doi.org/10.1007/978-3-540-87974-9_10.

Halama R and Bebout G (2021) Earth's nitrogen and carbon cycles. *Space Science Reviews* 217(3): 45.

Hammouda T (2003) High-pressure melting of carbonated eclogite and experimental constraints on carbon recycling and storage in the mantle. *Earth and Planetary Science Letters* 214(1): 357–368. https://doi.org/10.1016/S0012-821X(03)00361-3.

Hammouda T and Keshav S (2015) Melting in the mantle in the presence of carbon: Review of experiments and discussion on the origin of carbonatites. *Chemical Geology* 418: 171–188. https://doi.org/10.1016/j.chemgeo.2015.05.018.

Hammouda T and Laporte D (2000) Ultrafast mantle impregnation by carbonatite melts. *Geology* 28(3): 283–285. https://doi.org/10.1130/0091-7613(2000)28<283:UMIBCM>2.0.CO;2.

Hammouda T, Manthilake G, Goncalves P, Chantel J, Guignard J, Crichton W, and Gaillard F (2021) Is there a global carbonate layer in the oceanic mantle? *Geophysical Research Letters* 48(2): e2020GL089752. https://doi.org/10.1029/2020GL089752.

Harada H and Tsujimori T (2024) Methane genesis within olivine-hosted fluid inclusions in dolomitic marble of the Hida Belt, Japan. *Progress in Earth and Planetary Science* 11(1): 6. https://doi.org/10.1186/s40645-024-00609-y.

Hartmann J, Dürr HH, Moosdorf N, Meybeck M, and Kempe S (2012) The geochemical composition of the terrestrial surface (without soils) and comparison with the upper continental crust. *International Journal of Earth Sciences* 101(1): 365–376. https://doi.org/10.1007/s00531-010-0635-x.

Hauri EH, Cottrell E, Kelley KA, Tucker JM, Shimizu K, Le Voyer M, Marske JP, and Saal AE (2019) Carbon in the convecting mantle. In: Orcutt B, Dasgupta R, and Daniel I (eds.) *Deep Carbon: Past to Present*. Cambridge University Press.

Havlin C, Parmentier EM, and Hirth G (2013) Dike propagation driven by melt accumulation at the lithosphere–asthenosphere boundary. *Earth and Planetary Science Letters* 376: 20–28. https://doi.org/10.1016/j.epsl.2013.06.010.

Hay Mele B, Monticelli M, Leone S, Bastoni D, Barosa B, Cascone M, Migliaccio F, Montemagno F, Ricciardelli A, Tonietti L, Rotundi A, Cordone A, and Giovannelli D (2023) Oxidoreductases and metal cofactors in the functioning of the Earth. *Essays in Biochemistry* 67(4): 653–670. https://doi.org/10.1042/EBC20230012.

Hayes JM and Waldbauer JR (2006) The carbon cycle and associated redox processes through time. *Philosophical Transactions of the Royal Society of London B: Biological Sciences* 361(1470): 931–950. https://doi.org/10.1098/rstb.2006.1840.

Hayes CT, Costa KM, Anderson RF, Calvo E, Chase Z, Demina LL, Dutay J-C, German CR, Heimbürger-Boavida L-E, Jaccard SL, Jacobel A, Kohfeld KE, Kravchishina MD, Lippold J, Mekik F, Missiaen L, Pavia FJ, Paytan A, Pedrosa-Pamies R, et al. (2021) Global ocean sediment composition and burial flux in the deep sea. *Global Biogeochemical Cycles* 35(4): e2020GB006769. https://doi.org/10.1029/2020GB006769.

Hazen RM and Schiffries CM (2013) Why deep carbon? *Reviews in Mineralogy and Geochemistry* 75(1): 1–6. https://doi.org/10.2138/rmg.2013.75.1.

Hazen RM, Bromberg Y, Downs RT, Eleish A, Falkowski PG, Fox P, Giovannelli D, Hummer DR, Hystad G, Golden JJ, Knoll AH, Li C, Liu C, Moore EK, Morrison SM, Muscente AD, Prabhu A, Ralph J, Rucker MY, and Zhong H (2019) Deep carbon through deep time: Data-driven insights. In: Orcutt BN, Daniel I, and Dasgupta R (eds.) *Deep Carbon: Past to Present*, pp. 620–652. Cambridge University Press. https://www.cambridge.org/core/books/deep-carbon/deep-carbon-through-deep-time/F728FCC10F909246FD0FD9923FB6F4DC.

Hazen RM, Downs RT, Jones AP, and Kah L (2013a) Carbon mineralogy and crystal chemistry. *Reviews in Mineralogy and Geochemistry* 75(1): 7–46. https://doi.org/10.2138/rmg.2013.75.2.

Hazen RM, Downs RT, Kah L, and Sverjensky D (2013b) Carbon mineral evolution. *Reviews in Mineralogy and Geochemistry* 75(1): 79–107. https://doi.org/10.2138/rmg.2013.75.4.

Helffrich G and Kaneshima S (2010) Outer-core compositional stratification from observed core wave speed profiles. *Nature* 468(7325): 807–810. https://doi.org/10.1038/nature09636.

Herviou C, Verlaguet A, Agard P, Locatelli M, Raimbourg H, Lefeuvre B, and Dubacq B (2021) Along-dip variations of subduction fluids: The 30–80 km depth traverse of the Schistes Lustrés complex (Queyras-Monviso, W. Alps). *Lithos* 394–395: 106168. https://doi.org/10.1016/j.lithos.2021.106168.

Heuer VB, Inagaki F, Morono Y, Kubo Y, Spivack AJ, Viehweger B, Treude T, Beulig F, Schubotz F, Tonai S, Bowden SA, Cramm M, Henkel S, Hirose T, Homola K, Hoshino T, Ijiri A, Imachi H, Kamiya N, et al. (2020) Temperature limits to deep subseafloor life in the Nankai Trough subduction zone. *Science* 370(6521): 1230–1234. https://doi.org/10.1126/science.abd7934.

Hier-Majumder S and Hirschmann MM (2017) The origin of volatiles in the Earth's mantle. *Geochemistry, Geophysics, Geosystems* 18(8): 3078–3092. https://doi.org/10.1002/2017GC006937.

Higgins JA, Fischer WW, and Schrag DP (2009) Oxygenation of the ocean and sediments: Consequences for the seafloor carbonate factory. *Earth and Planetary Science Letters* 284(1): 25–33. https://doi.org/10.1016/j.epsl.2009.03.039.

Hirano N and Machida S (2022) The mantle structure below petit-spot volcanoes. *Communications Earth & Environment* 3(1): 1–11. https://doi.org/10.1038/s43247-022-00438-1.

Hirano N, Takahashi E, Yamamoto J, Abe N, Ingle SP, Kaneoka I, Hirata T, Kimura J-I, Ishii T, Ogawa Y, Machida S, and Suyehiro K (2006) Volcanism in response to plate flexure. *Science* 313(5792): 1426–1428. https://doi.org/10.1126/science.1128235.

Hirose K, Wood B, and Vočadlo L (2021) Light elements in the Earth's core. *Nature Reviews Earth and Environment* 2(9): 645–658. https://doi.org/10.1038/s43017-021-00203-6.

Hirschmann MM (2000) Mantle solidus: Experimental constraints and the effects of peridotite composition. *Geochemistry, Geophysics, Geosystems* 1(10). https://doi.org/10.1029/2000GC000070.

Hirschmann MM (2010) Partial melt in the oceanic low velocity zone. *Physics of the Earth and Planetary Interiors* 179(1): 60–71. https://doi.org/10.1016/j.pepi.2009.12.003.

Hirschmann MM (2016) Constraints on the early delivery and fractionation of Earth's major volatiles from C/H, C/N, and C/S ratios. *American Mineralogist* 101(3): 540–553. https://doi.org/10.2138/am-2016-5452.

Hirschmann MM (2018) Comparative deep Earth volatile cycles: The case for C recycling from exosphere/mantle fractionation of major (H_2O, C, N) volatiles and from H_2O/Ce, CO_2/Ba, and CO_2/Nb exosphere ratios. *Earth and Planetary Science Letters* 502: 262–273. https://doi.org/10.1016/j.epsl.2018.08.023.

Hirschmann MM, Tenner T, Aubaud C, and Withers AC (2009) Dehydration melting of nominally anhydrous mantle: The primacy of partitioning. *Physics of the Earth and Planetary Interiors* 176(1): 54–68. https://doi.org/10.1016/j.pepi.2009.04.001.

Holloway JR (1984) Graphite-CH_4-H_2O-CO_2 equilibria at low-grade metamorphic conditions. *Geology* 12(8): 455–458. https://doi.org/10.1130/0091-7613(1984)12<455:GEALMC>2.0.CO;2.

Howell D, Wood I, Nestola F, Nimis P, and Nasdala L (2012) Inclusions under remnant pressure in diamond: A multi-technique approach. *European Journal of Mineralogy* 24: 563–573. https://doi.org/10.1127/0935-1221/2012/0024-2183.

Howell D, Stachel T, Stern RA, Pearson DG, Nestola F, Hardman MF, Harris JW, Jaques AL, Shirey SB, Cartigny P, Smit KV, Aulbach S, Brenker FE, Jacob DE, Thomassot E, Walter MJ, and Navon O (2020) Deep carbon through time: Earth's diamond record and its implications for carbon cycling and fluid speciation in the mantle. *Geochimica et Cosmochimica Acta* 275: 99–122. https://doi.org/10.1016/j.gca.2020.02.011.

Hu H, Vitale Brovarone A, Zhang L, Piccoli F, Peng W, and Shen T (2021) Retrograde carbon sequestration in orogenic complexes: A case study from the Chinese southwestern Tianshan. *Lithos* 392–393: 106151. https://doi.org/10.1016/j.lithos.2021.106151.

Hu F, Jiang H, Wan B, Ducea MN, Gao L, and Wu FN (2024) Latitude-dependent oxygen fugacity in arc magmas. *Nature Communications* 15: 6050. https://doi.org/10.1038/s41467-024-50337-6.

Huang F, Daniel I, Cardon H, Montagnac G, and Sverjensky DA (2017) Immiscible hydrocarbon fluids in the deep carbon cycle. *Nature Communications* 8(1): 15798. https://doi.org/10.1038/ncomms15798.

Huang F, Barbier S, Tao R, Hao J, Garcia del Real P, Peuble S, Merdith A, Leichnig V, Perrillat J-P, Fontaine K, Fox P, Andreani M, and Daniel I (2021a) Dataset for H_2, CH_4 and organic compounds formation during experimental serpentinization. *Geoscience Data Journal* 8(1): 90–100. https://doi.org/10.1002/gdj3.105.

Huang Y, Nicholson D, Huang B, and Cassar N (2021b) Global estimates of marine gross primary production based on machine learning upscaling of field observations. *Global Biogeochemical Cycles* 35(3): e2020GB006718. https://doi.org/10.1029/2020GB006718.

Huang J, Daniel I, Sverjensky DA, Cardon H, and Montagnac G (2023) Formation of hydrocarbons favored by high pressure at subduction zone conditions. *Chemical Geology* 630: 121489. https://doi.org/10.1016/j.chemgeo.2023.121489.

Hügler M and Sievert SM (2011) Beyond the calvin cycle: Autotrophic carbon fixation in the ocean. *Annual Review of Marine Science* 3: 261–289. https://doi.org/10.1146/annurev-marine-120709-142712.

Hunt JM (1972) Distribution of carbon in crust of Earth. *AAPG Bulletin* 56(11): 2273–2277. https://doi.org/10.1306/819A4206-16C5-11D7-8645000102C1865D.

Hunt JA, Zafu A, Mather TA, Pyle DM, and Barry PH (2017) Spatially variable CO_2 degassing in the main Ethiopian rift: Implications for magma storage, volatile transport, and rift-related emissions. *Geochemistry, Geophysics, Geosystems* 18(10): 3714–3737. https://doi.org/10.1002/2017GC006975.

Husson JM and Peters SE (2017) Atmospheric oxygenation driven by unsteady growth of the continental sedimentary reservoir. *Earth and Planetary Science Letters* 460: 68–75. https://doi.org/10.1016/j.epsl.2016.12.012.

Iacono-Marziano G, Gaillard F, Scaillet B, Pichavant M, and Chiodini G (2009) Role of non-mantle CO_2 in the dynamics of volcano degassing: The Mount Vesuvius example. *Geology* 37(4): 319–322. https://doi.org/10.1130/G25446A.1.

Iacono-Marziano G, Morizet Y, Le Trong E, and Gaillard F (2012) New experimental data and semi-empirical parameterization of H_2O–CO_2 solubility in mafic melts. *Geochimica et Cosmochimica Acta* 97: 1–23. https://doi.org/10.1016/j.gca.2012.08.035.

Iacovino K, Matthews S, Wieser PE, Moore GM, and Bégué F (2021) VESIcal part I: An open-source thermodynamic model engine for mixed volatile (H_2O-CO_2) solubility in silicate melts. *Earth and Space Science* 8(11): e2020EA001584. https://doi.org/10.1029/2020EA001584.

Iddon F and Edmonds M (2020) Volatile-rich magmas distributed through the upper crust in the main Ethiopian rift. *Geochemistry, Geophysics, Geosystems* 21(6): e2019-GC008904. https://doi.org/10.1029/2019GC008904.

Isson TT and Planavsky NJ (2018) Reverse weathering as a long-term stabilizer of marine pH and planetary climate. *Nature* 560(7719): 471–475. https://doi.org/10.1038/s41586-018-0408-4.

Isson TT, Planavsky NJ, Coogan LA, Stewart EM, Ague JJ, Bolton EW, Zhang S, McKenzie NR, and Kump LR (2020) Evolution of the global carbon cycle and climate regulation on Earth. *Global Biogeochemical Cycles* 34(2): e2018GB006061. https://doi.org/10.1029/2018GB006061.

Jackson CG and Gibson SA (2023) Build-up of multiple volatiles in Earth's continental keels: Implications for craton stability. *Earth and Planetary Science Letters* 611: 118134. https://doi.org/10.1016/j.epsl.2023.118134.

Jacobson SA, Morbidelli A, Raymond SN, O'Brien DP, Walsh KJ, and Rubie DC (2014) Highly siderophile elements in Earth's mantle as a clock for the Moon-forming impact. *Nature* 508(7494): 84–87. https://doi.org/10.1038/nature13172.

Jahnke RA (1996) The global ocean flux of particulate organic carbon: Areal distribution and magnitude. *Global Biogeochemical Cycles* 10(1): 71–88. https://doi.org/10.1029/95GB03525.

Jarrard RD (2003) Subduction fluxes of water, carbon dioxide, chlorine, and potassium. *Geochemistry, Geophysics, Geosystems* 4(5). https://doi.org/10.1029/2002GC000392.

Javoy M, Pineau F, and Allègre CJ (1982) Carbon geodynamic cycle. *Nature* 300(5888): 171. https://doi.org/10.1038/300171a0.

Jian J, Bailey V, Dorheim K, Konings AG, Hao D, Shiklomanov AN, Snyder A, Steele M, Teramoto M, Vargas R, and Bond-Lamberty B (2022) Historically inconsistent productivity and respiration fluxes in the global terrestrial carbon cycle. *Nature Communications* 13(1): 1733. https://doi.org/10.1038/s41467-022-29391-5.

Jing Z and Karato S (2011) A new approach to the equation of state of silicate melts: An application of the theory of hard sphere mixtures. *Geochimica et Cosmochimica Acta* 75(22): 6780–6802. https://doi.org/10.1016/j.gca.2011.09.004.

Johansen A and Lambrechts M (2017) Forming planets via pebble accretion. *Annual Review of Earth and Planetary Sciences* 45: 359–387. https://doi.org/10.1146/annurev-earth-063016-020226.

Johansson L, Zahirovic S, and Müller RD (2018) The interplay between the eruption and weathering of large igneous provinces and the deep-time carbon cycle. *Geophysical Research Letters* 45(11): 5380–5389. https://doi.org/10.1029/2017GL076691.

Johnston FKB, Turchyn AV, and Edmonds M (2011) Decarbonation efficiency in subduction zones: Implications for warm Cretaceous climates. *Earth and Planetary Science Letters* 303(1): 143–152. https://doi.org/10.1016/j.epsl.2010.12.049.

Jones AP, Genge M, and Carmody L (2013) Carbonate melts and carbonatites. *Reviews in Mineralogy and Geochemistry* 75(1): 289–322. https://doi.org/10.2138/rmg.2013.75.10.

Jørgensen BB, Findlay AJ, and Pellerin A (2019) The biogeochemical sulfur cycle of marine sediments. *Frontiers in Microbiology* 10. https://doi.org/10.3389/fmicb.2019.00849.

Kallmeyer J, Pockalny R, Adhikari RR, Smith DC, and D'Hondt S (2012) Global distribution of microbial abundance and biomass in subseafloor sediment. *Proceedings of the National Academy of Sciences* 109(40): 16213–16216. https://doi.org/10.1073/pnas.1203849109.

Kaminsky F (2012) Mineralogy of the lower mantle: A review of 'super-deep' mineral inclusions in diamond. *Earth-Science Reviews* 110(1): 127–147. https://doi.org/10.1016/j.earscirev.2011.10.005.

Kaminsky F, Wirth R, Matsyuk S, Schreiber A, and Thomas R (2009) Nyerereite and nahcolite inclusions in diamond: Evidence for lower-mantle carbonatitic magmas. *Mineralogical Magazine* 73(5): 797–816. https://doi.org/10.1180/minmag.2009.073.5.797.

Kaminsky FV, Wirth R, and Schreiber A (2013) Carbonatitic inclusions in deep mantle diamond from Juina, Brazil: New minerals in the carbonate-halide association. *The Canadian Mineralogist* 51(5): 669–688. https://doi.org/10.3749/canmin.51.5.669.

Kaminsky FV, Ryabchikov ID, and Wirth R (2016) A primary natrocarbonatitic association in the Deep Earth. *Mineralogy and Petrology* 110(2): 387–398. https://doi.org/10.1007/s00710-015-0368-4.

Kandasamy S and Nagender Nath B (2016) Perspectives on the terrestrial organic matter transport and burial along the land-deep sea continuum: Caveats in our understanding of biogeochemical processes and future needs. *Frontiers in Marine Science* 3. https://doi.org/10.3389/fmars.2016.00259.

Kaneshima S (2018) Array analyses of SmKS waves and the stratification of Earth's outermost core. *Physics of the Earth and Planetary Interiors* 276: 234–246. https://doi.org/10.1016/j.pepi.2017.03.006.

Kaneshima S and Helffrich G (2013) Vp structure of the outermost core derived from analysing large-scale array data of SmKS waves. *Geophysical Journal International* 193(3): 1537–1555. https://doi.org/10.1093/gji/ggt042.

Kaneshima S and Matsuzawa T (2015) Stratification of earth's outermost core inferred from SmKS array data. *Progress in Earth and Planetary Science* 2(1): 15. https://doi.org/10.1186/s40645-015-0046-5.

Kawakatsu H and Utada H (2017) Seismic and Electrical Signatures of the Lithosphere–Asthenosphere System of the Normal Oceanic Mantle. *Annual Review of Earth and Planetary Sciences* 45: 139–167. https://doi.org/10.1146/annurev-earth-063016-020319.

Kawakatsu H, Kumar P, Takei Y, Shinohara M, Kanazawa T, Araki E, and Suyehiro K (2009) Seismic evidence for sharp lithosphere-asthenosphere boundaries of oceanic plates. *Science* 324(5926): 499–502. https://doi.org/10.1126/science.1169499.

Kelemen PB and Behn MD (2016) Formation of lower continental crust by relamination of buoyant arc lavas and plutons. *Nature Geoscience* 9(3): 197–205. https://doi.org/10.1038/ngeo2662.

Kelemen PB and Manning CE (2015) Reevaluating carbon fluxes in subduction zones, what goes down, mostly comes up. *Proceedings of the National Academy of Sciences* 112(30): E3997–E4006. https://doi.org/10.1073/pnas.1507889112.

Kelemen PB and Matter J (2008) In situ carbonation of peridotite for CO_2 storage. *Proceedings of the National Academy of Sciences* 105(45): 17295–17300. https://doi.org/10.1073/pnas.0805794105.

Kelemen PB, Matter J, Streit EE, Rudge JF, Curry WB, and Blusztajn J (2011) Rates and mechanisms of mineral carbonation in peridotite: Natural processes and recipes for enhanced, in situ CO_2 capture and storage. *Annual Review of Earth and Planetary Sciences* 39(1): 545–576. https://doi.org/10.1146/annurev-earth-092010-152509.

Kelemen PB, de Obeso JC, Leong JA, Godard M, Okazaki K, Kotowski AJ, Manning CE, Ellison ET, Menzel MD, Urai JL, Hirth G, Rioux M, Stockli DF, Lafay R, Beinlich AM, Coggon JA, Warsi NH, Matter JM, Teagle DAH, et al., and Team, T. O. D. P. S (2022) Listvenite formation during mass transfer into the leading edge of the mantle wedge: Initial results from oman drilling project hole BT1B. *Journal of Geophysical Research: Solid Earth* 127(2): e2021JB022352. https://doi.org/10.1029/2021JB022352.

Keller T, Katz RF, and Hirschmann MM (2017) Volatiles beneath mid-ocean ridges: Deep melting, channelised transport, focusing, and metasomatism. *Earth and Planetary Science Letters* 464: 55–68. https://doi.org/10.1016/j.epsl.2017.02.006.

Kelley DS, Karson JA, Früh-Green GL, Yoerger DR, Shank TM, Butterfield DA, Hayes JM, Schrenk MO, Olson EJ, Proskurowski G, Jakuba M, Bradley A, Larson B, Ludwig K, Glickson D, Buckman K, Bradley AS, Brazelton WJ, Roe K, et al. (2005) A serpentinite-hosted ecosystem: The lost city hydrothermal field. *Science* 307(5714): 1428–1434. https://doi.org/10.1126/science.1102556.

Keppler H, Wiedenbeck M, and Shcheka SS (2003) Carbon solubility in olivine and the mode of carbon storage in the Earth's mantle. *Nature* 424(6947): 414–416. https://doi.org/10.1038/nature01828.

Kerrick DM and Caldeira K (1998) Metamorphic CO_2 degassing from orogenic belts. *Chemical Geology* 145(3): 213–232. https://doi.org/10.1016/S0009-2541(97)00144-7.

Kerrick DM and Connolly JAD (2001) Metamorphic devolatilization of subducted marine sediments and the transport of volatiles into the Earth's mantle. *Nature* 411(6835): 293–296. https://doi.org/10.1038/35077056.

Kiseeva ES, Yaxley GM, Hermann J, Litasov KD, Rosenthal A, and Kamenetsky VS (2012) An experimental study of carbonated eclogite at 3.5–5.5 GPa—Implications for silicate and carbonate metasomatism in the cratonic mantle. *Journal of Petrology* 53(4): 727–759. https://doi.org/10.1093/petrology/egr078.

Kiseeva ES, Vasiukov DM, Wood BJ, McCammon C, Stachel T, Bykov M, Bykova E, Chumakov A, Cerantola V, Harris JW, and Dubrovinsky L (2018) Oxidized iron in garnets from the mantle transition zone. *Nature Geoscience* 11(2): 144–147. https://doi.org/10.1038/s41561-017-0055-7.

Klein C (2005) Some Precambrian banded iron-formations (BIFs) from around the world: Their age, geologic setting, mineralogy, metamorphism, geochemistry, and origins. *American Mineralogist* 90(10): 1473–1499. https://doi.org/10.2138/am.2005.1871.

Klein BZ and Behn MD (2021) On the evolution and fate of sediment diapirs in subduction zones. *Geochemistry, Geophysics, Geosystems* 22(11): e2021GC009873. https://doi.org/10.1029/2021GC009873.

Klein F, Grozeva NG, and Seewald JS (2019) Abiotic methane synthesis and serpentinization in olivine-hosted fluid inclusions. *Proceedings of the National Academy of Sciences* 116(36): 17666–17672. https://doi.org/10.1073/pnas.1907871116.

Klein F, Schroeder T, John CM, Davis S, Humphris SE, Seewald JS, Sichel S, Bach W, and Brunelli D (2024) Mineral carbonation of peridotite fueled by magmatic degassing and melt impregnation in an oceanic transform fault. *Proceedings of the National Academy of Sciences* 121(8): e2315662121. https://doi.org/10.1073/pnas.2315662121.

Kolesnikov A, Kutcherov VG, and Goncharov AF (2009) Methane-derived hydrocarbons produced under upper-mantle conditions. *Nature Geoscience* 2(8): 566–570. https://doi.org/10.1038/ngeo591.

Könneke M, Schubert DM, Brown PC, Hügler M, Standfest S, Schwander T, Schada von Borzyskowski L, Erb TJ, Stahl DA, and Berg IA (2014) Ammonia-oxidizing archaea use the most energy-efficient aerobic pathway for CO_2 fixation. *Proceedings of the National Academy of Sciences* 111(22): 8239–8244. https://doi.org/10.1073/pnas.1402028111.

Korenaga J (2021) Hadean geodynamics and the nature of early continental crust. *Precambrian Research* 359: 106178. https://doi.org/10.1016/j.precamres.2021.106178.

Kueter N, Soesilo J, Fedortchouk Y, Nestola F, Belluco L, Troch J, Wälle M, Guillong M, Von Quadt A, and Driesner T (2016) Tracing the depositional history of Kalimantan diamonds by zircon provenance and diamond morphology studies. *Lithos* 265: 159–176. https://doi.org/10.1016/j.lithos.2016.05.003.

Kumar N, Anderson RF, Mortlock RA, Froelich PN, Kubik P, Dittrich-Hannen B, and Suter M (1995) Increased biological productivity and export production in the glacial Southern Ocean. *Nature* 378(6558): 675–680. https://doi.org/10.1038/378675a0.

Kump LR and Arthur MA (1999) Interpreting carbon-isotope excursions: Carbonates and organic matter. *Chemical Geology* 161(1): 181–198. https://doi.org/10.1016/S0009-2541(99)00086-8.

Kump LR, Junium C, Arthur MA, Brasier A, Fallick A, Melezhik V, Lepland A, Črne AE, and Luo G (2011) Isotopic evidence for massive oxidation of organic matter following the great oxidation event. *Science* 334(6063): 1694–1696. https://doi.org/10.1126/science.1213999.

Kunhi Mouvenchery Y, Kučerík J, Diehl D, and Schaumann GE (2012) Cation-mediated cross-linking in natural organic matter: A review. *Reviews in Environmental Science and Bio/Technology* 11(1): 41–54. https://doi.org/10.1007/s11157-011-9258-3.

Kushiro I (1975) Carbonate-silicate reactions at high pressures and possible presence of dolomite and magnesite in the upper mantle. *Earth and Planetary Science Letters* 28(2): 116–120. https://doi.org/10.1016/0012-821X(75)90218-6.

Kushiro I (1976) Changes in viscosity and structure of melt of $NaAlSi_2O_6$ composition at high pressures. *Journal of Geophysical Research (1896-1977)* 81(35): 6347–6350. https://doi.org/10.1029/JB081i035p06347.

Kwon EY, DeVries T, Galbraith ED, Hwang J, Kim G, and Timmermann A (2021) Stable carbon isotopes suggest large terrestrial carbon inputs to the global ocean. *Global Biogeochemical Cycles* 35(4): e2020GB006684. https://doi.org/10.1029/2020GB006684.

Labrosse S, Hernlund JW, and Coltice N (2007) A crystallizing dense magma ocean at the base of the Earth's mantle. *Nature* 450(7171): 866–869. https://doi.org/10.1038/nature06355.

Lange RA and Carmichael ISE (1987) Densities of Na_2O-K_2O-CaO-MgO-FeO-Fe_2O_3-Al_2O_3-TiO_2-SiO_2 liquids: New measurements and derived partial molar properties. *Geochimica et Cosmochimica Acta* 51(11): 2931–2946. https://doi.org/10.1016/0016-7037(87)90368-1.

LaRowe DE, Arndt S, Bradley JA, Estes ER, Hoarfrost A, Lang SQ, Lloyd KG, Mahmoudi N, Orsi WD, Shah Walter SR, Steen AD, and Zhao R (2020) The fate of organic carbon in marine sediments—New insights from recent data and analysis. *Earth-Science Reviews* 204: 103146. https://doi.org/10.1016/j.earscirev.2020.103146.

Laumonier M, Gaillard F, Muir D, Blundy J, and Unsworth M (2017) Giant magmatic water reservoirs at mid-crustal depth inferred from electrical conductivity and the growth of the continental crust. *Earth and Planetary Science Letters* 457: 173–180. https://doi.org/10.1016/j.epsl.2016.10.023.

Lay T (2005) The deep mantle thermo-chemical boundary layer: The putative mantle plume source. In: Foulger GR, Natland JH, Presnall DC, and Anderson DL (eds.) *Plates, plumes and paradigms*. Geological Society of America. https://doi.org/10.1130/0-8137-2388-4.193.

Lazar C, Zhang C, Manning CE, and Mysen BO (2014) Redox effects on calcite-portlandite-fluid equilibria at forearc conditions: Carbon mobility, methanogenesis, and reduction melting of calcite†. *American Mineralogist* 99(8–9): 1604–1615. https://doi.org/10.2138/am.2014.4696.

Le Voyer M, Kelley KA, Cottrell E, and Hauri EH (2017) Heterogeneity in mantle carbon content from CO_2-undersaturated basalts. *Nature Communications* 8: 14062. https://doi.org/10.1038/ncomms14062.

Le Voyer M, Hauri EH, Cottrell E, Kelley KA, Salters VJM, Langmuir CH, Hilton DR, Barry PH, and Füri E (2019) Carbon fluxes and primary magma CO_2 contents along the global mid-ocean ridge system. *Geochemistry, Geophysics, Geosystems* 20(3): 1387–1424. https://doi.org/10.1029/2018GC007630.

Lee H, Muirhead JD, Fischer TP, Ebinger CJ, Kattenhorn SA, Sharp ZD, and Kianji G (2016) Massive and prolonged deep carbon emissions associated with continental rifting. *Nature Geoscience* 9(2): 145–149. https://doi.org/10.1038/ngeo2622.

Lee C-TA (2006) In: Benn K, Mareschal J-C, and Condie KC (eds.). *Geophysical Monograph Series*, Vol. 164, pp. 89–114. American Geophysical Union. https://doi.org/10.1029/164GM08.

Lee C-TA, Jiang H, Dasgupta R, and Torres M (2019) A framework for understanding whole Earth carbon cycling. In: Orcutt B, Dasgupta R, and Daniel I (eds.) *Deep Carbon: Past to Present*. Cambridge University Press.

Lefeldt M, Ranero CR, and Grevemeyer I (2012) Seismic evidence of tectonic control on the depth of water influx into incoming oceanic plates at subduction trenches. *Geochemistry, Geophysics, Geosystems* 13(5). https://doi.org/10.1029/2012GC004043.

Li Y (2017) Immiscible C-H-O fluids formed at subduction zone conditions. *Geochemical Perspectives Letters* 12–21. https://doi.org/10.7185/geochemlet.1702.

Li Y, Dasgupta R, Tsuno K, Monteleone B, and Shimizu N (2016) Carbon and sulfur budget of the silicate Earth explained by accretion of differentiated planetary embryos. *Nature Geoscience* 9(10): 781–785. https://doi.org/10.1038/ngeo2801.

Li K, Li L, Pearson DG, and Stachel T (2019) Diamond isotope compositions indicate altered igneous oceanic crust dominates deep carbon recycling. *Earth and Planetary Science Letters* 516: 190–201. https://doi.org/10.1016/j.epsl.2019.03.041.

Litasov K and Ohtani E (2010) The solidus of carbonated eclogite in the system CaO–Al_2O,–MgO–SiO_2–Na_2O–CO_2 to 32 GPa and carbonatite liquid in the deep mantle. *Earth and Planetary Science Letters* 295(1): 115–126. https://doi.org/10.1016/j.epsl.2010.03.030.

Litasov K, Shatskiy A, Podborodnikov I, and Arefiev A (2020) Phase diagrams of carbonate materials at high pressures, with implications for melting and carbon cycling in the deep Earth. In: *Carbon in Earth's Interior*, pp. 137–165. American Geophysical Union (AGU). https://doi.org/10.1002/9781119508229.ch14.

Liu J, Lin J-F, Mao Z, and Prakapenka VB (2014) Thermal equation of state and spin transition of magnesiosiderite at high pressure and temperature. *American Mineralogist* 99(1): 84–93. https://doi.org/10.2138/am.2014.4553.

Liu J, Li J, Hrubiak R, and Smith JS (2016) Origins of ultralow velocity zones through slab-derived metallic melt. *Proceedings of the National Academy of Sciences* 113(20): 5547–5551. https://doi.org/10.1073/pnas.1519540113.

Liu J, Cai R, Pearson DG, and Scott JM (2019) Thinning and destruction of the lithospheric mantle root beneath the North China Craton: A review. *Earth-Science Reviews* 196: 102873. https://doi.org/10.1016/j.earscirev.2019.05.017.

Liu Z, Perez-Gussinye M, García-Pintado J, Mezri L, and Bach W (2023) Mantle serpentinization and associated hydrogen flux at North Atlantic magma-poor rifted margins. *Geology*. https://doi.org/10.1130/G50722.1.

Lloyd KG (2020) Time as a microbial resource. *Environmental Microbiology Reports* 13(1). https://doi.org/10.1111/1758-2229.12892.

Lord OT, Walter MJ, Dasgupta R, Walker D, and Clark SM (2009) Melting in the Fe–C system to 70 GPa. *Earth and Planetary Science Letters* 284(1): 157–167. https://doi.org/10.1016/j.epsl.2009.04.017.

Lorenzon S, Wenz M, Nimis P, Jacobsen SD, Pasqualetto L, Pamato MG, Novella D, Zhang D, Anzolini C, Regier M, Stachel T, Pearson DG, Harris JW, and Nestola F (2023) Dual origin of ferropericlase inclusions within super-deep diamonds. *Earth and Planetary Science Letters* 608: 118081. https://doi.org/10.1016/j.epsl.2023.118081.

Lowenstern JB (2001) Carbon dioxide in magmas and implications for hydrothermal systems. *Mineralium Deposita* 36(6): 490–502. https://doi.org/10.1007/s001260100185.

Lu Q, Liu H, Wei L, Zhong Y, and Zhou Z (2024) Global prediction of gross primary productivity under future climate change. *Science of the Total Environment* 912: 169239. https://doi.org/10.1016/j.scitotenv.2023.169239.

Luque del Villar FJ, Pasteris JD, Wopenka B, Rodas M, and Fernández Barrenechea JM (1998) Natural fluid-deposited graphite: Mineralogical characteristics and mechanisms of formation. *American Journal of Science* 298: 471–498.

Luque FJ, Huizenga J-M, Crespo-Feo E, Wada H, Ortega L, and Barrenechea JF (2014) Vein graphite deposits: Geological settings, origin, and economic significance. *Mineralium Deposita* 49(2): 261–277. https://doi.org/10.1007/s00126-013-0489-9.

Lv M, Dorfman SM, Badro J, Borensztajn S, Greenberg E, and Prakapenka VB (2021) Reversal of carbonate-silicate cation exchange in cold slabs in Earth's lower mantle. *Nature Communications* 12(1): 1712. https://doi.org/10.1038/s41467-021-21761-9.

Magnabosco C, Lin L-H, Dong H, Bomberg M, Ghiorse W, Stan-Lotter H, Pedersen K, Kieft TL, van Heerden E, and Onstott TC (2018) The biomass and biodiversity of the continental subsurface. *Nature Geoscience* 11(10). https://doi.org/10.1038/s41561-018-0221-6. Article 10.

Malinverno A and Martinez EA (2015) The effect of temperature on organic carbon degradation in marine sediments. *Scientific Reports* 5(1): 17861. https://doi.org/10.1038/srep17861.

Malvoisin B, Chopin C, Brunet F, and Galvez ME (2012) Low-temperature wollastonite formed by carbonate reduction: A marker of serpentinite redox conditions. *Journal of Petrology* 53(1): 159–176. https://doi.org/10.1093/petrology/egr060.

Manning CE, Shock EL, and Sverjensky DA (2013) The chemistry of carbon in aqueous fluids at crustal and upper-mantle conditions: Experimental and theoretical constraints. *Reviews in Mineralogy and Geochemistry* 75(1): 109–148. https://doi.org/10.2138/rmg.2013.75.5.

Marty B (2012) The origins and concentrations of water, carbon, nitrogen and noble gases on Earth. *Earth and Planetary Science Letters* 313–314: 56–66. https://doi.org/10.1016/j.epsl.2011.10.040.

Marty B, Alexander CMO, and Raymond SN (2013) Primordial origins of Earth's carbon. *Reviews in Mineralogy and Geochemistry* 75(1): 149–181. https://doi.org/10.2138/rmg.2013.75.6.

Marty B, Avice G, Sano Y, Altwegg K, Balsiger H, Hässig M, Morbidelli A, Mousis O, and Rubin M (2016) Origins of volatile elements (H, C, N, noble gases) on Earth and Mars in light of recent results from the ROSETTA cometary mission. *Earth and Planetary Science Letters* 441: 91–102. https://doi.org/10.1016/j.epsl.2016.02.031.

Mason E, Edmonds M, and Turchyn AV (2017) Remobilization of crustal carbon may dominate volcanic arc emissions. *Science* 357(6348): 290–294. https://doi.org/10.1126/science.aan5049.

Massuyeau M, Gardés E, Morizet Y, and Gaillard F (2015) A model for the activity of silica along the carbonatite–kimberlite–melilitite–basanite melt compositional joint. *Chemical Geology* 418: 206–216. https://doi.org/10.1016/j.chemgeo.2015.07.025.

Massuyeau M, Gardés E, Rogerie G, Aulbach S, Tappe S, Le Trong E, Sifré D, and Gaillard F (2021) MAGLAB: A computing platform connecting geophysical signatures to melting processes in Earth's mantle. *Physics of the Earth and Planetary Interiors* 314: 106638. https://doi.org/10.1016/j.pepi.2020.106638.

Massuyeau M, Ritter X, and Sanchez-Valle C (2023) A density model for high-pressure carbonate-rich melts applied to carbonatitic magmatism in the upper mantle. *Chemical Geology* 622: 121275. https://doi.org/10.1016/j.chemgeo.2022.121275.

Mather BR, Müller RD, Alfonso CP, Seton M, and Wright NM (2023) Kimberlite eruptions driven by slab flux and subduction angle. *Scientific Reports* 13(1). https://doi.org/10.1038/s41598-023-36250-w. Article 1.

Matter JM and Kelemen PB (2009) Permanent storage of carbon dioxide in geological reservoirs by mineral carbonation. *Nature Geoscience* 2(12): 837–841. https://doi.org/10.1038/ngeo683.

Mattila A, Pylkkänen T, Rueff J-P, Huotari S, Vankó G, Hanfland M, Lehtinen M, and Hämäläinen K (2007) Pressure induced magnetic transition in siderite FeCO3 studied by x-ray emission spectroscopy. *Journal of Physics: Condensed Matter* 19(38): 386206. https://doi.org/10.1088/0953-8984/19/38/386206.

McCammon C (1997) Perovskite as a possible sink for ferric iron in the lower mantle. *Nature* 387(6634): 694–696. https://doi.org/10.1038/42685.

McCollom TM (2013) Laboratory simulations of abiotic hydrocarbon formation in Earth's deep subsurface. *Reviews in Mineralogy and Geochemistry* 75(1): 467–494. https://doi.org/10.2138/rmg.2013.75.15.

McCollom TM, Lollar BS, Lacrampe-Couloume G, and Seewald JS (2010) The influence of carbon source on abiotic organic synthesis and carbon isotope fractionation under hydrothermal conditions. *Geochimica et Cosmochimica Acta* 74(9): 2717–2740. https://doi.org/10.1016/j.gca.2010.02.008.

McDermott JM, Seewald JS, German CR, and Sylva SP (2015) Pathways for abiotic organic synthesis at submarine hydrothermal fields. *Proceedings of the National Academy of Sciences* 112(25): 7668–7672. https://doi.org/10.1073/pnas.1506295112.

McDonough WF and Sun SS (1995) The composition of the Earth. *Chemical Geology* 120: 223–253. https://doi.org/10.1016/0009-2541(94)00140-4.

McKenzie D (1989) Some remarks on the movement of small melt fractions in the mantle. *Earth and Planetary Science Letters* 95(1): 53–72. https://doi.org/10.1016/0012-821X(89)90167-2.

McKenzie NR, Horton BK, Loomis SE, Stockli DF, Planavsky NJ, and Lee C-TA (2016) Continental arc volcanism as the principal driver of icehouse-greenhouse variability. *Science* 352(6284): 444–447. https://doi.org/10.1126/science.aad5787.

McNamara AK (2019) A review of large low shear velocity provinces and ultra low velocity zones. *Tectonophysics* 760: 199–220. https://doi.org/10.1016/j.tecto.2018.04.015.

Meister P, Brunner B, Picard A, Böttcher ME, and Jørgensen BB (2019) Sulphur and carbon isotopes as tracers of past sub-seafloor microbial activity. *Scientific Reports* 9(1): 604. https://doi.org/10.1038/s41598-018-36943-7.

Ménez B (2020) Abiotic hydrogen and methane: Fuels for life. *Elements* 16(1): 39–46. https://doi.org/10.2138/gselements.16.1.39.

Ménez B, Pisapia C, Andreani M, Jamme F, Vanbellingen QP, Brunelle A, et al. (2018) Abiotic synthesis of amino acids in the recesses of the oceanic lithosphere. *Nature* 564(7734): 59–63.

Menzel MD, Garrido CJ, López Sánchez-Vizcaíno V, Marchesi C, Hidas K, Escayola MP, and Delgado Huertas A (2018) Carbonation of mantle peridotite by CO_2-rich fluids: The formation of listvenites in the Advocate ophiolite complex (Newfoundland, Canada). *Lithos* 323: 238–261. https://doi.org/10.1016/j.lithos.2018.06.001.

Menzel MD, Garrido CJ, and Sánchez-Vizcaíno VL (2020) Fluid-mediated carbon release from serpentinite-hosted carbonates during dehydration of antigorite-serpentinite in subduction zones. *Earth and Planetary Science Letters* 531: 115964.

Menzel MD, Sieber MJ, and Godard M (2024) From peridotite to listvenite – perspectives on the processes, mechanisms and settings of ultramafic mineral carbonation to quartz-magnesite rocks. *Earth-Science Reviews* 255: 104828. https://doi.org/10.1016/j.earscirev.2024.104828.

Merdith AS, Atkins SE, and Tetley MG (2019) Tectonic controls on carbon and serpentinite storage in subducted upper oceanic lithosphere for the past 320 Ma. *Frontiers in Earth Science* 7. https://www.frontiersin.org/articles/10.3389/feart.2019.00332.

Merdith AS, del Real PG, Daniel I, Andreani M, Wright NM, and Coltice N (2020) Pulsated global hydrogen and methane flux at mid-ocean ridges driven by Pangea breakup. *Geochemistry, Geophysics, Geosystems* 21(4): e2019GC008869. https://doi.org/10.1029/2019GC008869.

Merino N, Aronson HS, Bojanova DP, Feyhl-Buska J, Wong ML, Zhang S, and Giovannelli D (2019) Living at the extremes: Extremophiles and the limits of life in a planetary context. *Frontiers in Microbiology* 10. https://doi.org/10.3389/fmicb.2019.00780.

Merlini M, Milani S, and Maurice J (2020) Structures and crystal chemistry of carbonate at Earth's mantle conditions. In: *Carbon in Earth's Interior*, pp. 87–95. American Geophysical Union (AGU). https://doi.org/10.1002/9781119508229.ch9.

Middelburg JJ (2011) Chemoautotrophy in the ocean. *Geophysical Research Letters* 38(24). https://doi.org/10.1029/2011GL049725.

Mikhail S and Füri E (2019) On the origin(s) and evolution of Earth's carbon. *Elements* 15(5): 307–312. https://doi.org/10.2138/gselements.15.5.307.

Milliman JD (1974) Precipitation and cementation of deep-sea carbonate sediments. In: Inderbitzen AL (ed.) *Deep-Sea Sediments: Physical and Mechanical Properties*, pp. 463–476. Springer US. https://doi.org/10.1007/978-1-4684-2754-7_23.

Minarik WG and Watson EB (1995) Interconnectivity of carbonate melt at low melt fraction. *Earth and Planetary Science Letters* 133(3): 423–437. https://doi.org/10.1016/0012-821X(95)00085-Q.

mindat.org (n.d.) https://www.mindat.org/chemsearch.php?inc=CO3%2C&exc=&class=0&sub=Search+Minerals - mindat.org search query for carbonate minerals (CO_3^{2-}), last visited June 2024.

Morard G, Nakajima Y, Andrault D, Antonangeli D, Auzende AL, Boulard E, Cervera S, Clark AN, Lord OT, Siebert J, Svitlyk V, Garbarino G, and Mezouar M (2017) Structure and density of Fe-C liquid alloys under high pressure. *Journal of Geophysical Research: Solid Earth* 122(10): 7813–7823. https://doi.org/10.1002/2017JB014779.

Mottl MJ, Komor SC, Fryer P, and Moyer CL (2003) Deep-slab fluids fuel extremophilic Archaea on a Mariana forearc serpentinite mud volcano: Ocean Drilling Program Leg 195. *Geochemistry, Geophysics, Geosystems* 4(11). https://doi.org/10.1029/2003GC000588.

Moussallam Y, Longpré M-A, McCammon C, Gomez-Ulla A, Rose-Koga EF, Scaillet B, Peters N, Gennaro E, Paris R, and Oppenheimer C (2019) Mantle plumes are oxidised. *Earth and Planetary Science Letters* 527: 115798. https://doi.org/10.1016/j.epsl.2019.115798.

Muirhead JD, Fischer TP, Oliva SJ, Laizer A, van Wijk J, Currie CA, Lee H, Judd EJ, Kazimoto E, Sano Y, Takahata N, Tiberi C, Foley SF, Dufek J, Reiss MC, and Ebinger CJ (2020) Displaced cratonic mantle concentrates deep carbon during continental rifting. *Nature* 582(7810). https://doi.org/10.1038/s41586-020-2328-3. Article 7810.

Müller RD and Dutkiewicz A (2018) Oceanic crustal carbon cycle drives 26-million-year atmospheric carbon dioxide periodicities. *Science Advances* 4(2): eaaq0500. https://doi.org/10.1126/sciadv.aaq0500.

Müller RD, Mather B, Dutkiewicz A, Keller T, Merdith A, Gonzalez CM, Gorczyk W, and Zahirovic S (2022) Evolution of Earth's tectonic carbon conveyor belt. *Nature* 605(7911). https://doi.org/10.1038/s41586-022-04420-x. Article 7911.

Mullis J, Dubessy J, Poty B, and O'Neil J (1994) Fluid regimes during late stages of a continental collision: Physical, chemical, and stable isotope measurements of fluid inclusions in fissure quartz from a geotraverse through the Central Alps, Switzerland. *Geochimica et Cosmochimica Acta* 58(10): 2239–2267. https://doi.org/10.1016/0016-7037(94)90008-6.

Mungall JE, Brenan JM, Godel B, Barnes SJ, and Gaillard F (2015) Transport of metals and sulphur in magmas by flotation of sulphide melt on vapour bubbles. *Nature Geoscience* 8(3): 216–219. https://doi.org/10.1038/ngeo2373.

Nabyl Z, Massuyeau M, Gaillard F, Tuduri J, Iacono-Marziano G, Rogerie G, Le Trong E, Di Carlo I, Melleton J, and Bailly L (2020) A window in the course of alkaline magma differentiation conducive to immiscible REE-rich carbonatites. *Geochimica et Cosmochimica Acta* 282: 297–323. https://doi.org/10.1016/j.gca.2020.04.008.

Nakajima Y, Imada S, Hirose K, Komabayashi T, Ozawa H, Tateno S, Tsutsui S, Kuwayama Y, and Baron AQR (2015) Carbon-depleted outer core revealed by sound velocity measurements of liquid iron–carbon alloy. *Nature Communications* 6(1): 8942. https://doi.org/10.1038/ncomms9942.

Nestola F, Korolev N, Kopylova M, Rotiroti N, Pearson DG, Pamato MG, Alvaro M, Peruzzo L, Gurney JJ, Moore AE, and Davidson J (2018) CaSiO3 perovskite in diamond indicates the recycling of oceanic crust into the lower mantle. *Nature* 555(7695): 237–241. https://doi.org/10.1038/nature25972.

Nestola F, Regier ME, Luth RW, Pearson DG, Stachel T, McCammon C, Wenz MD, Jacobsen SD, Anzolini C, Bindi L, and Harris JW (2023) Extreme redox variations in a superdeep diamond from a subducted slab. *Nature* 613(7942): 85–89. https://doi.org/10.1038/s41586-022-05392-8.

Ni H and Keppler H (2013) Carbon in silicate melts. *Reviews in Mineralogy and Geochemistry* 75(1): 251–287. https://doi.org/10.2138/rmg.2013.75.9.

Novella D, Frost DJ, Hauri EH, Bureau H, Raepsaet C, and Roberge M (2014) The distribution of H_2O between silicate melt and nominally anhydrous peridotite and the onset of hydrous melting in the deep upper mantle. *Earth and Planetary Science Letters* 400: 1–13. https://doi.org/10.1016/j.epsl.2014.05.006.

O'Reilly SY and Griffin WL (2010) The continental lithosphere–asthenosphere boundary: Can we sample it? *Lithos* 120(1): 1–13. https://doi.org/10.1016/j.lithos.2010.03.016.

O'Reilly SY and Griffin WL (2013) Mantle metasomatism. In: Harlov DE and Austrheim H (eds.) *Metasomatism and the Chemical Transformation of Rock: The Role of Fluids in Terrestrial and Extraterrestrial Processes*, pp. 471–533. Springer. https://doi.org/10.1007/978-3-642-28394-9_12.

Oganov AR, Hemley RJ, Hazen RM, and Jones AP (2013) Structure, bonding, and mineralogy of carbon at extreme conditions. *Reviews in Mineralogy and Geochemistry* 75(1): 47–77. https://doi.org/10.2138/rmg.2013.75.3.

Ohara Y, Reagan MK, Fujikura K, Watanabe H, Michibayashi K, Ishii T, Stern RJ, Pujana I, Martinez F, Girard G, Ribeiro J, Brounce M, Komori N, and Kino M (2012) A serpentinite-hosted ecosystem in the Southern Mariana Forearc. *Proceedings of the National Academy of Sciences* 109(8): 2831–2835. https://doi.org/10.1073/pnas.1112005109.

Okamoto A, Oyanagi R, Yoshida K, Uno M, Shimizu H, and Satish-Kumar M (2021) Rupture of wet mantle wedge by self-promoting carbonation. *Communications Earth & Environment* 2(1): 151.

Olivieri OS and Miglioli A (2021) Hopper quartz crystals from Porretta Terme and Val Nervia, northern Italy. *Australian Journal of Mineralogy* 22(2): 13–29.

Olson P, Reynolds E, Hinnov L, and Goswami A (2016) Variation of ocean sediment thickness with crustal age. *Geochemistry, Geophysics, Geosystems* 17(4): 1349–1369. https://doi.org/10.1002/2015GC006143.

Pall J, Zahirovic S, Doss S, Hassan R, Matthews KJ, Cannon J, Gurnis M, Moresi L, Lenardic A, and Müller RD (2018) The influence of carbonate platform interactions with subduction zone volcanism on palaeo-atmospheric CO_2 since the Devonian. *Climate of the Past* 14(6): 857–870. https://doi.org/10.5194/cp-14-857-2018.

Pattison DRM (2006) The fate of graphite in prograde metamorphism of pelites: An example from the Ballachulish aureole, Scotland. *Lithos* 88(1): 85–99. https://doi.org/10.1016/j.lithos.2005.08.006.

Peltonen P, Kinnunen KA, and Huhma H (2002) Petrology of two diamondiferous eclogite xenoliths from the Lahtojoki kimberlite pipe, eastern Finland. *Lithos* 63(3): 151–164. https://doi.org/10.1016/S0024-4937(02)00119-6.

Peña-Alvarez M, Vitale Brovarone A, Donnelly M-E, Wang M, Dalladay-Simpson P, Howie R, and Gregoryanz E (2021) In-situ abiogenic methane synthesis from diamond and graphite under geologically relevant conditions. *Nature Communications* 12(1): 6387. https://doi.org/10.1038/s41467-021-26664-3.

Peng W, Zhang L, Tumiati S, Vitale Brovarone A, Hu H, Cai Y, and Shen T (2021) Abiotic methane generation through reduction of serpentinite-hosted dolomite: Implications for carbon mobility in subduction zones. *Geochimica et Cosmochimica Acta* 311: 119–140. https://doi.org/10.1016/j.gca.2021.07.033.

Piccoli F, Vitale Brovarone A, Beyssac O, Martinez I, Ague JJ, and Chaduteau C (2016) Carbonation by fluid–rock interactions at high-pressure conditions: Implications for carbon cycling in subduction zones. *Earth and Planetary Science Letters* 445: 146–159. https://doi.org/10.1016/j.epsl.2016.03.045.

Piccoli F, Hermann J, Pettke T, Connolly J, Kempf e, and Vieira Duarte JF (2019) Subducted serepntinites release reduced, not oxidized, aqueous fluids. *Scientific Reports* 9(1): 19573.

Piccoli F, Vitale Brovarone A, and Ague JJ (2018) Field and petrological study of metasomatism and high-pressure carbonation from lawsonite eclogite-facies terrains, Alpine Corsica. *Lithos* 304–307: 16–37. https://doi.org/10.1016/j.lithos.2018.01.026.

Piccoli F, Ague JJ, Chu X, Tian M, and Vitale Brovarone A (2021) Field-based evidence for intra-slab high-permeability channel formation at eclogite-facies conditions during subduction. *Geochemistry, Geophysics, Geosystems* 22(3): e2020GC009520. https://doi.org/10.1029/2020GC009520.

Pilet S, Abe N, Rochat L, Kaczmarek M-A, Hirano N, Machida S, Buchs DM, Baumgartner PO, and Müntener O (2016) Pre-subduction metasomatic enrichment of the oceanic lithosphere induced by plate flexure. *Nature Geoscience* 9(12): 898–903. https://doi.org/10.1038/ngeo2825.

Plank T (2014) 4.17—The Chemical Composition of Subducting Sediments. In: Holland HD and Turekian KK (eds.) *Treatise on Geochemistry*, 2nd edn, pp. 607–629. Elsevier. https://doi.org/10.1016/B978-0-08-095975-7.00319-3.

Plank T and Langmuir CH (1998) The chemical composition of subducting sediment and its consequences for the crust and mantle. *Chemical Geology* 145(3): 325–394. https://doi.org/10.1016/S0009-2541(97)00150-2.

Plank T and Manning CE (2019) Subducting carbon. *Nature* 574(7778): 343–352. https://doi.org/10.1038/s41586-019-1643-z.

Plümper O, King HE, Geisler T, Liu Y, Pabst S, Savov IP, Rost D, and Zack T (2017) Subduction zone forearc serpentinites as incubators for deep microbial life. *Proceedings of the National Academy of Sciences* 114(17): 4324–4329. https://doi.org/10.1073/pnas.1612147114.

Potter J and Longstaffe FJ (2007) A gas-chromatograph, continuous flow-isotope ratio mass-spectrometry method for $\delta^{13}C$ and δD measurement of complex fluid inclusion volatiles: Examples from the Khibina alkaline igneous complex, northwest Russia and the south Wales coalfields. *Chemical Geology* 244(1): 186–201. https://doi.org/10.1016/j.chemgeo.2007.06.014.

Power IM, Wilson SA, and Dipple GM (2013) Serpentinite Carbonation for CO_2 Sequestration. *Elements* 9(2): 115–121. https://doi.org/10.2113/gselements.9.2.115.

Ranero CR, Phipps Morgan J, McIntosh K, and Reichert C (2003) Bending-related faulting and mantle serpentinization at the Middle America trench. *Nature* 425(6956): 367–373. https://doi.org/10.1038/nature01961.

Ranero CR and von Huene R (2000) Subduction erosion along the Middle America convergent margin. *Nature* 404(6779): 748–752. https://doi.org/10.1038/35008046.

Raven JA (2009) Contributions of anoxygenic and oxygenic phototrophy and chemolithotrophy to carbon and oxygen fluxes in aquatic environments. *Aquatic Microbial Ecology* 56(2–3): 177–192. https://doi.org/10.3354/ame01315.

Rea DK and Ruff LJ (1996) Composition and mass flux of sediment entering the world's subduction zones: Implications for global sediment budgets, great earthquakes, and volcanism. *Earth and Planetary Science Letters* 140(1): 1–12. https://doi.org/10.1016/0012-821X(96)00036-2.

Reeder RJ (1983) Crystal chemistry of the rhombohedral carbonates. In: Reeder RJ (ed.) *Carbonates*, Vol. 11, pp. 1–48. De Gruyter. https://doi.org/10.1515/9781501508134-005.

Regier ME, Pearson DG, Stachel T, Luth RW, Stern RA, and Harris JW (2020) The lithospheric-to-lower-mantle carbon cycle recorded in superdeep diamonds. *Nature* 585(7824): 234–238. https://doi.org/10.1038/s41586-020-2676-z.

Ridgwell A (2005) A mid mesozoic revolution in the regulation of ocean chemistry. *Marine Geology* 217(3): 339–357. https://doi.org/10.1016/j.margeo.2004.10.036.

Ridgwell A and Zeebe RE (2005) The role of the global carbonate cycle in the regulation and evolution of the Earth system. *Earth and Planetary Science Letters* 234(3–4): 299–315. https://doi.org/10.1016/j.epsl.2005.03.006.

Ritter X, Sanchez-Valle C, Sator N, Desmaele E, Guignot N, King A, Kupenko I, Berndt J, and Guillot B (2020) Density of hydrous carbonate melts under pressure, compressibility of volatiles and implications for carbonate melt mobility in the upper mantle. *Earth and Planetary Science Letters* 533: 116043. https://doi.org/10.1016/j.epsl.2019.116043.

Ritter X, Guillot B, Sator N, Desmaele E, Massuyeau M, and Sanchez-Valle C (2021) Non-arrhenian temperature-dependent viscosity of alkali(ne) carbonate melts at mantle pressures. *Frontiers in Earth Science* 9. https://doi.org/10.3389/feart.2021.674770.

Rizo H, Andrault D, Bennett NR, Humayun M, Brandon A, Vlastélic I, Moine BN, Poirier A, Bouhifd MAMA, and Murphy DT (2019) ^{182}W evidence for core-mantle interaction in the source of mantle plumes. *Geochemical Perspectives Letters* 11: 6. https://doi.org/10.7185/geochemlet.1917.

Rogers TJ, Buongiorno J, Jessen GL, Schrenk MO, Fordyce JA, de Moor JM, Ramírez CJ, Barry PH, Yücel M, Selci M, Cordone A, Giovannelli D, and Lloyd KG (2023) Chemolithoautotroph distributions across the subsurface of a convergent margin. *The ISME Journal* 17(1). https://doi.org/10.1038/s41396-022-01331-7. Article 1.

Rohrbach A and Schmidt MW (2011) Redox freezing and melting in the Earth's deep mantle resulting from carbon–iron redox coupling. *Nature* 472(7342): 209–212. https://doi.org/10.1038/nature09899.

Rohrbach A, Ghosh S, Schmidt MW, Wijbrans CH, and Klemme S (2014) The stability of Fe–Ni carbides in the Earth's mantle: Evidence for a low Fe–Ni–C melt fraction in the deep mantle. *Earth and Planetary Science Letters* 388: 211–221. https://doi.org/10.1016/j.epsl.2013.12.007.

Rooney TO, Nelson WR, Dosso L, Furman T, and Hanan B (2014) The role of continental lithosphere metasomes in the production of HIMU-like magmatism on the northeast African and Arabian plates. *Geology* 42(5): 419–422. https://doi.org/10.1130/G35216.1.

Rooney TO, Nelson WR, Ayalew D, Hanan B, Yirgu G, and Kappelman J (2017) Melting the lithosphere: Metasomes as a source for mantle-derived magmas. *Earth and Planetary Science Letters* 461: 105–118. https://doi.org/10.1016/j.epsl.2016.12.010.

Rudnick RL, McDonough WF, and Chappell BW (1993) Carbonatite metasomatism in the northern Tanzanian mantle: Petrographic and geochemical characteristics. *Earth and Planetary Science Letters* 114(4): 463–475. https://doi.org/10.1016/0012-821X(93)90076-L.

Rumble D III, Duke EF, and Hoering TL (1986) Hydrothermal graphite in New Hampshire: Evidence of carbon mobility during regional metamorphism. *Geology* 14(6): 452–455. https://doi.org/10.1130/0091-7613(1986)14<452:HGINHE>2.0.CO;2.

Rychert CA, Harmon N, Constable S, and Wang S (2020) The nature of the lithosphere-asthenosphere boundary. *Journal of Geophysical Research: Solid Earth* 125(10): e2018JB016463. https://doi.org/10.1029/2018JB016463.

Saha S, Peng Y, Dasgupta R, Mookherjee M, and Fischer KM (2021) Assessing the presence of volatile-bearing mineral phases in the cratonic mantle as a possible cause of mid-lithospheric discontinuities. *Earth and Planetary Science Letters* 553: 116602. https://doi.org/10.1016/j.epsl.2020.116602.

Sakamaki T, Suzuki A, and Ohtani E (2006) Stability of hydrous melt at the base of the Earth's upper mantle. *Nature* 439(7073): 192–194. https://doi.org/10.1038/nature04352.

Sakamaki T, Suzuki A, Ohtani E, Terasaki H, Urakawa S, Katayama Y, Funakoshi K, Wang Y, Hernlund JW, and Ballmer MD (2013) Ponded melt at the boundary between the lithosphere and asthenosphere. *Nature Geoscience* 6(12): 1041–1044. https://doi.org/10.1038/ngeo1982.

Salvi S and Williams-Jones AE (1997) Fischer-Tropsch synthesis of hydrocarbons during sub-solidus alteration of the Strange Lake peralkaline granite, Quebec/Labrador, Canada. *Geochimica et Cosmochimica Acta* 61(1): 83–99. https://doi.org/10.1016/S0016-7037(96)00313-4.

Sapienza GT, Scambelluri M, and Braga R (2009) Dolomite-bearing orogenic garnet peridotites witness fluid-mediated carbon recycling in a mantle wedge (Ulten Zone, Eastern Alps, Italy). *Contributions to Mineralogy and Petrology* 158: 401–420. https://doi.org/10.1007/s00410-009-0389-2.

Sarmiento JL, Gruber N, Brzezinski MA, and Dunne JP (2004) High-latitude controls of thermocline nutrients and low latitude biological productivity. *Nature* 427(6969): 56–60. https://doi.org/10.1038/nature02127.

Sawyer DS, Whitmarsh RB, Klaus A, et al. (eds.) (1994) vol. 149. *Proceedings of the Ocean Drilling Program, 149 Initial Reports*. Ocean Drilling Program. https://doi.org/10.2973/odp.proc.ir.149.1994.

Scambelluri M, Bebout GE, Belmonte D, Gilio M, Campomenosi N, Collins N, and Crispini L (2016) Carbonation of subduction-zone serpentinite (high-pressure ophicarbonate; Ligurian Western Alps) and implications for the deep carbon cycling. *Earth and Planetary Science Letters* 441: 155–166.

Scheller EL, Swindle C, Grotzinger J, Barnhart H, Bhattacharjee S, Ehlmann BL, Farley K, Fischer WW, Greenberger R, Ingalls M, Martin PE, Osorio-Rodriguez D, and Smith BP (2021) Formation of magnesium carbonates on Earth and implications for mars. *Journal of Geophysical Research: Planets* 126(7): e2021JE006828. https://doi.org/10.1029/2021JE006828.

Schettino E and Poli S (2020) Hydrous carbonatitic liquids drive CO_2 recycling from subducted marls and limestones. In: *Carbon in Earth's Interior*, pp. 209–221. American Geophysical Union (AGU). https://doi.org/10.1002/9781119508229.ch18.

Schidlowski M (1988) A 3,800-million-year isotopic record of life from carbon in sedimentary rocks. *Nature* 333(6171): 313–318. https://doi.org/10.1038/333313a0.

Schmerr N (2012) The Gutenberg discontinuity: Melt at the lithosphere-asthenosphere boundary. *Science (New York, N.Y.)* 335(6075): 1480–1483. https://doi.org/10.1126/science.1215433.

Schwarzenbach EM, Früh-Green GL, Bernasconi SM, Alt JC, and Plas A (2013) Serpentinization and carbon sequestration: A study of two ancient peridotite-hosted hydrothermal systems. *Chemical Geology* 351: 115–133. https://doi.org/10.1016/j.chemgeo.2013.05.016.

Scott HP, Hemley RJ, Mao H, Herschbach DR, Fried LE, Howard WM, and Bastea S (2004) Generation of methane in the Earth's mantle: In situ high pressure–temperature measurements of carbonate reduction. *Proceedings of the National Academy of Sciences* 101(39): 14023–14026. https://doi.org/10.1073/pnas.0405930101.

Seewald JS, Zolotov MY, and McCollom T (2006) Experimental investigation of single carbon compounds under hydrothermal conditions. *Geochimica et Cosmochimica Acta* 70(2): 446–460. https://doi.org/10.1016/j.gca.2005.09.002.

Selway K and O'Donnell JP (2019) A small, unextractable melt fraction as the cause for the low velocity zone. *Earth and Planetary Science Letters* 517: 117–124. https://doi.org/10.1016/j.epsl.2019.04.012.

Selway K, O'Donnell JP, and Özaydin S (2019) Upper mantle melt distribution from petrologically constrained magnetotellurics. *Geochemistry, Geophysics, Geosystems* 20(7): 3328–3346. https://doi.org/10.1029/2019GC008227.

Sephton MA and Hazen RM (2013) On the origins of deep hydrocarbons. *Reviews in Mineralogy and Geochemistry* 75(1): 449–465. https://doi.org/10.2138/rmg.2013.75.14.

Serovaiskii A, Mukhina E, Dubrovinsky L, Chernoutsan A, Kudryavtsev D, McCammon C, Aprilis G, Kupenko I, Chumakov A, Hanfland M, and Kutcherov V (2019) Fate of hydrocarbons in iron-bearing mineral environments during subduction. *Minerals* 9(11): 651. https://doi.org/10.3390/min9110651.

Sforna MC, Brunelli D, Pisapia C, Pasini V, Malferrari D, and Ménez B (2018) Abiotic formation of condensed carbonaceous matter in the hydrating oceanic crust. *Nature Communications* 9(1): 5049. https://doi.org/10.1038/s41467-018-07385-6.

Shcheka SS, Wiedenbeck M, Frost DJ, and Keppler H (2006) Carbon solubility in mantle minerals. *Earth and Planetary Science Letters* 245(3): 730–742. https://doi.org/10.1016/j.epsl.2006.03.036.

Sherwood Lollar B, Lacrampe-Couloume G, Voglesonger K, Onstott TC, Pratt LM, and Slater GF (2008) Isotopic signatures of CH_4 and higher hydrocarbon gases from Precambrian Shield sites: A model for abiogenic polymerization of hydrocarbons. *Geochimica et Cosmochimica Acta* 72(19): 4778–4795. https://doi.org/10.1016/j.gca.2008.07.004.

Sherwood Lollar B, Onstott TC, Lacrampe-Couloume G, and Ballentine CJ (2014) The contribution of the Precambrian continental lithosphere to global H_2 production. *Nature* 516(7531): 379–382. https://doi.org/10.1038/nature14017.

Shi GU, Tropper P, Cui W, Tan J, and Wang C (2005) Methane (CH4)-bearing fluid inclusions in the Myanmar jadeitite. *Geochemical Journal* 39(6): 503–516. https://doi.org/10.2343/geochemj.39.503.

Shilobreeva S, Martinez I, Busigny V, Agrinier P, and Laverne C (2011) Insights into C and H storage in the altered oceanic crust: Results from ODP/IODP Hole 1256D. *Geochimica et Cosmochimica Acta* 75(9): 2237–2255. https://doi.org/10.1016/j.gca.2010.11.027.

Shimizu K, Saal AE, Hauri EH, Perfit MR, and Hékinian R (2019) Evaluating the roles of melt-rock interaction and partial degassing on the CO_2/Ba ratios of MORB: Implications for the CO_2 budget in the Earth's depleted upper mantle. *Geochimica et Cosmochimica Acta* 260: 29–48. https://doi.org/10.1016/j.gca.2019.06.013.

Shirey SB and Richardson SH (2011) Start of the Wilson cycle at 3 Ga Shown by diamonds from subcontinental mantle. *Science* 333(6041): 434–436. https://doi.org/10.1126/science.1206275.

Shirey SB, Cartigny P, Frost DJ, Keshav S, Nestola F, Nimis P, Pearson DG, Sobolev NV, and Walter MJ (2013) Diamonds and the geology of mantle carbon. *Reviews in Mineralogy and Geochemistry* 75(1): 355–421. https://doi.org/10.2138/rmg.2013.75.12.

Shirey SB, Smit KV, Pearson DG, Walter MJ, Aulbach S, Brenker FE, Bureau H, Burnham AD, Cartigny P, Chacko T, Frost DJ, Hauri EH, Jacob DE, Jacobsen SD, Kohn SC, Luth RW, Mikhail S, Navon O, Nestola F, et al. (2019) Diamonds and the mantle geodynamics of carbon: Deep mantle carbon evolution from the diamond record. In: Orcutt BN, Daniel I, and Dasgupta R (eds.) *Deep Carbon: Past to Present*, pp. 89–128. Cambridge University Press. https://www.cambridge.org/core/books/deep-carbon/diamonds-and-the-mantle-geodynamics-of-carbon/E46212484DDAA32B1DA14B796EB3D9BC.

Sidorin I, Gurnis M, and Helmberger DV (1999) Evidence for a ubiquitous seismic discontinuity at the base of the mantle. *Science* 286(5443): 1326–1331. https://doi.org/10.1126/science.286.5443.1326.

Sieber MJ, Hermann J, and Yaxley GM (2018) An experimental investigation of C–O–H fluid-driven carbonation of serpentinites under forearc conditions. *Earth and Planetary Science Letters* 496: 178–188. https://doi.org/10.1016/j.epsl.2018.05.027.

Siegel DA, DeVries T, Cetinić I, and Bisson KM (2023) Quantifying the ocean's biological pump and its carbon cycle impacts on global scales. *Annual Review of Marine Science* 15: 329–356. https://doi.org/10.1146/annurev-marine-040722-115226.

Sievert SM and Vetriani C (2012) Chemoautotrophy at deep-sea vents: Past, present, and future. *Oceanography* 25(1): 218–233.

Sifré D, Gardés E, Massuyeau M, Hashim L, Hier-Majumder S, and Gaillard F (2014) Electrical conductivity during incipient melting in the oceanic low-velocity zone. *Nature* 509(7498): 81–85. https://doi.org/10.1038/nature13245.

Skelton A (2011) Flux rates for water and carbon during greenschist facies metamorphism. *Geology* 39(1): 43–46. https://doi.org/10.1130/G31328.1.

Sleep NH (2009) Stagnant lid convection and carbonate metasomatism of the deep continental lithosphere. *Geochemistry, Geophysics, Geosystems* 10(11). https://doi.org/10.1029/2009GC002702.

Sleep NH, Bird DK, and Pope EC (2011) Serpentinite and the dawn of life. *Philosophical Transactions of the Royal Society B: Biological Sciences* 366(1580): 2857–2869. https://doi.org/10.1098/rstb.2011.0129.

Smit KV, Timmerman S, Aulbach S, Shirey SB, Richardson SH, Phillips D, and Pearson DG (2022) Geochronology of diamonds. *Reviews in Mineralogy and Geochemistry* 88(1): 567–636. https://doi.org/10.2138/rmg.2022.88.11.

Smith EM, Shirey SB, Nestola F, Bullock ES, Wang J, Richardson SH, and Wang W (2016) Large gem diamonds from metallic liquid in Earth's deep mantle. *Science* 354(6318): 1403–1405. https://doi.org/10.1126/science.aal1303.

Smith EM, Shirey SB, Richardson SH, Nestola F, Bullock ES, Wang J, and Wang W (2018) Blue boron-bearing diamonds from Earth's lower mantle. *Nature* 560(7716): 84–87. https://doi.org/10.1038/s41586-018-0334-5.

Smith EM, Krebs MY, Genzel P-T, and Brenker FE (2022) Raman identification of inclusions in diamond. *Reviews in Mineralogy and Geochemistry* 88(1): 451–473. https://doi.org/10.2138/rmg.2022.88.08.

Sobolev NV, Logvinova AM, Tomilenko AA, Wirth R, and Bul'bak, T. A., Luk'yanova, L. I., Fedorova, E. N., Reutsky, V. N., & Efimova, E. S. (2019) Mineral and fluid inclusions in diamonds from the Urals placers, Russia: Evidence for solid molecular N_2 and hydrocarbons in fluid inclusions. *Geochimica et Cosmochimica Acta* 266: 197–219. https://doi.org/10.1016/j.gca.2019.08.028.

Soltanmohammadi A, Grégoire M, Rabinowicz M, Gerbault M, Ceuleneer G, Rahgoshay M, Bystricky M, and Benoit M (2018) Transport of volatile-rich melt from the mantle transition zone via compaction pockets: Implications for mantle metasomatism and the origin of alkaline lavas in the Turkish–Iranian plateau. *Journal of Petrology* 59(12): 2273–2310. https://doi.org/10.1093/petrology/egy097.

Sossi PA, Burnham AD, Badro J, Lanzirotti A, Newville M, O'Neill HS, and C. (2020) Redox state of Earth's magma ocean and its Venus-like early atmosphere. *Science Advances* 6(48): eabd1387. https://doi.org/10.1126/sciadv.abd1387.

Stachel T and Harris JW (2008) The origin of cratonic diamonds—Constraints from mineral inclusions. *Ore Geology Reviews* 34(1): 5–32. https://doi.org/10.1016/j.oregeorev.2007.05.002.

Stachel T, Brey GP, and Harris JW (2000a) Kankan diamonds (Guinea) I: From the lithosphere down to the transition zone. *Contributions to Mineralogy and Petrology* 140(1): 1–15. https://doi.org/10.1007/s004100000173.

Stachel T, Harris JW, Brey GP, and Joswig W (2000b) Kankan diamonds (Guinea) II: Lower mantle inclusion parageneses. *Contributions to Mineralogy and Petrology* 140(1): 16–27. https://doi.org/10.1007/s004100000174.

Stachel T, Chacko T, and Luth RW (2017) Carbon isotope fractionation during diamond growth in depleted peridotite: Counterintuitive insights from modelling water-maximum CHO fluids as multi-component systems. *Earth and Planetary Science Letters* 473: 44–51. https://doi.org/10.1016/j.epsl.2017.05.037.

Stachel T, Aulbach S, and Harris JW (2022a) Mineral inclusions in lithospheric diamonds. *Reviews in Mineralogy and Geochemistry* 88(1): 307–391. https://doi.org/10.2138/rmg.2022.88.06.

Stachel T, Cartigny P, Chacko T, and Pearson DG (2022b) Carbon and nitrogen in mantle-derived diamonds. *Reviews in Mineralogy and Geochemistry* 88(1): 809–875. https://doi.org/10.2138/rmg.2022.88.15.

Stagno V and Fei Y (2020) The redox boundaries of Earth's interior. *Elements* 16(3): 167–172. https://doi.org/10.2138/gselements.16.3.167.

Stagno V and Frost DJ (2010) Carbon speciation in the asthenosphere: Experimental measurements of the redox conditions at which carbonate-bearing melts coexist with graphite or diamond in peridotite assemblages. *Earth and Planetary Science Letters* 300(1): 72–84. https://doi.org/10.1016/j.epsl.2010.09.038.

Stagno V, Ojwang DO, McCammon CA, and Frost DJ (2013) The oxidation state of the mantle and the extraction of carbon from Earth/'s interior. *Nature* 493(7430): 84–88. https://doi.org/10.1038/nature11679.

Stagno V, Cerantola V, Aulbach S, Lobanov S, McCammon CA, and Merlini M (2019) Carbon-bearing phases throughout Earth's interior: Evolution through space and time. In: Orcutt BN, Daniel I, and Dasgupta R (eds.) *Deep Carbon*, 1st edn, pp. 66–88. Cambridge University Press. https://doi.org/10.1017/9781108677950.004.

Stamm N and Schmidt MW (2017) Asthenospheric kimberlites: Volatile contents and bulk compositions at 7 GPa. *Earth and Planetary Science Letters* 474: 309–321. https://doi.org/10.1016/j.epsl.2017.06.037.

Staudigel H, Hart SR, Schmincke H-U, and Smith BM (1989) Cretaceous ocean crust at DSDP Sites 417 and 418: Carbon uptake from weathering versus loss by magmatic outgassing. *Geochimica et Cosmochimica Acta* 53(11): 3091–3094. https://doi.org/10.1016/0016-7037(89)90189-0.

Stern CR (2011) Subduction erosion: Rates, mechanisms, and its role in arc magmatism and the evolution of the continental crust and mantle. *Gondwana Research* 20(2): 284–308. https://doi.org/10.1016/j.gr.2011.03.006.

Stern CR (2020) The role of subduction erosion in the generation of Andean and other convergent plate boundary arc magmas, the continental crust and mantle. *Gondwana Research* 88: 220–249. https://doi.org/10.1016/j.gr.2020.08.006.

Stewart EM and Ague JJ (2018) Infiltration-driven metamorphism, New England, USA: Regional CO_2 fluxes and implications for Devonian climate and extinctions. *Earth and Planetary Science Letters* 489: 123–134. https://doi.org/10.1016/j.epsl.2018.02.028.

Stewart EM, Ague JJ, Ferry JM, Schiffries CM, Tao R-B, Isson TT, and Planavsky NJ (2019) Carbonation and decarbonation reactions: Implications for planetary habitability. *American Mineralogist* 104(10): 1369–1380. https://doi.org/10.2138/am-2019-6884.

Stixrude L, de Koker N, Sun N, Mookherjee M, and Karki BB (2009) Thermodynamics of silicate liquids in the deep Earth. *Earth and Planetary Science Letters* 278(3): 226–232. https://doi.org/10.1016/j.epsl.2008.12.006.

Stolte N, Yu J, Chen Z, Sverjensky DA, and Pan D (2021) Water–gas shift reaction produces formate at extreme pressures and temperatures in deep Earth fluids. *The Journal of Physical Chemistry Letters* 12(17): 4292–4298. https://doi.org/10.1021/acs.jpclett.1c00563.

Straub SM, Gómez-Tuena A, Bindeman IN, Bolge LL, Brandl PA, Espinasa-Perena R, Solari L, Stuart FM, Vannucchi P, and Zellmer GF (2015) Crustal recycling by subduction erosion in the central Mexican Volcanic Belt. *Geochimica et Cosmochimica Acta* 166: 29–52. https://doi.org/10.1016/j.gca.2015.06.001.

Straub SM, Gómez-Tuena A, and Vannucchi P (2020) Subduction erosion and arc volcanism. *Nature Reviews Earth and Environment* 1(11): 574–589. https://doi.org/10.1038/s43017-020-0095-1.

Suzuki A, Ohtani E, and Kato T (1995) Flotation of diamond in mantle melt at high pressure. *Science* 269(5221): 216–218. https://doi.org/10.1126/science.269.5221.216.

Svensen H, Planke S, Malthe-Sørenssen A, Jamtveit B, Myklebust R, Rasmussen Eidem T, and Rey SS (2004) Release of methane from a volcanic basin as a mechanism for initial Eocene global warming. *Nature* 429(6991): 542–545. https://doi.org/10.1038/nature02566.

Sverjensky DA and Huang F (2015) Diamond formation due to a pH drop during fluid–rock interactions. *Nature Communications* 6(1): 8702. https://doi.org/10.1038/ncomms9702.

Sverjensky DA, Harrison B, and Azzolini D (2014) Water in the deep Earth: The dielectric constant and the solubilities of quartz and corundum to 60kb and 1200°C. *Geochimica et Cosmochimica Acta* 129: 125–145. https://doi.org/10.1016/j.gca.2013.12.019.

Sverjensky D, Daniel I, and Vitale Brovarone A (2020) The changing character of carbon in fluids with pressure: Organic geochemistry of Earth's upper mantle fluids. In: Manning CE, Lin J, and Mao WL (eds.) *Carbon in Earth's Interior*, 1st edn, pp. 259–269. Wiley. https://doi.org/10.1002/9781119508229.ch22.

Symonds RB, Rose WI, Bluth GJS, and Gerlach TM (1994) Volcanic-gas studies: Methods, results, and applications. In: Carroll MR and Holloway JR (eds.) *Volatiles in Magmas*, 30, pp. 1–66. De Gruyter. https://doi.org/10.1515/9781501509674-007.

Takai K, Nakamura K, Toki T, Tsunogai U, Miyazaki M, Miyazaki J, Hirayama H, Nakagawa S, Nunoura T, and Horikoshi K (2008) Cell proliferation at 122°C and isotopically heavy CH_4 production by a hyperthermophilic methanogen under high-pressure cultivation. *Proceedings of the National Academy of Sciences* 105(31): 10949–10954. https://doi.org/10.1073/pnas.0712334105.

Tamburello G, Pondrelli S, Chiodini G, and Rouwet D (2018) Global-scale control of extensional tectonics on CO_2 earth degassing. *Nature Communications* 9(1): 4608. https://doi.org/10.1038/s41467-018-07087-z.

Tao R, Zhang L, Fei Y, and Liu Q (2014) The effect of Fe on the stability of dolomite at high pressure: Experimental study and petrological observation in eclogite from southwestern Tianshan, China. *Geochimica et Cosmochimica Acta* 143: 253–267. https://doi.org/10.1016/j.gca.2014.02.031.

Tao R, Zhang L, Tian M, Zhu J, Liu X, Liu J, Höfer HE, Stagno V, and Fei Y (2018) Formation of abiotic hydrocarbon from reduction of carbonate in subduction zones: Constraints from petrological observation and experimental simulation. *Geochimica et Cosmochimica Acta* 239: 390–408. https://doi.org/10.1016/j.gca.2018.08.008.

Tappe S, Foley SF, Stracke A, Romer RL, Kjarsgaard BA, Heaman LM, and Joyce N (2007) Craton reactivation on the Labrador Sea margins: $^{40}Ar/^{39}Ar$ age and Sr–Nd–Hf–Pb isotope constraints from alkaline and carbonatite intrusives. *Earth and Planetary Science Letters* 256(3): 433–454. https://doi.org/10.1016/j.epsl.2007.01.036.

Tarantola A, Mullis J, Vennemann T, Dubessy J, and de Capitani C (2007) Oxidation of methane at the CH_4/H_2O–(CO_2) transition zone in the external part of the Central Alps, Switzerland: Evidence from stable isotope investigations. *Chemical Geology* 237(3): 329–357. https://doi.org/10.1016/j.chemgeo.2006.07.007.

Tassi F, Garofalo PS, Turchetti F, De Santis D, Capecchiacci F, Vaselli O, et al. (2022) Insights into the Porretta Terme (northern Apennines, Italy) hydrothermal system revealed by geochemical data on presently discharging thermal waters and paleofluids. *Environmental Geochemistry and Health*: 1–24.

Tewksbury-Christle CM, Behr WM, and Helper MA (2021) Tracking deep sediment underplating in a fossil subduction margin: Implications for interface rheology and mass and volatile recycling. *Geochemistry, Geophysics, Geosystems* 22(3): e2020GC009463. https://doi.org/10.1029/2020GC009463.

Thomassot E, Cartigny P, Harris JW, and (Fanus) Viljoen, K. S. (2007) Methane-related diamond crystallization in the Earth's mantle: Stable isotope evidences from a single diamond-bearing xenolith. *Earth and Planetary Science Letters* 257(3): 362–371. https://doi.org/10.1016/j.epsl.2007.02.020.

Thomsen TB and Schmidt MW (2008) Melting of carbonated pelites at 2.5–5.0 GPa, silicate–carbonatite liquid immiscibility, and potassium–carbon metasomatism of the mantle. *Earth and Planetary Science Letters* 267(1): 17–31. https://doi.org/10.1016/j.epsl.2007.11.027.

Thomson AR, Kohn SC, Bulanova GP, Smith CB, Araujo D, and Walter MJ (2016) Trace element composition of silicate inclusions in sub-lithospheric diamonds from the Juina-5 kimberlite: Evidence for diamond growth from slab melts. *Lithos* 265: 108–124. https://doi.org/10.1016/j.lithos.2016.08.035.

Thomson AR, Crichton WA, Brodholt JP, Wood IG, Siersch NC, Muir JMR, Dobson DP, and Hunt SA (2019) Seismic velocities of $CaSiO_3$ perovskite can explain LLSVPs in Earth's lower mantle. *Nature* 572(7771): 643–647. https://doi.org/10.1038/s41586-019-1483-x.

Thybo H, Ross AR, and Egorkin AV (2003) Explosion seismic reflections from the Earth's core. *Earth and Planetary Science Letters* 216(4): 693–702. https://doi.org/10.1016/S0012-821X(03)00532-6.

Timmerman S, Stachel T, Koornneef JM, Smit KV, Harlou R, Nowell GM, Thomson AR, Kohn SC, Davies JHFL, Davies GR, Krebs MY, Zhang Q, Milne SEM, Harris JW, Kaminsky F, Zedgenizov D, Bulanova G, Smith CB, Cabral Neto I, et al. (2023) Sublithospheric diamond ages and the supercontinent cycle. *Nature* 623(7988): 752–756. https://doi.org/10.1038/s41586-023-06662-9.

Tissot BP and Welte DH (1984) *Petroleum Formation and Occurrence*. Springer. https://doi.org/10.1007/978-3-642-87813-8.

Toffolo L, Tumiati S, Villa A, Fumagalli P, Amalfa A, and Miozzi F (2023) Experimental dissolution of carbonaceous materials in water at 1 GPa and 550° C: Assessing the role of carbon forms and redox state on COH fluid production and composition during forearc subduction of organic matter. *Frontiers in Earth Science* 11: 1013014.

Trestrail KR, Rooney TO, Girard G, Svoboda C, Yirgu G, Ayalew D, and Keppelman J (2017) Sub-continental lithospheric mantle deformation in the Yerer-Tullu Wellel Volcanotectonic Lineament: A study of peridotite xenoliths. *Chemical Geology* 455: 249–263. https://doi.org/10.1016/j.chemgeo.2016.10.013.

Tumiati S, Tiraboschi C, Sverjensky DA, Pettke T, Recchia S, Ulmer P, Miozzi F, and Poli S (2017) Silicate dissolution boosts the CO2 concentrations in subduction fluids. *Nature Communications* 8(1): 616.

Tumiati S, Tiraboschi C, Miozzi F, Vitale-Brovarone A, Manning CE, Sverjensky DA, Milani S, and Poli S (2020) Dissolution susceptibility of glass-like carbon versus crystalline graphite in high-pressure aqueous fluids and implications for the behavior of organic matter in subduction zones. *Geochimica et Cosmochimica Acta* 273: 383–402. https://doi.org/10.1016/j.gca.2020.01.030.

Tucker JM, Mukhopadhyay S, and Gonnermann HM (2018) Reconstructing mantle carbon and noble gas contents from degassed mid-ocean ridge basalts. *Earth and Planetary Science Letters* 496: 108–119. https://doi.org/10.1016/j.epsl.2018.05.024.

Tumiati S, Recchia S, Remusat L, Tiraboschi C, Sverjensky DA, Manning CE, Vitale Brovarone A, Boutier A, Spanu D, and Poli S (2022) Subducted organic matter buffered by marine carbonate rules the carbon isotopic signature of arc emissions. *Nature Communications* 13(1): 2909. https://doi.org/10.1038/s41467-022-30421-5.

Urey HC (1952) On the early chemical history of the Earth and the origin of life. *Proceedings of the National Academy of Sciences* 38(4): 351–363. https://doi.org/10.1073/pnas.38.4.351.

Valentine DL (2002) Biogeochemistry and microbial ecology of methane oxidation in anoxic environments: A review. *Antonie Van Leeuwenhoek* 81(1): 271–282. https://doi.org/10.1023/A:1020587206351.

van Andel TH (1975) Mesozoic/Cenozoic calcite compensation depth and the global distribution of calcareous sediments. *Earth and Planetary Science Letters* 26(2): 187–194. https://doi.org/10.1016/0012-821X(75)90086-2.

van Avendonk HJA, Holbrook WS, Lizarralde D, and Denyer P (2011) Structure and serpentinization of the subducting Cocos plate offshore Nicaragua and Costa Rica. *Geochemistry, Geophysics, Geosystems* 12(6). https://doi.org/10.1029/2011GC003592.

Vandenbroucke M and Largeau C (2007) Kerogen origin, evolution and structure. *Organic Geochemistry* 38(5): 719–833. https://doi.org/10.1016/j.orggeochem.2007.01.001.

Vannucchi P, Scholl DW, Meschede M, and McDougall-Reid K (2001) Tectonic erosion and consequent collapse of the Pacific margin of Costa Rica: Combined implications from ODP Leg 170, seismic offshore data, and regional geology of the Nicoya Peninsula. *Tectonics* 20(5): 649–668. https://doi.org/10.1029/2000TC001223.

Vannucchi P, Sage F, Phipps Morgan J, Remitti F, and Collot J-Y (2012) Toward a dynamic concept of the subduction channel at erosive convergent margins with implications for interplate material transfer. *Geochemistry, Geophysics, Geosystems* 13(2). https://doi.org/10.1029/2011GC003846.

Vannucchi P, Morgan JP, and Balestrieri ML (2016) Subduction erosion, and the de-construction of continental crust: The Central America case and its global implications. *Gondwana Research* 40: 184–198. https://doi.org/10.1016/j.gr.2016.10.001.

Vernadsky VI (1926) *Biosfera (The Biosphere). Nauchnoe khimiko-techniche-skoye izdatel'stvo*. Scientific Chemico-Technical Publishing.
Vitale Brovarone A, Martinez I, Elmaleh A, Compagnoni R, Chaduteau C, Ferraris C, and Esteve I (2017) Massive production of abiotic methane during subduction evidenced in metamorphosed ophicarbonates from the Italian Alps. *Nature Communications* 8(1): 14134. https://doi.org/10.1038/ncomms14134.
Vitale Brovarone AV, Chu X, Martin L, Ague JJ, Monie P, Groppo C, Martinez I, and Chaduteau C (2018) Intra-slab COH fluid fluxes evidenced by fluid-mediated decarbonation of lawsonite eclogite-facies altered oceanic metabasalts. *Lithos* 304: 211–229.
Vitale Brovarone A, Sverjensky DA, Piccoli F, Ressico F, Giovannelli D, and Daniel I (2020a) Subduction hides high-pressure sources of energy that may feed the deep subsurface biosphere. *Nature Communications* 11(1). https://doi.org/10.1038/s41467-020-17342-x. Article 1.
Vitale Brovarone A, Tumiati S, Piccoli F, Ague JJ, Connolly JAD, and Beyssac O (2020b) Fluid-mediated selective dissolution of subducting carbonaceous material: Implications for carbon recycling and fluid fluxes at forearc depths. *Chemical Geology* 549: 119682. https://doi.org/10.1016/j.chemgeo.2020.119682.
Walker RJ (2009) Highly siderophile elements in the Earth, Moon and Mars: Update and implications for planetary accretion and differentiation. *Chemie der Erde - Geochemistry* 69(2): 101–125. https://doi.org/10.1016/j.chemer.2008.10.001.
Wallace ME and Green DH (1988) An experimental determination of primary carbonatite magma composition. *Nature* 335(6188): 343–346. https://doi.org/10.1038/335343a0.
Walling DE and Fang D (2003) Recent trends in the suspended sediment loads of the world's rivers. *Global and Planetary Change* 39(1): 111–126. https://doi.org/10.1016/S0921-8181(03)00020-1.
Wallmann K, Aloisi G, Haeckel M, Tishchenko P, Pavlova G, Greinert J, Kutterolf S, and Eisenhauer A (2008) Silicate weathering in anoxic marine sediments. *Geochimica et Cosmochimica Acta* 72(12): 2895–2918. https://doi.org/10.1016/j.gca.2008.03.026.
Walter MJ, Kohn SC, Araujo D, Bulanova GP, Smith CB, Gaillou E, Wang J, Steele A, and Shirey SB (2011) Deep mantle cycling of oceanic crust: Evidence from diamonds and their mineral inclusions. *Science* 334(6052): 54–57. https://doi.org/10.1126/science.1209300.
Walther JV and Long MI (1986) Experimental determination of calcite solubilities in supercritical H_2O. In: *Int Symp Water-Rock Interaction*, pp. 609–611.
Walton CR and Shorttle O (2024) Phanerozoic biological reworking of the continental carbonate rock reservoir. *Earth and Planetary Science Letters* 632: 118640. https://doi.org/10.1016/j.epsl.2024.118640.
Wang Z and Becker H (2013) Ratios of S, Se and Te in the silicate Earth require a volatile-rich late veneer. *Nature* 499(7458): 328–331. https://doi.org/10.1038/nature12285.
Wang C, Tao R, Walters JB, Höfer HE, and Zhang L (2022) Favorable P–T–fO_2 conditions for abiotic CH_4 production in subducted oceanic crusts: A comparison between CH_4-bearing ultrahigh- and CO_2-bearing high-pressure eclogite. *Geochimica et Cosmochimica Acta* 336: 269–290. https://doi.org/10.1016/j.gca.2022.09.010.
Wang W, Walter MJ, Brodholt JP, Huang S, and Petaev MI (2023) Chalcogen isotopes reveal limited volatile contribution from late veneer to Earth. *Science Advances* 9(49): eadh0670. https://doi.org/10.1126/sciadv.adh0670.
Wang H, Liu L, Gao Z, Yang L, Naren G, and Mao S (2024) Structure and elasticity of CaC_2O_5 suggests carbonate contribution to the seismic anomalies of Earth's mantle. *Nature Communications* 15(1): 755. https://doi.org/10.1038/s41467-024-44925-9.
Warr O, Young ED, Giunta T, Kohl IE, Ash JL, and Sherwood Lollar B (2021) High-resolution, long-term isotopic and isotopologue variation identifies the sources and sinks of methane in a deep subsurface carbon cycle. *Geochimica et Cosmochimica Acta* 294: 315–334. https://doi.org/10.1016/j.gca.2020.12.002.
Wedepohl KH (1995) The composition of the continental crust. *Geochimica et Cosmochimica Acta* 59(7): 1217–1232. https://doi.org/10.1016/0016-7037(95)00038-2.
Weidendorfer D, Schmidt MW, and Mattsson HB (2017) A common origin of carbonatite magmas. *Geology* 45(6): 507–510. https://doi.org/10.1130/G38801.1.
Weis D, Harpp KS, Harrison LN, Boyet M, Chauvel C, Farnetani CG, Finlayson VA, Lee KKM, Parai R, Shahar A, and Williamson NMB (2023) Earth's mantle composition revealed by mantle plumes. *Nature Reviews Earth and Environment* 4(9): 604–625. https://doi.org/10.1038/s43017-023-00467-0.
White BS and Wyllie PJ (1992) Solidus reactions in synthetic lherzolite-H_2O-CO_2 from 20–30 kbar, with applications to melting and metasomatism. *Journal of Volcanology and Geothermal Research* 50(1): 117–130. https://doi.org/10.1016/0377-0273(92)90040-K.
Werner C, Fischer TP, Aiuppa A, Edmonds M, Cardellini C, Carn S, Chiodini G, Cottrell E, Burton MR, Shinohara H, and Allard P (2019) Carbon Dioxide Emissions from Subaerial Volcanic Regions: Two decades in review. In: Orcutt B, Dasgupta R, and Daniel I (eds.) *Deep Carbon: Past to Present*. Cambridge University Press.
White RS, Minshull TA, Bickle MJ, and Robinson CJ (2001) Melt generation at very slow-spreading oceanic ridges: Constraints from geochemical and geophysical data. *Journal of Petrology* 42(6): 1171–1196. https://doi.org/10.1093/petrology/42.6.1171.
Whiticar MJ (1999) Carbon and hydrogen isotope systematics of bacterial formation and oxidation of methane. *Chemical Geology* 161(1): 291–314. https://doi.org/10.1016/S0009-2541(99)00092-3.
Whittington AG, Hellwig BM, Behrens H, Joachim B, Stechern A, and Vetere F (2009) The viscosity of hydrous dacitic liquids: Implications for the rheology of evolving silicic magmas. *Bulletin of Volcanology* 71(2): 185–199. https://doi.org/10.1007/s00445-008-0217-y.
Wieser PE, Iacovino K, Matthews S, Moore G, and Allison CM (2022) VESIcal: 2. A critical approach to volatile solubility modeling using an open-source Python3 engine. *Earth and Space Science* 9(2): e2021EA001932. https://doi.org/10.1029/2021EA001932.
Wong K, Mason E, Brune S, East M, Edmonds M, and Zahirovic S (2019) Deep carbon cycling over the past 200 million years: A review of fluxes in different tectonic settings. Frontiers. *Earth Science* 7(263). https://doi.org/10.3389/feart.2019.00263.
Wong K, Ferguson D, Wieser P, Morgan D, Edmonds M, Tadesse AZ, Yirgu G, Harvey J, and Hammond S (2023) Focused mid-crustal magma intrusion during continental break-up in Ethiopia. *Geophysical Research Letters* 50(11): e2023GL103257. https://doi.org/10.1029/2023GL103257.
Wood BJ (1993) Carbon in the core. *Earth and Planetary Science Letters* 117(3): 593–607. https://doi.org/10.1016/0012-821X(93)90105-I.
Wood RA (2011) Paleoecology of the earliest skeletal metazoan communities: Implications for early biomineralization. *Earth-Science Reviews* 106(1): 184–190. https://doi.org/10.1016/j.earscirev.2011.01.011.
Wood BJ, Li J, and Shahar A (2013) Carbon in the core: Its influence on the properties of core and mantle. *Reviews in Mineralogy and Geochemistry* 75(1): 231–250. https://doi.org/10.2138/rmg.2013.75.8.
Woodland AB and Koch M (2003) Variation in oxygen fugacity with depth in the upper mantle beneath the Kaapvaal craton, Southern Africa. *Earth and Planetary Science Letters* 214(1): 295–310. https://doi.org/10.1016/S0012-821X(03)00379-0.
Wyllie PJ, Huang W-L, Otto J, and Byrnes AP (1983) Carbonation of peridotites and decarbonation of siliceous dolomites represented in the system CaO-MgO-SiO_2-CO_2 to 30 kbar. *Tectonophysics* 100(1): 359–388. https://doi.org/10.1016/0040-1951(83)90194-4.
Yaroshevsky AA (2006) Abundances of chemical elements in the Earth's crust. *Geochemistry International* 44(1): 48–55. https://doi.org/10.1134/S001670290601006X.
Yaxley GM and Brey GP (2004) Phase relations of carbonate-bearing eclogite assemblages from 2.5 to 5.5 GPa: Implications for petrogenesis of carbonatites. *Contributions to Mineralogy and Petrology* 146(5): 606–619. https://doi.org/10.1007/s00410-003-0517-3.
Yaxley GM, Green DH, and Kamenetsky V (1998) Carbonatite metasomatism in the Southeastern Australian lithosphere. *Journal of Petrology* 39(11–12): 1917–1930. https://doi.org/10.1093/petroj/39.11-12.1917.
Yaxley GM, Anenburg M, Tappe S, Decree S, and Guzmics T (2022) Carbonatites: Classification, sources, evolution, and emplacement. *Annual Review of Earth and Planetary Sciences* 50: 261–293. https://doi.org/10.1146/annurev-earth-032320-104243.
Yoshino T, Laumonier M, McIsaac E, and Katsura T (2010) Electrical conductivity of basaltic and carbonatite melt-bearing peridotites at high pressures: Implications for melt distribution and melt fraction in the upper mantle. *Earth and Planetary Science Letters* 295(3): 593–602. https://doi.org/10.1016/j.epsl.2010.04.050.
Yoshino T, Gruber B, and Reinier C (2018) Effects of pressure and water on electrical conductivity of carbonate melt with implications for conductivity anomaly in continental mantle lithosphere. *Physics of the Earth and Planetary Interiors* 281: 8–16. https://doi.org/10.1016/j.pepi.2018.05.003.
Young ED (2019) A two-dimensional perspective on CH_4 isotope clumping: Distinguishing process from source. In: Orcutt BN, Daniel I, and Dasgupta R (eds.) *Deep Carbon: Past to Present*, pp. 388–414. Cambridge University Press. https://www.cambridge.org/core/books/deep-carbon/twodimensional-perspective-on-ch4-isotope-clumping/B2F63149CB9D2732418BE275D06FD8E0.

Young ED, Kohl IE, Lollar BS, Etiope G, Rumble D, Li (李姝宁) S, Haghnegahdar MA, Schauble EA, McCain KA, Foustoukos DI, Sutclife C, Warr O, Ballentine CJ, Onstott TC, Hosgormez H, Neubeck A, Marques JM, Pérez-Rodríguez I, Rowe AR, et al. (2017) The relative abundances of resolved $^{12}CH_2D_2$ and $^{13}CH_3D$ and mechanisms controlling isotopic bond ordering in abiotic and biotic methane gases. *Geochimica et Cosmochimica Acta* 203: 235–264. https://doi.org/10.1016/j.gca.2016.12.041.

Zeebe RE (2012) History of seawater carbonate chemistry, atmospheric CO_2, and ocean acidification. *Annual Review of Earth and Planetary Sciences* 40(1): 141–165. https://doi.org/10.1146/annurev-earth-042711-105521.

Zhang C, Lin J-F, Liu Y, Feng S, Jin C, Hou M, and Yoshino T (2018a) Electrical resistivity of Fe-C alloy at high pressure: Effects of carbon as a light element on the thermal conductivity of the Earth's core. *Journal of Geophysical Research: Solid Earth* 123(5): 3564–3577. https://doi.org/10.1029/2017JB015260.

Zhang S, Ague JJ, and Vitale Brovarone A (2018b) Degassing of organic carbon during regional metamorphism of pelites, Wepawaug Schist, Connecticut, USA. *Chemical Geology* 490: 30–44. https://doi.org/10.1016/j.chemgeo.2018.05.003.

Zhang L, Zhang L, Tang M, Wang X, Tao R, Xu C, and Bader T (2023) Massive abiotic methane production in eclogite during cold subduction. *National Science Review* 10(1): nwac207. https://doi.org/10.1093/nsr/nwac207.

Zhang F, Lai S, Stagno V, Chen L, Zhang C, Zhu R, Zhu Y, Wang X, Qin J, and Wang J (2024) The redox state of the asthenospheric mantle and the onset of melting beneath mid-ocean ridges. *Journal of Geophysical Research: Solid Earth* 129(5): e2023JB027033. https://doi.org/10.1029/2023JB027033.